UNIVERSITÉ DE MONTRÉAL

OPTIMIZATION OF MAGNESIA BASED, CEMENT-FREE, SPINEL BONDED CASTABLES

CHENG XING

DÉPARTEMENT DE GÉNIE PHYSIQUE ET DE GÉNIE DES MATÉRIAUX

ÉCOLE POLYTECHNIQUE DE MONTRÉAL

THÈSE PRÉSENTÉE EN VUE DE L'OBTENTION

DU DIPLÔME DE PHILOSOPHIAE DOCTOR (Ph.D.)

(GÉNIE MÉTALLURGIQUE)

DÉCEMBRE 1999

UNIVERSITÉ DE MONTRÉAL

ÉCOLE POLYTECHNIQUE DE MONTRÉAL

Cette thèse intitulée:

OPTIMIZATION OF MAGNESIA BASED, CEMENT-FREE, SPINEL BONDED CASTABLES

Présentée par: XING Cheng

En vue de l'obtention du diplôme de: Philosophiae Doctor

A été dûment acceptée par le jury d'examen constitué de:

Mr. Allaire Claude, Ph.D., président

Mr. Rigaud Michel, Ph.D., membre et directeur de recherche

Mr. Pelton Authur, Ph.D., membre

Mr. Dallaire Serge Ph.D., membre

ACKNOWLEDGEMENTS

I would like to express my deepest appreciation and sincere gratitude to my supervisor, Prof. M. Rigaud, for his expert guidance, valuable advice and constant support and encouragement.

I sincerely thank Dr. Claude Allaire who has accepted to act as chairman of the jury, Dr. Authur Pelton and Dr. Serge Dallaire for accepting to be members of the jury.

In no particular order, grateful acknowledgement is also made to my friends and colleagues in CIREP, Mr. V. Kovac, Dr. S. Afshar, Dr. C.L.Feng, Dr. S. Palco, N.S.Zhou, Z.Q.Guo, H.Q.He, and J. Sebbani, R. Pelletier, N. Ntakaburimvo, H. Rioux, M. E. Perron A. Pulido and L.Rebouillat for their friendship, fruiful discussions and valuable assistance.

Special thanks are also extended to Prof. L. Nan, Prof. V. Pandolfelli, Dr. X. Li, Dr. N. Wang, F. B. Ye, Dr. W. Zhong, M. Lagace and J. Chamberlain for their constant encouragement and help.

I also sincerely thank Mr. Jean-Philippe Bouchard for his great help with some experimental works.

Finally, the author would like to thank his family and in particular, to express his deepest appreciation to his wife and son for their love, encouragement and constant support.

RÉSUMÉ

L'optimisation de bétons réfractaires de $MgO-Al_2O_3$, à base de magnésie, sans ciment, à liaison spinelle, avec au moins 70% de magnésie, 5% d'alumine hydratable comme liant hydraulique, a été accomplie. Les points principaux de cette mise au point ont porté sur l'étude de la coulabilité de ces bétons et la stabilité dimensionnelle des mélanges de magnésie et d'alumine, et la détermination des propriétés physiques, mécaniques et chimiques, notamment la résistance à la corrosion vis à vis de scories basiques ferritiques.

Les essais de coulabilité ont été conduits pour déterminer le type et la quantité de défloculant nécessaire. Pour cela, une procédure originale a été suivie, en isolant la partie matrice des agrégats du béton et en mesurant des temps d'écoulement de différentes barbotines avec différents défloculants, à partir d'un montage décrit dans cette thèse. Il a été par la suite démontré que ces mesures de temps correspondent très bien avec des mesures de coulabilité sur les mélanges eux-mêmes ; cette procédure expérimentale s'est avérée fiable, et nous a permis d'économiser temps et matériaux.

L'étude de la stabilité dimensionnelle des mélanges de magnésie et d'alumine, a été conduite en établissant les courbes de dilatométrie de deux types distincts de mélanges; l'un constitué de MgO, d'alumine et de spinelle synthétique, l'autre avec en plus addition de fumée de silice.

Dans la première catégorie de mélanges, 35 compositions avec diverses proportions (0, 5 et 10%) de spinelle riche en alumine (AR_{90}), de spinelle riche en

magnésie (MR_{66}) et de spinelle stœchiométrique (AR_{78}) ont été évaluées. Il a été établi que la formation de spinelle s'amorce à 1100°C. Jusqu' à cette température, la dilatation réversible des mélanges est contrôlée par la dilatation de la magnésie. De 1100°C à 1600°C, l'expansion puis la contraction due au frittage des particules sont contrôlées par trois phénomènes concurrents: la dilatation continue des particules, la réaction de formation de spinelle qui s'accompagne d'une forte augmentation de volume et le frittage des particules qui impose un rétrécissement important. Suite à des mesures semi-quantitatives de diffraction-X pour déterminer la quantité de spinelle in-situ formée pour chaque composition, il a été possible de corréler les effets d'expansion-frittage aux quantités respectives de magnésie (M), alumine (A) et spinelle synthétique (MA) utilisées et de différencier le rôle des trois types de spinelle synthétique utilisés (AR_{90}, MR_{66}, AR_{78}). Il a été principalement démontré qu'il était possible de limiter les effets néfastes dûs à l'augmentation volumique in-situ, en ajustant les proportions de M, A et MA. Il a été aussi vérifié que dans les cas étudiés, la spinelle in-situ formée été de type quasi-stœchiométrique. Suite à cette étude centrale, pour la poursuite des travaux, il a été possible de prévoir la mise au point de bétons magnésiens avec des limites de variations dimensionnelles, lors de leur mise en œuvre, de l'ordre de 1% ou moins.

Dans la deuxième catégorie d'essais dilatométriques, l'influence de faibles quantités de fumée de silice (entre 0 et 3%) a été précisée sur des mélanges contenant 0, 5 ou 10% de spinelle AR_{78}. Il a été ainsi vérifié de nouveau que cette addition ne perturbe pas les limites de variations dimensionnelles escomptées. Lors de tous ces essais, les effets au refroidissement ont aussi été enregistrés. Il a été possible de mettre

en évidence une température (dite TG dans la thèse, pour Température Gap) où il y a systématiquement apparition de microfissures entre les grains de magnésie et de spinelle formés in-situ, due à la différence intrinsèque des coefficients d'expansion thermique des deux oxydes.

Les effets dûs aux additions de spinelle synthétique et de fumée de silice sur les propriétés physiques et mécaniques des bétons étudiés sont discutés au chapitre 5. Le rapport magnésie/alumine total et les quantités de spinelle synthétique et de silice influencent directement la porosité, la densité et le module de rupture à froid. L'ajout de spinelle est néfaste aux propriétés mécaniques après cuisson à température intermédiaire (1000°C) mais permet une amélioration des valeurs de module de rupture à chaud. L'ajout de fumée de silice permet d'améliorer les propriétés mécaniques après cuisson à température intermédiaire mais il est nuisible aux valeurs de module de rupture à chaud. Dès lors, une proportion adéquate des deux ajouts est requise.

La mesure de la résistance à la corrosion des bétons vis-à-vis d'une scorie basique ferritique (C/S=2.2 ; Fe_2O_3=29%) a été effectuée en suivant la norme ASTM C-874, à l'aide d'un four rotatif. L'effet de la nature du grain de spinelle utilisé a été étudié au niveau de 5%. Les résultats expérimentaux démontrent que la résistance à la dissolution est améliorée lorsqu'on utilise le spinelle AR_{78}; l'ajout de MR_{66} est le plus bénéfique pour la résistance à la pénétration; l'utilisation de AR_{90} n'est pas recommandable (en rapport avec les AR_{78} et MR_{66}) dans les bétons MgO-Al_2O_3 étudiés.

Les effets dûs à l'addition de silice sur la résistance à la corrosion ont été considérés en détail. La proportion la mieux appropriée se situe au niveau de 1% tant

pour la résistance à la corrosion que pour l'amélioration des propriétés mécaniques, après cuisson, à température intermédiaire. Avec plus de 1% de silice, les propriétés de corrosion décroissent.

Le contraste entre la résistance à la corrosion de bétons, bien optimisés, de MgO-Al_2O_3 par rapport à un béton commercial du type Al_2O_3-MgO est aussi mis en évidence, dans le chapitre 6. La résistance à la dissolution (érosion) des bétons MgO-Al_2O_3 est, comme compté, nettement supérieure.

La caractérisation microstructurale des bétons de MgO-Al_2O_3, avant et après corrosion, a été effectuée à l'aide de la microscopie optique et électronique à balayage (MEB), avec analyses spectrales et aussi à l'aide d'un diffractométre à rayons-X. Trois épaisseurs ont été clairement identifiées sur les échantillons corrodés. La couche de scorie résiduelle en face chaude, la zone pénétrée et la zone non-attaquée. La zone pénétrée doit être divisée en deux sous-couches, l'une colorée plus poreuse, l'autre plus dense et non colorée. La zone colorée résulte de la pénétration du fer, sous forme d'oxyde de fer dans les grains de magnésie et de spinelle, où le FeO se retrouve sous forme de solution solide. Dans la zone incolore, des phases de CMS et C_3MS_2 ont été identifiées, témoignant ainsi de la pénétration du CaO et SiO_2 de la scorie. À l'orée entre la zone colorée et la zone incolore, là où il y a densification, une proportion accrue de spinelle, dite secondaire, sous forme aciculaire, a été détectée; cette zone densifiée permettrait de minimiser l'importance de la pénétration de la scorie.

Le but ultime de ce travail qui était de contribuer au développement de bétons basiques adéquats pour être utilisés dans les poches de coulée d'aciers, à la ligne de

laitier, n'a pas été atteint de façon pleinement satisfaisante. Ce travail a néanmoins permis de révéler les limitations intrinsèques des bétons à base de magnésie, qui s'avèrent limités pour leur faible résistance à la pénétration par les laitiers contenant des oxydes de fer et par voie de conséquence à leur mauvaise résistance à l'écaillage structural. La seule solution semble être de développer dorénavant des bétons magnésiens contenant du carbone et du graphite.

Les objectifs qui ont été atteints sont : le développement de bétons magnésiens, sans ciment à liaison spinelle, ayant surmonté les difficultés suivantes : la coulabilité et la prise de ces bétons en minimisant l'eau de gâchage requise, la stabilité volumique et les propriétés mécaniques après cuisson.

ABSTRACT

The optimization of magnesia-based, cement-free and spinel bonded $MgO-Al_2O_3$ castables with more than 70% magnesia and 5% hydratable alumina as binder has been conducted. The major aspects which have been covered during this study are: flowability, volume stability, physical and mechanical properties and corrosion resistance.

Flowability tests have been carried out to determine the appropriate deflocculant type and addition level. Based on the developed "Extracting-Matrix" method, the "flow-time" of MgO, Al_2O_3 and castable matrix slurries have been tested with four types of inorganic or organic deflocculant at five addition levels each. The shortest "flow-time" corresponds to the most appropriate deflocculant. The flowability of $MgO-Al_2O_3$ castables have then been predicted from those "flow-time" measurements, which also correlate well with the physical and mechanical properties of $MgO-Al_2O_3$ castables.

Volume stability study is divided into two parts, one emphases on the effects of pre-reacted spinel addition on thermal expansion behaviors, the other focuses on the effect of silica fume additions.

For the first part, thirty five mixes in three series have been tested with additions of 0%, 5%, 10% pre-reacted spinel AR_{90} (alumina-rich), MR_{66} (magnesia-rich) and AR_{78} (close to stochoiomtric) respectively. The starting temperature of in-situ spinel formed is around 1100°C. The reversible thermal expansion coefficient of $MgO-Al_2O_3$ castable corresponds to the expansion of the magnesia for temperature up to 1100°C. Above

1100°C, the thermal expansion of $MgO-Al_2O_3$ castable is consistent with phenomenological model with three distinct contributions: the reversible thermal expansion of MgO aggregate, the volume exchange due to the formation of spinel from the reaction of MgO, Al_2O_3 and the high temperature shrinkage from fine powders sintering.

By means of X-ray quantitative analysis, the relationships among maximum thermal expansion, in-situ spinel formation and pre-reacted spinel addition are established. The maximum thermal expansion is proportional to the amount of in-situ spinel formed; adding pre-reacted spinel into the mixes, does reduce the maximum thermal expansion. However, the thermal expansion behavior of AR_{90} in the castable is different from MR_{66} and AR_{78}, due to the further reaction between AR_{90} and MgO in the castable mix.

The temperature at maximum thermal expansion (T_{max}) is strongly related to the ratio of MgO to Al_2O_3 in the castable mix. With an increase of pre-reacted spinel addition, T_{max} goes up.

Adding pre-reacted spinel also can compensate for permanent linear change of $MgO-Al_2O_3$ castables.

For the second part, silica fume was added at 0-3% to ten mixes of two series, with or without pre-reacted spinel AR_{78} addition. With silica fume addition, the in-situ spinel formation is enhanced. Adding silica fume into castable doesn't change the thermal expansion behavior below 1100°C, but does at higher temperature, increasing the maximum thermal expansion and decreasing the temperature at maximum thermal

expansion. The additional level also remarkably affects thermal expansion of MgO-Al_2O_3 castable at high temperature. Adding pre-reacted spinel AR_{78} still can control the expansion.

The sintering shrinkage during first cycle cooling is also addressed with both pre-reacted spinel and silica additions. The beginning temperature of gap formation (TG) is a function of alumina content, the SiO_2 and the pre-reacted spinel amount in MgO-Al_2O_3 castable mixes. By adding pre-reacted spinel, TG formation increases, however, with the addition of silica fume, the TG formation decreases.

The effects of pre-reacted spinel and SiO_2 fume addition on physical and mechanical properties of MgO-Al_2O_3 castable are discussed in Chapter 5. The MgO to Al_2O_3 ratio in the mix, the amount of pre-reacted spinel and the silica fume used significantly influence the porosity, the bulk density and the cold modulus of rupture. Properties after firing at intermediate temperature (1000°C) are reduced with pre-reacted spinel additions, but the hot modulus of rupture can be increased thereby. SiO_2 fume can be used to improve intermediate temperature strength, but due to harmful effect on HMOR, an appropriate amount has to be selected.

Corrosion resistance measurement in highly ferritic basic slag (Fe_2O_3: 29%, C/S: 2.2) was conducted through rotary slag testing. For the purpose of comparison, three different grades of pre-reacted spinel AR_{90}, AR_{78} and MR_{66} were also adopted respectively. It shows that the erosion resistance are improved by adding 5% of AR_{78}. Adding 5% MR_{66} is beneficial for the penetration resistance, however, AR_{90} is not appropriate for MgO-Al_2O_3 castable.

The effects of SiO_2 fume addition on corrosion resistance are considered in details. With the proper amount, up to 1% silica fume, not only the intermediate temperature strength has been improved, but the corrosion resistance has not been affected in comparison with a castable without SiO_2 addition.

The contrast of corrosion resistance between optimized MgO-Al_2O_3 castable and commercial Al_2O_3-MA castable is also given in Chapter 6. The erosion resistance of MgO-Al_2O_3 castable in ferritic basic slag is much higher than that of Al_2O_3-MA castable.

The microstructural characteristics of corroded MgO-Al_2O_3 castable have been analyzed through OPM, SEM, EDS and X-Ray diffraction. Three different layers, a slag layer, a penetrated layer and an unattacked layer are distinguishable in the castable. Due to FeO, CaO, SiO_2 penetration, the penetrated layer appears successively as a colored dense, a colored porous and an uncolored dense sub-layers. The microstructural analyses showed that both MgO and MA capture FeO from slag to form solid solutions. Needle crystals of C_2S are abundantly distributed in the slag layer, while the low melting phases in the system CaO-MgO-SiO_2-(Fe_xO-MnO-TiO_2) and $(Mg, Fe)_xO$, $(Mg, Fe)(Fe,Al)_2O_4$ do appear in the penetration layer. The mixed MgO (with solid solutions), primary spinel (with solid solutions) and a great amount of precipitated angular secondary spinel formed the colored dense layer, and this dense layer do protect the further penetration from slag.

The purpose of this work which was to contribute to the development of suitable basic castable, to be used in ladle steelmaking applications at the slag line zone, has not

been met. This thesis has nevertheless revealed the intrinsic limitations of the magnesia based castables, which are plagued by their poor resistance to penetration to slags containing iron oxide and hence their poor structural spalling resistance. The only foreseen solution will be the development of basic castables containing carbons.

The objectives that have been met are: the development of cement-free, spinel-bonded, magnesia based castables, having resolved the following issues: the flowability and setting minimizing, the water demand, the volume stability and the mechanical properties after firing as well as erosion resistance.

CONDENSÉ

Cette thèse a pour titre « L'optimisation de la composition de bétons magnésiens, sans ciment, à liaison spinelle ». Elle a été amorcée en septembre 1995, dans le but ultime de contribuer au développement de bétons adéquats pour le garnissage des parois de travail des poches de coulée d'aciers, en sidérurgie. Ces bétons devaient répondre aux exigences d'utilisation dans la zone dite ligne de laitier, c'est-à-dire qu'ils devaient avoir avant tout une excellente résistance à la corrosion des scories basiques, donc une excellente réfractairité à 1600°C, aussi une bonne résistance à l'écaillage et aux chocs thermiques.

Ce développement faisait partie des priorités des partenaires industriels associés au financement de la Chaire des Matériaux Réfractaires du Conseil de Recherche en Sciences Naturelles et en Génie du Canada (CRSNG) et constituait un des éléments d'un projet plus vaste sur l'étude des bétons dans le système MgO-Al_2O_3-SiO_2. Ce travail porte sur le pôle magnésie, ces bétons devant contenir a priori 70% de MgO, par opposition aux bétons dits « basiques » présentement connus, mais centrés sur le pôle alumine avec au plus 10 à 12% de magnésie. Pour préserver la réfractairité, il fut décidé de travailler avec des liaisons spinelles, donc avec ajout d'alumine et/ou de spinelle ($MgAl_2O_4$), et par conséquent de privilégier dès le départ des bétons, sans ciment, les liens hydrauliques à température ambiante et à basses températures étant assurés par l'ajout d'alumine hydratable, dite alumine-ρ. Il était en effet reconnu dès le départ que

tout ajout de chaux (CaO) dans ce système conduirait infailliblement à la formation de composés binaires et ternaires à bas point de fusion, surtout en présence de silice.

La thèse a donc porté sur une classe de béton n'ayant aucun équivalent commercial au départ. Il s'agissait d'entamer un travail original, pour surmonter les deux difficultés prévisibles suivantes : l'hydratation poussée de la magnésie et la perte de cohésion des bétons entre 800°C et 1000°C et ensuite de mesurer l'avantage des compositions riches en magnésie par rapport aux compositions riches en alumine, en ce qui a trait à la résistance à la corrosion par des scories basiques d'aciérage.

Dans une thèse précédente élaborée au sein de la Chaire des Matériaux Réfractaires, Ning Wang (88) « Spinel Bonded Magnesia Based Castables with Hydratable Alumina as Binder », Ph.D. 1996, avait démontré qu'il était possible d'élaborer des bétons à partir de magnésie et d'alumine pure, mais que l'expansion thermique résultant de la formation *in situ* de spinelle selon la réaction $MgO+Al_2O_3 \rightarrow MgAl_2O_4$, devait être contrôlée, ce qui limitait les quantités respectives des particules fines, par ailleurs requises. Il fut décidé de contrer ce problème en partant avec des compositions comprenant, en plus de la magnésie et de l'alumine, du spinelle synthétique, c'est-à-dire des agrégats de $MgAl_2O_4$ pré-synthétisés.

Le travail expérimental a donc porté, i) sur l'étude détaillée de la stabilité dimensionnelle des mélanges de magnésie, alumine et spinelle avec ou sans addition de microsilice (de 0 à 2% poids), ii) sur l'étude systématique de la coulabilité de bétons comprenant ces trois agrégats principaux (MgO, Al_2O_3 et $MgAl_2O_4$) en fonction de la nature et de la quantité de différents additifs dispersants, iii) sur la détermination des

propriétés physiques, mécaniques et chimiques de ces bétons. Ces trois aspects sont traités aux chapitres 3, 4, 5 et 6 de la thèse. En guise d'introduction, au chapitre 1, sont repris les buts et objectifs déjà énoncés et le contexte général déjà évoqué, à partir desquels la thèse a été menée. Le chapitre 2 sert à décrire brièvement l'état des connaissances sur les bétons utilisés en sidérurgie, et l'évolution de la technologie depuis 1960. Il en découle, en condensé, que de nos jours, certains utilisent des bétons riches en alumine avec addition de spinelle et d'autres avec addition de magnésie et de spinelle dans les fonds et le bas des parois des poches, mais que ces matériaux sont inadéquats pour garnir les lignes de laitier. En fait on doit recourir là à des briques de magnésie-carbone ce qui empêche de promouvoir la solution des poches entièrement en béton. Ceci est reconnu comme un désavantage majeur.

L'étude de la stabilité dimensionnelle des mélanges de magnésie et d'alumine a été conduite en établissant les courbes de dilatométrie de deux types distincts de mélanges ; l'un constitué de MgO, d'alumine et de spinelle synthétique, l'autre avec en plus addition de fumée de silice.

Dans la première catégorie de mélanges, 35 compositions avec diverses proportions (0,5 et 10%) de spinelle riche en alumine (AR_{90}), de spinelle riche en magnésie (MR_{66}) et de spinelle stœchiométrique (AR_{78}) ont été évaluées. Il a été établi que la formation de spinelle s'amorce à 1100°C. Jusqu'à cette température, la dilatation réversible des mélanges est contrôlée par la dilatation de la magnésie. De 1100°C à 1600°C, l'expansion puis la contraction due au frittage des particules sont contrôlées par trois phénomènes concurrents : la dilatation continue des particules, la réaction de

formation de spinelle qui s'accompagne d'une forte augmentation de volume et le frittage des particules qui impose un rétrécissement important. Suite à des mesures semi-quantitatives de diffraction-X pour déterminer la quantité de spinelle *in situ* formée pour chaque composition, il a été possible de corréler les effets d'expansion-frittage aux quantités respectives de magnésie (M), alumine (A) et spinelle synthétique (MA) utilisées et de différencier le rôle des trois types de spinelle synthétique utilisés (AR_{90}, MR_{66}, AR_{78}). Il a été principalement démontré qu'il était possible de limiter les effets néfastes dus à l'augmentation volumique *in situ*, en ajustant les proportions de M, A et MA. Il a été aussi vérifié que dans les cas étudiés, la spinelle *in situ* formée était de type quasi-stœchiométrique. Suite à cette étude centrale, pour la poursuite des travaux, il a été possible de prévoir la mise au point de bétons magnésiens avec des limites de variations dimensionnelles, lors de leur mise en œuvre, de l'ordre de 1% ou moins.

Dans la deuxième catégorie d'essais dilatométriques, l'influence de faibles quantités de fumée de silice (entre 0 et 3%) a été précisée sur des mélanges contenant 5% ou 10% de spinelle AR_{78}. Il a été ainsi vérifié de nouveau que cette addition ne perturbe pas les limites de variations dimensionnelles escomptées. Lors de tous ces essais, les effets au refroidissement ont aussi été enregistrés. Il a été possible de mettre en évidence une température (dite TG dans la thèse, pour Température Gap) où il y a systématiquement apparition de micro fissures entre les grains de magnésie et de spinelle formés *in situ*, due à la différence intrinsèque des coefficients d'expansion thermique des deux oxydes.

Cette étude détaillée de la stabilité dimensionnelle des mélanges de magnésie et d'alumine a donc complété de façon définitive les travaux de mon collègue Ning Wang (88) déjà cités, tout en confirmant les travaux récents de Z. Nakagaura (14, 17).

Quant aux essais de coulabilité ils ont été conduits pour déterminer le type et la quantité de défloculants à base de lignosulphonate, de sulfite, de phosphate et de sels organiques, à des niveaux de 0.1, 0.5, 1.0, 5.0 et 10.0% poids ont été utilisés. Une méthode originale dite d'extraction de la matrice du béton est considérée séparément. On mesure alors un temps d'écoulement d'une quantité fixe de barbotine avec défloculant d'un entonnoir que l'on fait vibrer. Il a été démontré dans cette thèse que ces mesures de temps d'écoulement correspondent aux mesures de coulabilité sur les mélanges de béton eux-mêmes, la corrélation obtenue entre les deux mesures étant statistiquement valable cette procédure expérimentale s'est avérée fiable et a permis d'économiser temps et matériaux. À partir de ces essais de coulabilité, il a donc été possible de fixer les distributions granulométriques des constituants solides des bétons et les quantités minimales d'eau de gâchage sur un ensemble de soixante-quatorze compositions comprenant des additions de trois types de spinelle synthétique : la spinelle AR-90, riche en alumine, la spinelle AR-78, dite stœchiométrique, et la spinelle MR-66, riche en magnésie ; et différents additifs (19) au niveau des fines dont la liste se retrouve au tableau 5.11, en page 112. Les compositions évaluées sont définies aux tableaux 5.1 à 5.10 ; elles comprennent aussi des compositions de magnésie-alumine sans spinelle, une série de 5 compositions, répétées 2 fois pour pouvoir comparer avec des compositions contenant 5 et 10% d'un des 3 spinelles synthétiques considérés.

Les effets dus aux additions de spinelle synthétique et de fumée de silice sur les propriétés physiques et mécaniques des bétons étudiés sont discutés au chapitre 5. Le rapport magnésie/alumine total et les quantités de spinelle synthétique et de silice influencent directement la porosité, la densité et le module de rupture à froid. L'ajout de spinelle est néfaste aux propriétés mécaniques après cuisson à température intermédiaire (1000°C) mais permet une amélioration des valeurs de module de rupture à chaud. L'ajout de fumée de silice permet d'améliorer les propriétés mécaniques après cuisson à température intermédiaire mais il est nuisible aux valeurs de module de rupture à chaud. Dès lors, une proportion adéquate des deux ajouts est requise.

La mesure de la résistance à la corrosion des bétons vis-à-vis d'une scorie basique ferritique (C/S=2.2 ; Fe2O3=29%) a été effectuée en suivant la norme ASTM C-874, à l'aide d'un four rotatif. L'effet de la nature du grain de spinelle utilisé a été étudiée au niveau de 5%. Les résultats expérimentaux démontrent que la résistance à la dissolution est améliorée lorsqu'on utilise le spinelle AR_{78} ; l'ajout de MR_{66} est le plus bénéfique pour la résistance à la pénétration ; l'utilisation de AR_{90} n'est pas recommandable (en rapport avec les AR_{78} et MR_{66}) dans les bétons $MgO-Al_2O_3$ étudiés.

Les effets dus à l'addition de silice sur la résistance à la corrosion ont été considérés en détail. La proportion la mieux appropriée se situe au niveau de 1% tant pour la résistance à la corrosion que pour l'amélioration des propriétés mécaniques, après cuisson, à température intermédiaire. Avec plus de 1% de silice, les propriétés de corrosion décroissent.

Le contraste entre la résistance à la corrosion de bétons, bien optimisés, de MgO-Al_2O_3 par rapport à un béton commercial du type Al_2O_3-MgO est aussi mis en évidence, dans le chapitre 6. La résistance à la dissolution (érosion) des bétons de MgO-Al_2O_3 est, comme escomptée, nettement supérieure.

La caractérisation microstructurale des bétons de MgO-Al_2O_3, avant et après corrosion, a été effectuée à l'aide de la microscopie optique et électronique à balayage (MEB), avec analyses spectrales et aussi à l'aide d'un diffractomètre à rayons-X. Trois épaisseurs ont été clairement identifiées sur les échantillons corrodés. La couche de scorie résiduelle en face chaude, la zone pénétrée et la zone non-attaquée. La zone pénétrée doit être divisée en deux sous-couches, l'une colorée plus poreuse, l'autre plus dense et non colorée. La zone colorée résulte de la pénétration du fer, sous forme d'oxyde de fer dans les grains de magnésie et de spinelle, où le FeO se retrouve sous forme de solution solide. Dans la zone incolore, des phases de CMS et C_3MS_2 ont été identifiées, témoignant ainsi de la pénétration du CaO et SiO_2 de la scorie. À l'orée entre la zone colorée et la zone incolore, là où il y a densification, une proportion accrue de spinelle, dite secondaire, sous forme aciculaire, a été détectée ; cette zone densifiée permettrait de minimiser l'importance de la pénétration de la scorie.

Au total, cette thèse a permis de révéler les limitations intrinsèques des bétons à base de magnésie, qui s'avèrent limités par leur faible résistance à la pénétration par les scories contenant de l'oxyde de fer et par voie de conséquence à leur mauvaise résistance à l'écaillage structural. La seule solution pour les bétons magnésiens semble être de développer dorénavant des bétons contenant du carbone et du graphite. Cette

solution est attrayante parce que d'une part il a été prouvé que les bétons magnésiens développés dans cette thèse possèdent une excellente résistance à la corrosion-dissolution par les scories d'aciérage et que d'autre part la solution magnésie-graphite sous forme de brique, offre des performances imbattables à date.

TABLE OF CONTENTS

LIST OF TABLES

LIST OF FIGURES

CHAPTER 1 INTRODUCTION

Looking back on the last three decades, refractory linings used in steel ladles, were all installed with bricks. However, in the last ten years, steelmakers have sparked off a completely new approach, to construct steel ladle lining using monolithics.

Monolithic lings have distinct advantages as compared with conventional brick linings, such as short manufacturing cycle; energy and materials saving; flexibility for complex structure shaping; local repairs possible and minimized joints available. Nowadays, some monolithic refractories are considered having superior performances in terms of resistance to high temperature erosion, penetration and structural degradation [1,2,3,4,5].

Focusing still on steel ladle linings, Al_2O_3-MA castables are of the most successful type used in steel ladles [6,7,8,9]. Nevertheless, this kind of castable is satisfactory only in barrel and bottom zones. An adequate castable for slag line, that is able to replace, performance-wise, magnesia-carbon bricks in order to achieve full monolithic lining is still being expected. To tackle this critical issue, the optimization of a magnesia based basic castable has been undertaken.

A rational solution for a castable to be used in slag zone is to develop a truly basic castable in order to resist to highly basic slags [7]. Magnesia based castable is a prospective candidate because of its high refractoriness in contact with basic slag. However, the first question coming to the mind is how to produce a water added magnesia based castable with very fine magnesia particles, which would not hydrate.

One solution to overcome this challenge is to use magnesia aggregates with mostly alumina fine particles in the matrix. The alumina fine grains added into matrix not only avoid the hydration of MgO fine particles, but also create in-situ spinel ceramic bonding at high temperatures due to the reaction of MgO and Al_2O_3 [7,8]. Additionally, the in-situ formed spinel, $MgAl_2O_4$, is also a stable material, like MgO or Al_2O_3, with high refractoriness, hence beneficial for the castable to present high performance at high temperatures.

However, the question now still waiting to be answered is: what kind of binders should be used? As we know, high alumina calcium aluminate cement is not appropriate, since in MgO-Al_2O_3-CaO system, liquid formation could start around 1300°C. Hydratable alumina [10,11] as a binder, which has been used in cement-free alumina based castables recently [12,13], could be considered, because using hydratable alumina can avoid the formation of calcium aluminosilicate and should provide superior mechanical properties at high temperatures. Nevertheless, a major drawback of this binder is the lost of strength at intermediate temperature, which will significantly affect the thermal spalling resistance of such castable. The next question, how to increase castable's intermediate temperature strength when using hydratable alumina as a binder, becomes another critical issue.

Spinel formation, as a result of the reaction between MgO and Al_2O_3 fine powders, could result in a volume expansion of 8% or 2.6% in linear expansion, if simply based on the theoretical calculation from density differences [14], but practically, linear expansion of more than 5% is frequently observed [15,16]. Such large expansion is

unacceptable. Hence, how to control the volume stability of $MgO-Al_2O_3$ castable will be another question to be considered.

Moreover, to improve the properties of material, we do need to understand the corrosion mechanism of $MgO-Al_2O_3$ castable. Is it possible to find a way to enhance slag erosion and penetration resistance for $MgO-Al_2O_3$ castable? Actually, it has been shown in Al_2O_3-MA castable, that Al_2O_3-rich spinel, with plenty of lattice defects, has a stronger capability to capture FeO from slag and is efficient to suppress slag penetration [17]. Will MgO-rich spinel added into magnesia based $MgO-Al_2O_3$ castable have an equivalent effect?

The general purpose of this study is to develop a magnesia based $MgO-Al_2O_3$ castable for steel ladle slag line on the basis of the above discussion. In the present work, highly amorphous hydratable alumina has been adopted as hydraulic binder. This cement free castable system is to contain up to 75% of sintered magnesia. To adjust the composition and to obtain good ceramic-bonds, ultrafine alumina additions is used. The flowability issue of such $MgO-Al_2O_3$ castables in order to optimize physical and mechanical properties is considered in Chapter 3. An "extracting-matrix" method to investigate the effects of five different deflocculants at five different level addition is described and the most appropriate deflocculant is selected. In Chapter 4, volume stability issue is addressed. Typical thermal expansion characteristics are shown using phenomenological and a mathematical model. The influences of three different grades and additions of pre-reacted spinel, alumina-rich spinel AR_{90}, magnesia-rich spinel MR_{66} and close to stoichiometric spinel AR_{78}, on thermal expansion behaviors are

discussed in details. Effects of SiO_2 fume additions on thermal expansion behavior from room temperature to 1600°C is also documented. On the other hand, the shrinkage behavior during cooling and repeated heating and cooling cycles are also discussed. In Chapter 5, physical and mechanical properties such as bulk density, porosity, permanent linear change, cold and hot modulus of rupture are represented as a function of MgO/Al_2O_3 ratio in the matrix and the amount of pre-reacted spinel addition used. Those properties are also considered in case of both pre-reacted spinel and SiO_2 fume added together. Special attention has been paid to the intermediate temperature strength of $MgO-Al_2O_3$ castable. To find an appropriate additive to improve the cold modulus of rupture at 1000°C, a number of tests have been carried out. The last Chapter 6 is focusing on the analysis of the corrosion mechanisms of $MgO-Al_2O_3$ castables. The corrosion behavior of castables with different grades, amounts of pre-reacted spinel and SiO_2 fume is discussed in details in conjunction with SEM, OPM and X-ray etc.

Through this investigation, the approach to control volume stability of the $MgO-Al_2O_3$ castables is revealed. One of the effective methods is to add appropriate pre-reacted spinel into the mixes. Adding SiO_2 fume can't control the expansion, but does improve the intermediate temperature strength. Using a proper deflocculant, it is possible to obtain $MgO-Al_2O_3$ castables with good flowability and better physical and mechanical properties. With magnesia-rich pre-reacted spinel MR_{66} added, the penetration resistance of $MgO-Al_2O_3$ castable can be improved. Additionally, the erosion resistance is enhanced with a certain amount of AR_{78} and SiO_2 fume addition.

From the corrosion point of view, alumina-rich pre-reacted spinel AR_{90} is not suitable for such MgO-Al_2O_3 castables.

In this work, the following raw materials will be used: i) The dead-burned seawater MgO (the specific density of 3.58 g/cm^3) has been selected as both aggregates (denoted as MG afterward 3-170 mesh) and fine grains (BMF, -170 mesh). Some fused magnesia (-48 mesh) has also been used. The chemical compositions of those materials are shown in Table 1.1, and Figure 1.1 gives the size distribution of fine magnesia powder BMF.

Table 1.1 The Chemical Composition of Magnesia Raw Materials

	MgO	Al_2O_3	CaO	SiO_2	Fe_2O_3	K_2O	Na_2O	TiO_2	LOI
Sintered MgO (MG)	97.6	0.13	1.04	0.15	0.17	0.01	0.18	0.01	1.10
Ball Milled MgO (BMF)	98.2	0.33	0.68	0.10	0.36	0.01	0.10	0.01	0.15

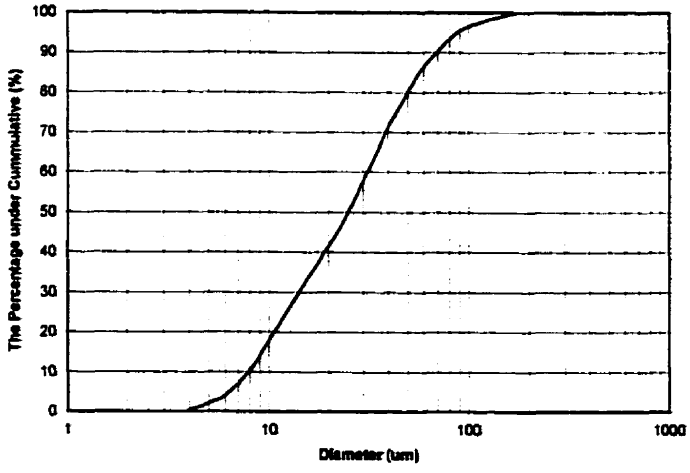

Figure 1.1 The Size Distribution of Fine Magnesia Powders

(Sedigraph 5100, FOLIO Instruments Inc.)

ii) Four kinds of alumina, which are tabular alumina, fine and ultrafine ground alumina as well as hydratable alumina, have also been used.

(a) Tabular alumina is defined as sintered aluminas having a median α-Al_2O_3 crystal size which averages 50μm and greater, with the occurrence of large flat tablet-like α-Al_2O_3 crystals. Because of the grain-boundary porosity entrapped during rapid sintering, tabular alumina has a particle bulk density, in the range 3.40 to 3.65 g/cm^3, with characteristic closed spherical porosity and typical of a fully sintered ceramic with secondary really crystallization[1]. Those <1 to >10 μm closed spherical pores which apparently act as crack arresters contribute their excellent thermal shock resistance. Tabular alumina T64 , -325 mesh with the specific density of 3.99 g/cm^3, was used in this research work. The chemical composition of T64 is given in Table 1.2.

(b) The Bayer process alumina trihydrate by calcining in rotary kilns produces Alcan fine ground aluminas (FGA). During calcination, the combined water is driven off and the oxides formed pass through several intermediate phases until the stable alpha-alumina structure is reached. As the exist of the transformation between trihydrate and α-Al_2O_3, the resulting α-Al_2O_3 is a porous aggregation of monocrystal platelets (Figure 1.2). The porous structure within the aggregate makes the alumina easily grind into its component crystals (Figure 1.3). The specific density of FGA used in the test is 3.98g/cm^3, however, the bulk density is only 1.1g/cm^3.

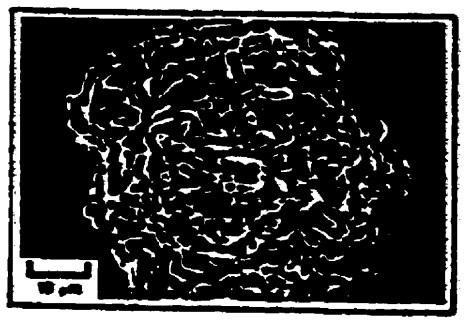

Figure 1.2 Scanning Micrograph of a Porous Aggregate of Monocrystal Platelet

Figure 1.3 FGA after Ground

(c) Ultrafine Ground Alumina (UGA) is a new, highly reactive alumina at Alcan alumina family. They were ground in dry ball mill and near ultimate crystals with their high sinterability was reached. The specific density of UGA in this work is 3.98 g/cm^3.

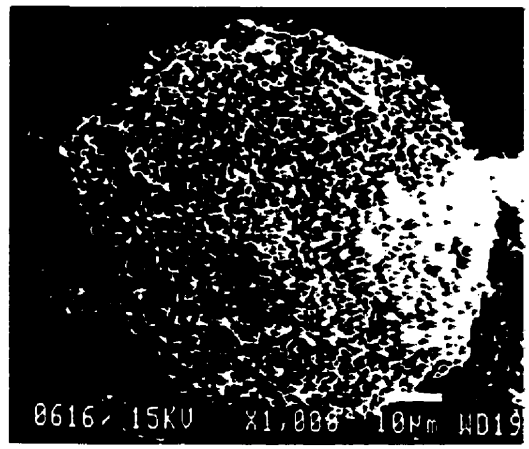

Figure 1.4 A single particle of UGA

The chemical compositions and size distributions of FGA and UGA powders are given in Figure 1.5 and Table 1.2 respectively.

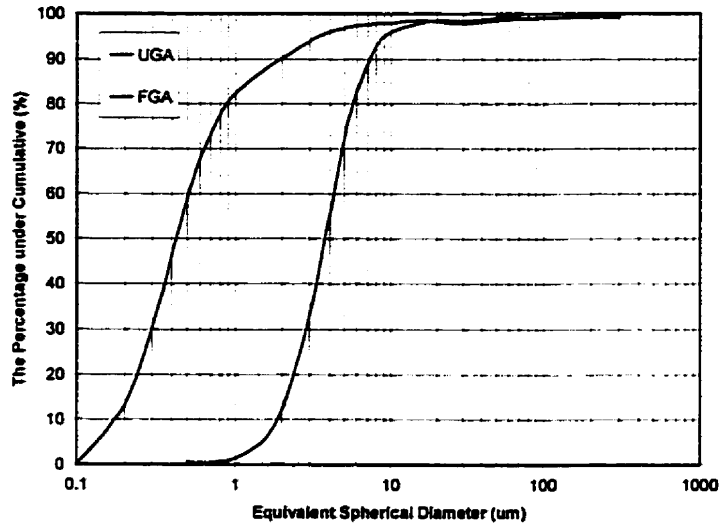

Figure 1.5 The Size Distributions of FGA and UGA Powders

(Sedigraph 5100, Folio Instruments Inc.)

(d) Hydratable alumina is an activated alumina powder which is produced from aluminum hydroxides by controlled heating to eliminate most of the water of constitution. The crystal phases are predominant chi phase and small amount of other phases [10]. In a refractory mix, hydratable alumina can react with water to form a hydraulic bond. Since hydratable alumina is composed of more than 95% Al_2O_3 and less than 0.05% calcium oxide, comparing to the traditional calcium aluminate cements with 15% of CaO at least, a higher refractoriness and good corrosion resistance are

expected. The size and distributions, TGA curves and chemical composition of hydratable alumina used in tests are given in Figures 1.6, 1.7 and Table 1.2 separately.

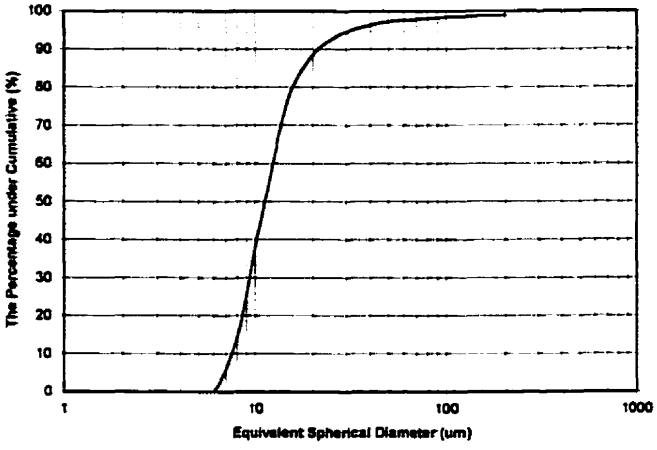

Figure 1.6 The Size Distribution of Hydratable Alumina (Sedigraph 5100, FOLIO Instruments Inc.)

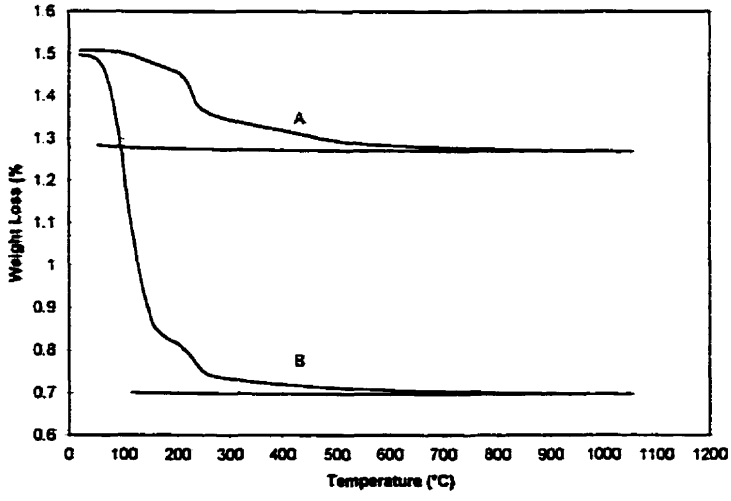

Figure 1.7 The TGA Curves of Hydratable Alumina

A: Hydratable Alumina after Dried at 110°C×24hrs. B: As-received Hydratable Alumina

Table 1.2 The Chemical Compositions of Alumina TA, FGA and UGA

	Al_2O_3	Na_2O	Fe_2O_3	SiO_2	MgO	CaO	LOI
TA	99.7	0.16	0.06	0.04	0.001	0.04	
FGA	99.8	0.18	0.03	0.03			
UGA	99.8	0.05	0.03	0.002	0.05	0.01	
HA	95.5	0.4	0.02	0.02		0.03	4.0

iii). Magnesium aluminate spinel, as one of important raw materials used in tests, belongs to the family of mixed oxide spinels with cubic structures. It is considered as one of high performance refractory materials due to its superior physical and chemical properties.

Magnesium aluminate spinel can be produced by sintering or fusing method. The stochiometric spinel is composed of 72wt% Al_2O_3 and 28wt%MgO. Both magnesia rich and alumina rich spinel are available by varying mixture compositions and processing conditions.

The typical chemical compositions of alumina-rich pre-reacted spinel AR_{90}, close to stoichiometric spinel AR_{78} and magnesia-rich spinel MR_{66} which have been used are shown in Table 1.3. The X-ray diffraction, the size distributions of those three kinds of spinels are given in Figure 1.8 and 1.9 respectively.

Table 1.3 The Chemical Compositions of Spinel AR_{90}, AR_{78} and MR_{66}

	Al_2O_3	Na_2O	Fe_2O_3	SiO_2	MgO	CaO
AR_{90}	90	0.17	0.1	0.05	9.0	0.25
AR_{78}	76.0	0.15	0.1	0.06	23.0	0.3
MR_{66}	66.0	0.05	0.1	0.09	33.0	0.4

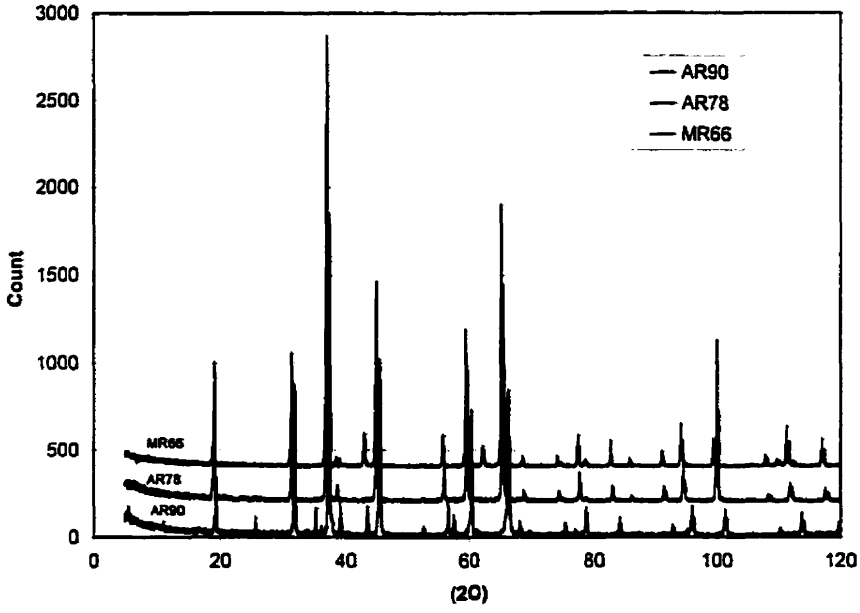

Figure 1.8 The X-ray Diffractions of Spinel Powder AR_{90}, AR_{78} and MR_{66}

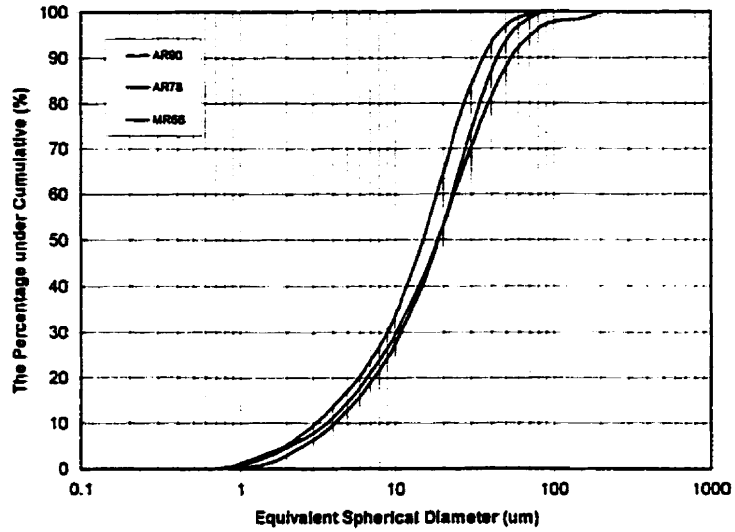

Figure 1.9 The Size Distributions of Pre-reacted Spinel AR_{90}, AR_{78} and MR_{66}

CHAPTER 2 MAGNESIA, ALUMINA, SPINEL CASTABLES FOR STEELMAKING APPLICATIONS

2.1 Introduction

Like the wheel, monolithic refractories are cautiously being reinvented. Archeological evidence shows that as long ago as 6000 B.C., vitrified clay hearths were used in Asia [18]. This may be considered as the first application of monolithic refractories, then around 1850s, Saint-Claire Deville [19], in France, contributed to this technology with his great "discovery" --- calcium aluminate as a refractory concrete. He heated the mixtures of alumina and lime, mixed the reaction products with alumina aggregates and water to produce crucible for successful usage at high temperatures. This practice established the basis of modern monolithic refractories.

In this century , no exact date can be assigned to the beginning of modern monolithic refractories. However, during the last three decades, a considerable technical evolution in monolithic refractories has led to significant improvements in high temperature resistance, mechanical resistance and corrosion resistance of these materials [20,21,22,23].

Back to the 1960s, castables were only simple mixtures of fine grains, cements and aggregates [24]. The fines and cement particles (10-100μm) where added in enough quantity, to serve both as filling media and binder at room temperature, however, the high content of CaO and sometimes Fe_2O_3 in such castables had detrimental effects on corrosion resistance and hot strength.

In the '70s, with the availability of higher quality synthetic aggregates and higher alumina content cement, castable performances were really improved [25,26]. Since the '80s, the cement content in the castable has been systematically reduced to 8 - 3% [27,28], at the same time, calcium aluminate cements with 80% Al_2O_3 have become readily available, and more cement fraction has been replaced by SiO_2 [29], Al_2O_3 or ZrO_2, as ultrafine particles (0.5 - 5μm) [30,31,32,33,34], so as to reduce water addition from previous 15-8% to 8-4%. Nowadays, it is possible to produce low-cement, ultra-low and even no cement castables with remarkable properties for refractory castables[35,36,37].

Focusing on steel ladle linings, in order to adjust 1) to the changes in steelmaking processing; 2) to the requirements for improving steel quality; 3) to the reduction of labor costs and to overcome the environmental and safety aspects related to bricklaying, use of monolithic linings instead of bricks has emerged in many countries over the last thirty years.

At the beginning, monolithic castables were cast in side walls only, and gradually spread to be used in bottoms, eventually in slag lines. In Japan, monolithic steel ladle linings actually have become a reality, those ladles are also maintained and repaired using gunning materials [26,38].

The development of castables in steel ladles still present many challenges. In the earlier years, the '70s, high SiO_2 and zircon containing castables were adopted because of their availability and low price. However, with the requirements of low silica or silica-free refractories to improve steel quality, those raw materials had to be changed. In

the mid '80s, starting in Japan, a new type of Al_2O_3-MA castable containing synthetic spinel powders in matrix portion, was successfully put into practice in side wall of steel ladles [39,40,41]. Those Al_2O_3-MA castables dramatically increased the service life of steel ladle lining as compared with the previous zircon, or zircon–silicate castables. It is now an accepted class of castable, for steel ladle lining, in the world. Very interestingly, adding MgO powders into Al_2O_3-MA castables instead of pre-synthetic spinel fine grains has been used to obtain superior performances [42,43,44]. Finally, in the mid '90s, in parallel with Al_2O_3-MA castable developments, some results on MgO-Al_2O_3 and MgO-C castables [43,45] have also been reported as prospective materials to replace MgO-C bricks at slag line.

2.2 MgO-Al_2O_3 System

2.2.1 MgO, Al_2O_3 and Solid Solutions

MgO and Al_2O_3, with melting points at 2800°C and 2050°C respectively, are to be perfect refractory raw materials. The compound, $MgAl_2O_4$ spinel, still possesses a high melting point at 2109°C, especially, with a wide range of solid solution [46] as shown in Figure 2.1.

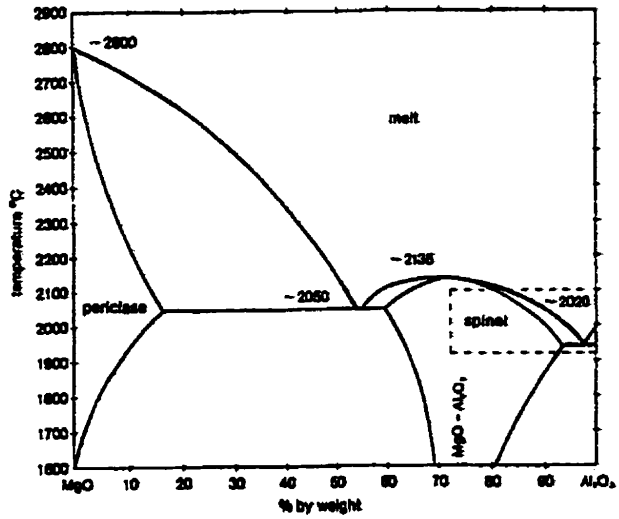

Figure 2.1 $MgO-Al_2O_3$ System Phase Diagram [46]

$MgO-Al_2O_3$ phase diagram was first reported by Rankin and Merwin [47]. They described no spinel stability beyond stoichiometry. Della M. Roy et al. [48] have remedied this mistake and reported that the solid solution was observed in Al_2O_3-$MgAl_2O_4$ subsystem. They examined the samples under petrographic microscope and determined the X-ray diffraction patterns. A homogeneous isotropic spinel solid solution was observed from 50 to 85 mol% Al_2O_3. The unit cell dimension of the spinel solid solution is shown in Figure 2.2 as a function of composition. The lattice dimensions decrease from 0.806 nm for stoichiometric $MgO:Al_2O_3$ to 0.793 nm for $12MgO:88Al_2O_3$. The maximum solid solution is at 86 mol % (approximately 94 wt%) Al_2O_3.

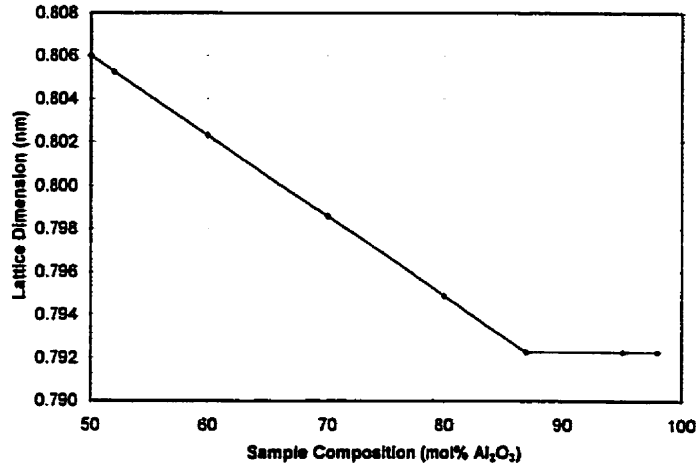

Figure 2.2 Lattice Constant of Spinel Solid Solutions as a Function of Composition [48]

However, the lattice constants for spinel solid solution shown in Table 2.1, calculated by Nakagawa [14], differ a little from the previous ones.

Table 2.1 The Lattice Constants of Different Molar Ratio Of Spinel Solid Solutions [14]

Chemical Composition	Lattice Constant (nm)	Density (g/cm^3)	Molar Ratio
$MgO \bullet Al_2O_3$	0.8083	3.579	1.000
$MgO \bullet 2Al_2O_3$	0.8010	3.607	1.008
$MgO \bullet 3Al_2O_3$	0.7978	3.623	1.012
$MgO \bullet 4Al_2O_3$	0.7962	3.630	1.014

D. Viechnicki et al [49] also presented X-ray diffraction results which indicated that the limit of solubility of α-Al_2O_3 in spinel solid solutions was around 85 mol% Al_2O_3 at the eutectic temperature. Later, Kouhei Shirasuka et al. further confirmed this conclusion.

In 1962, A.M.Alper et al. [50] conducted the determinations of liquidus, solidus and subsolidus of the system MgO-$MgAl_2O_4$ as well as the solid solution limits of Al^{3+} ions in periclase and Mg^{2+} ions in spinel. They [50] found that the periclase solid solution may contain a maximum of 18wt% Al_2O_3 and the spinel solid solution may contain as low as 61 wt% Al_2O_3. Above 1500°C, periclase and spinel solid solutions were in easily detectable amounts. However, contrary to Alper [50], A.M.Lejus et al. [51,52] by X-ray diffractometry and optical techniques indicated that MgO is nearly insoluble in $MgAl_2O_4$.

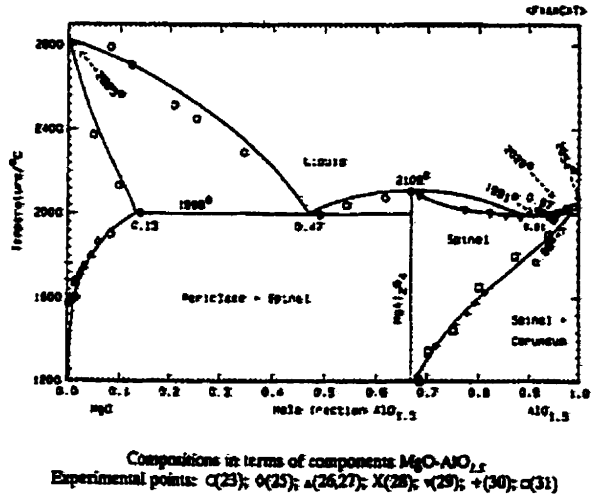

Figure 2.3. Optimized MgO-Al_2O_3 Phase Diagram By G. Eriksson et al. [53]

In 1993, G. Eriksson, P. Wu and A. Pelton [53] calculated the $MgO-Al_2O_3$ phase equilibria system, their results supporting the conclusion from A.M.Lejus. Figure 2.3 shows the optimized $MgO-Al_2O_3$ phase diagram [53].

2.2.2 Reactivity of MgO and Al_2O_3

MgO and Al_2O_3 start reacting to form $MgAl_2O_4$ at around 1100°C [54], but it can be formed even at lower temperatures if MgO and/or Al_2O_3 active powders are used. R. Russell [55] has reported initial temperatures of spinel formation to be in between 925 °C and 950 °C, with alumina and magnesia powders having an average particle sizes of 1.6 and 2.5 μm respectively.

Wagner et al. [56,57,58,59] studied the solid state reaction between MgO and Al_2O_3. He reported that the reaction proceeds by counter diffusion of the cation Mg^{+2} and Al^{+3} through the product layer $MgAl_2O_4$. To keep the electroneutrality, $3Mg^{2+}$ diffuse towards the alumina side and $2Al^{3+}$ diffuse towards the magnesia side. At the MgO/Spinel boundary, $2Al^{3+}$ react with MgO to form $MgAl_2O_4$ while $3Mg^{2+}$ react with $3Al_2O_3$ to form $3MgAl_2O_4$ at the Al_2O_3/Spinel boundary [56,60,61]. As a consequence, the spinel thickness ratio formed at alumina side and magnesia side is 3:1 as shown in Figure 2.4.

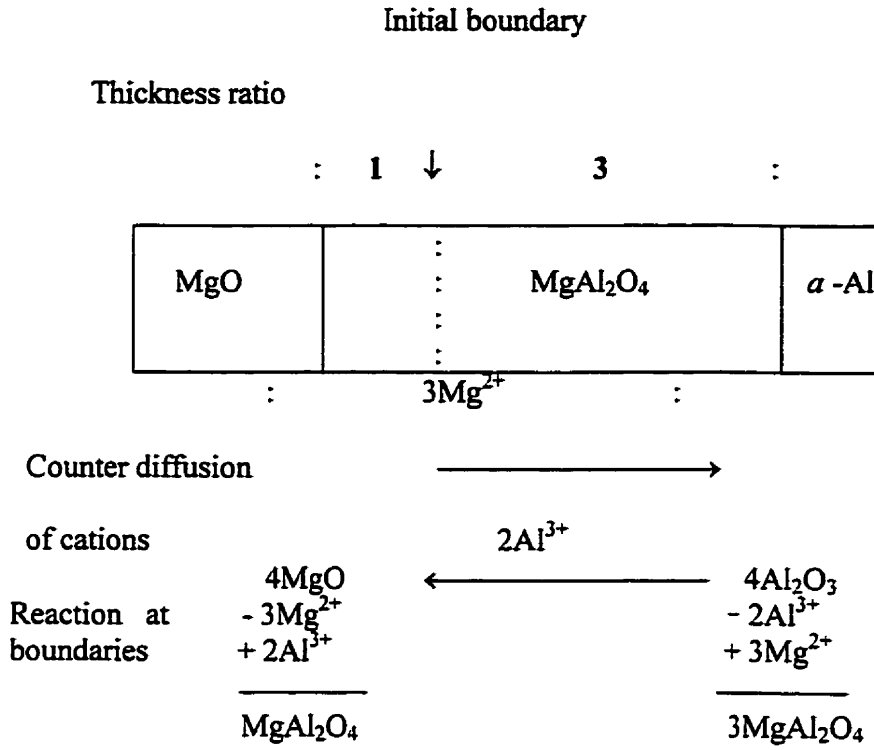

Figure 2.4 Wagner's Representation of $MgAl_2O_4$ Formation [56]

According to Wagner, the thickness ratio R is 3. However, two factors may increase R value at high temperatures: one is the solid solubility of alumina in spinel and the other is the transportation of MgO vapor [62]. In the case of alumina solid solution, the R value for the composition of $MgO.nAl_2O_3$ was formulated as $R = \frac{3(7n+1)}{3n+5}$ [63]. Yamaguchi et al. [64] reported values of R is between 4.1 to 4.6 at temperature range 1495 – 1595°C, and those R values were independent of whether single- or poly-crystalline materials were used.

For MgO vapor transportation, Nakagawa [16] calculated the saturated vapor pressure of MgO gas coexisting with periclase and spinel as 2.5×10^{-5} Pa and 6.2×10^{-7} Pa at 1527°C respectively. Those data imply that MgO molecules could be vaporized from periclase and sunk onto corundum to form spinel. Obviously, it results in an increase of R value.

Additionally, Nakagawa [16,62,64] also concluded that R increases if the contact surface between magnesia and alumina is rough; the diffusion of MgO vapor occurs through the gap and spinel forms at alumina side only. Actually, G. Yamaguchi [65] has reported that R could reach 5.6 at 1535°C based on the rough contact model for a diffusion couple. Also, if MgO is transported to alumina side, only in one direction, R could become infinite.

The variation of R is an important characteristic in MgO and Al_2O_3 reactivity, meanwhile, another significant characteristic could be the volumetric reaction expansion.

It was accepted that $MgAl_2O_4$ formation from mixture of MgO and Al_2O_3 may result in a linear expansion of 2.6% [14] through theoretical calculation and in practical up to 5% [15,16] as reported in the previous chapter. The expansion values are actually a function of temperature, particle size, particle configurations and chemical compositions of the raw materials.

As temperature increases, the expansion of MgO and Al_2O_3 mixture increases up to a maximum value. A "Mountain Peak" outline normally represents the expansion

characteristic. Of course, the shrinkage, after maximum thermal expansion, will significantly depend on the reaction extent and sinterability of mixture [15,66].

The influence of particle sizes on expansion of stoichiometric spinel formation was discussed by Nakagawa et al. [67]. As a comparison for a packing model of equimolar mixture of Al_2O_3 and MgO, in case of large Al_2O_3 and small MgO particles, the linear expansion is only slightly larger than the expansion of mixtures with similar particle size MgO and Al_2O_3; however, with large MgO and small Al_2O_3 particles, the expansion value is definitively enhanced.

Particle configuration significantly affects the thermal expansion of MgO, Al_2O_3 mixture, because the configuration is directly related to the number of pairs among $MgO-Al_2O_3$, MgO-MgO and $Al_2O_3-Al_2O_3$. Nakagawa [16,67] et al experimentally confirmed this conclusion. They chose two same specimens, pressed at different pressures, 98 and 350Mpa respectively. After heating from room temperature to 1500°C, it was observed that the maximum thermal expansion of sample with higher forming pressure is twice that of sample with the lower forming pressure.

2.2.3 Spinel Structure

The spinel ($MgAl_2O_4$) is a cubic crystal with eight formula molecules per unit cell [68,69,70]. The oxygen ions form an almost perfect cubic close-packed array with the metal ions distributed among the resulting position of fourfold and sixfold oxygen coordination. The maximum number of possible tetrahedral and octahedral sites is 64 and 32 respectively. The unit cell contains thirty-two oxygen ions in a close-packed fcc

array, giving rise to the formula $A_8B_{16}O_{32}$, i.e. the 32 oxygen ions occupy the 32-fold positions and the cations possess the 8-fold and 16-fold positions. The distribution in $MgAl_2O_4$ is 8 Mg^{2+} ions on tetrahedral sites, and 16 Al^{3+} ions on octahedral sites, therefore, the spinel structure has great potential to form solid solutions because such a close-packed array generates sixty-four tetrahedral and thirty-two octahedral available sites to accommodate only twenty-four cations. Figure 2.5 gives the schematic representation of a spinel structure unit cell.

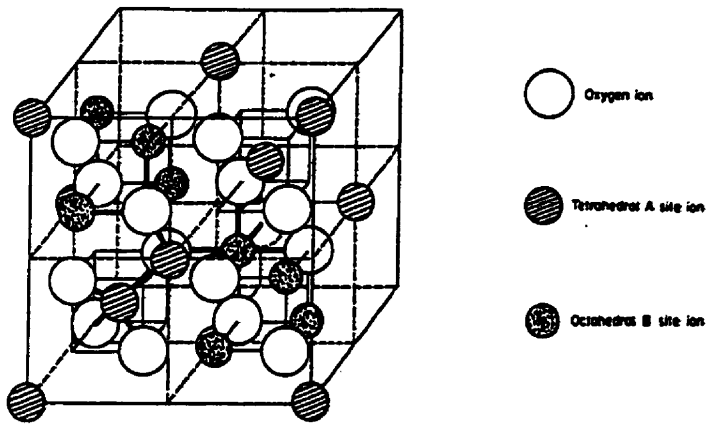

Figure 2.5 Four Quadrants of the Unit Cell of Spinel [70]

2.3 MgO-based Castables

MgO-based castable is expected to be a perspective candidate to be applied in the slag zone of steel ladles to resist basic slags. However, before it can be successfully

used, several technical difficulties have to be overcome. First of all, magnesia must possess sufficient hydration resistance to be mixed with water, put in place and dried without incurring cracking and damaging. Second, the castables have to be designed to avoid slag penetration during service, so to increase its structural spalling resistance. Third, castables must be volume stable. Chromite which has been used [71] in the past to control volume change of MgO is not anymore an acceptable solution because of the inherent environmental problem associated with it.

2.3.1 Hydration Resistance of Magnesia Clinkers

2.3.1.1 Hydration of Magnesia

Hydration may occur not only during mixing, but also during drying [72]. When water vapor is between 150-200°C, magnesia forms $Mg(OH)_2$ and therefore leads to a volume expansion because of the crystalization of brucite and subsequent cracking. The hydration reaction can be described by the following equation [73]:

$$MgO + H_2O \xrightarrow{\Delta V} Mg(OH)_2$$

The hydration mechanisms for fused single crystal magnesia and polycrystalline magnesia clinker have been studied by Kitamura et al. [74]. The hydration reaction of single crystal magnesia presents the initial mild, but shorter period with dense layer formation, and quickly changed into a longer active period with hydrated layer formation. During the active period, the hydrated layer forms pyramid shape $Mg(OH)_2$

with loose texture because of volume expansion, but no slaking was observed. However, this mechanism is different from the mechanism in polycrystals, the interactions among the hydrated crystals result in many cracks along grain boundaries, and finally produce a lot of fine grains with polycrystals disintegration. This is so-called the "dusting phenomenon" which continues until the ultimate size of single crystal is eventually reached. The extent of grain boundary destruction depends on the hydration temperature.

2.3.1.2 Effect of Impurities on the Hydration of Magnesia Clinkers

Different clinkers have different hydration resistance. The hydration of magnesia clinkers depends significantly on impurity content, not as much on bulk density or crystal size [75]. The influence of impurities is rather complex. For instance, boric oxide content does reduce MgO hydration propensity, because the glass phase (composed with B_2O_3, CaO and SiO_2) distributed among the magnesia grain boundary does protect against hydration [76], but it reduces its refractoriness. Matsui et al [75] revealed that the best hydration resistance impurity composition is $xCaO.ySiO_2.zB_2O_3(x+y+z=1)$, with $x>0.2$, $y>0.2$ and $z>0.1$, in magnesia clinker. For low B_2O_3 95% MgO magnesia grains, low CaO, high SiO_2 levels have higher hydration resistance than high CaO, low SiO_2, 98% MgO grains [26,27], because the liquid phase coating of periclase crystals after cooling does protect from hydration; however, the hydration resistance of those pulverized powders decreases due to the destruction of such coating upon crushing. The schematic explanation of those hydration mechanisms is illustrated in Figure 2.6.

(a) A MgO Clinker without Crushing

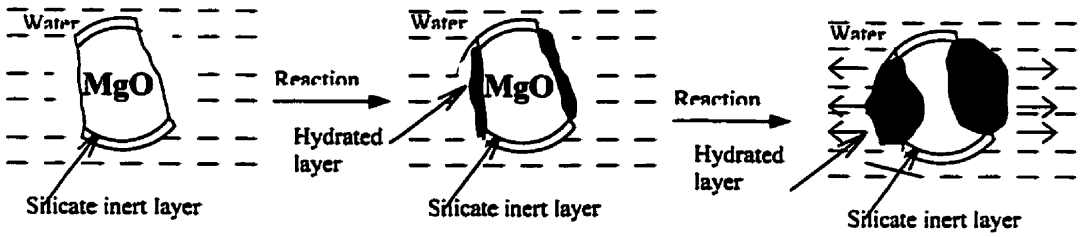

(b) A MgO Clinker after Crushing

Figure 2.6 Schematic Expression of the Slaking Mechanisms of Magnesia Clinker [77]

2.3.1.3 Improvement for MgO Hydration Resistance with Additives

Several methods have been developed to improve MgO hydration resistance. Arira Watanabe et al. [78] got the improved magnesia clinker with adding 2 to 4% Al_2O_3 into raw materials prior to sintering. Because in-situ spinel was formed and oriented on periclase boundary during the process, it was believed to prevent hydration of magnesia.

Various surface treatments have also been tried, through embodiment of MgO particles in solution of various acids [79] such as inorganic, organic, oxalic, citric, acetic, boric, etc.; in solution with various organometallic compounds [80,81], and in slurry of very fine silica [73,82,83]. For example, Kaneyasu et al. [80] found that for MgO particles treated in an organosilicon compound solution at temperatures between 350 °C and 500 °C, the hydration resistance was greatly improved; Samukana et al. [77] mixed magnesia clinker, fume silica with water and placed the slurry into a pressurized container; after hydration test at 150°C×3hr×5atm, they found that the hydration resistance of the magnesia was improved. They believed it is because an inert layer $Mg_mSi_nO_2.xH_2O$ is formed and decreases MgO particles hydration, as shown in Figure 2.7 .

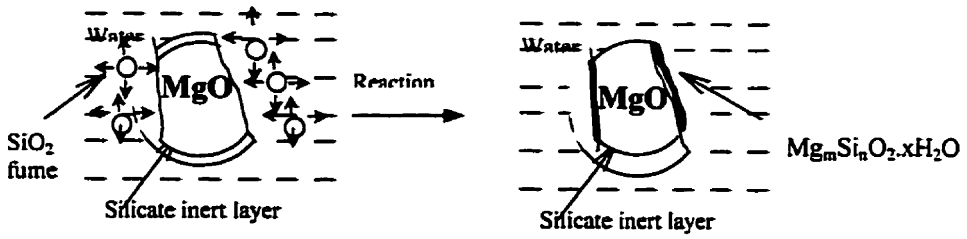

Figure 2.7 The Schematic Representation of Hydration Resistance of MgO Clinker after Adding SiO_2 Fume [77]

Another experiment [79] has shown that by mixing calcined magnesia with low solubility phosphate glass, it was possible to improve the hydration resistance of fine magnesia grains very significantly. This low solubility phosphate glass has a nominal

composition of 23% Na_2O, 64% P_2O_5, 7% Al_2O_3, 2% SiO_2, 3.5%B_2O_3. Additionally, using phosphate salt rather than low solubility phosphate glass, Kyoden et al. [73] have found that addition of sodium polyphosphate increases the pH of a magnesia slurry from 10.75 to 11.7, due to sodium polyphosphate capturing more Mg^{2+} ions, therefore hydration of magnesia could be improved by formation of an inert compound consisting of one molecule of sodium polyphosphate and one Mg^{2+} ion.

2.3.2 Binders for MgO-based Castables

Having decided to use water as a fluid to homogenize the mixes of aggregates and matrix components, three type of binders can be considered: 1)the classic calcium aluminate (CA) cements (70 or 80% alumina) by far the most well-known; 2) the hydratable alumina or the silica gel or the silica-alumina gel; 3)the chemical binder systems: mainly silicates and phosphates.

Using CA cement in basic castables, as a binder, is not the best to ensure adequate hot strength or adequate bonding at temperatures above 1500°C, because a lot of low melting constituents are to be formed in MgO-CaO-SiO_2 system. Cement-free castables are more preferable.

Watanabe et al [81] reported on the use of superfine SiO_2 powder as binder combination with organometallic compound. It was found to provide good flowability and high slaking resistance to the magnesia castables prepared. No cracking, even in large cast blocks, was observed after drying. Meanwhile, for the purpose of improving mechanical properties, siliceous mineral introduced was regarded as an effective agent.

Nishi et al. [84] used uneasily soluble phosphate glass as binder in magnesia castable, since the uneasily soluble phosphate hardly dissolves in the water during mixing, and produced castable with good flowability and workability. It has high intermediate temperature strength at T = 400-800 °C , but quite low hot strength at T = 1400°C.

Many papers have reported the use of hydraulic alumina as a binder and obtained good results, but mostly in Al_2O_3-based castable [10,71]. M. W. Vance et al [85,86] utilized hydraulic alumina in Al_2O_3 castables and attained success in components such as lances and impact pads, where controlling slag resistance, hot erosion, impact and thermal shock resistance are important. They reported the improved result for HMOR and fracture toughness when using hydratable alumina in castable fired at temperatures exceeding 1371°C. However, they also pointed out that the initial heat-up must be performed very carefully, in the temperature interval 204°C- 276°C, to avoid explosive spalling. Once the entire part has been above 276°C, it then can be heated more rapidly without problem.

Since hydratable alumina loses the crystal water at around 200°C [13], those castables with hydratable alumina as binder may have weak mechanical properties at intermediate temperature if no other additives are used. B. Myhre et al. [12,87] have tried to combine hydraulic alumina and fume silica in fused alumina castables and showed that at the intermediate temperature strength does improved.

Nevertheless, using hydratable alumina as a binder in MgO-based castable was rarely reported so far. Ning [88] has exploratorily studied the possibility to use

hydratable alumina in MgO based castable, the results were encouraging. Therefore, it could be a valuable approach to apply hydratable alumina into basic castables, instead of calcium aluminate cement or high content of SiO_2 as a binder, combination with proper additives.

2.3.3 Bonding for MgO-based Castables

2.3.3.1 Forsterite Bonding

MgO-SiO_2 castables have been used successfully in tundish baffles, electric arc furnace tap blocks etc. [81,89], and trials have been achieved in various steelmaking ladles in Japan [90,91]. It is important to minimize the use of alumina cement in such systems, because the addition of microsilica in cement bonded MgO will form low melting monticellite and merwinite, thus giving low strength products in service [83]. To replace cement, a magnesium-silicate hydrate gel has been successfully used [30]. With 6 to 10% SiO_2 , a good forsterite bond is formed at intermediate temperatures, but hot strengths are still too low to be useful at service temperatures in ladles, since liquid starts forming in the matrix at 1400°C [91]. Additions of silicon nitride and silicon metal have been considered suitable bond phase modifiers [83]. Hot modulus of rupture values were significantly improved.

For corrosion resistance in basic slag, silica additions inhibit slag penetration, but impair the dissolution resistance. Kyoden Nishi et al. [81,90,92] reported that a minimum of 6% fine silica addition is needed to cut penetration by ¼ , but dissolution increases steadily by a factor of 3 between 2 and 16% SiO_2 addition [90]. Having a

better penetration resistance increases the spalling resistance of castables. Nishii et al [93] have suggested that 8% SiO_2 was an optimum for thermal spalling, penetration and dissolution resistance in MgO-SiO_2 castable.

Although there is still work to be done in this system and there is still room for further improvement, it is believed that for steel-quality cleanliness, silica-free solutions have a better long-term chance of success.

2.3.3.2 Spinel Bonding

A phosphate and spinel bonded high magnesia castables were developed by Henry et al [94]. Starting with a high level of phosphate salts to avoid hydration of the aggregates, fused alumina clinker was added at a level of 20% or more to obtain a slightly positive permanent volume change once fired at 1600°C. They documented that the presence of liquids caused by the phosphate salt readily enhanced the formation of spinel and promoted rapid grain growth. Slag tests showed that slag penetration resistance and structure spalling were improved, but hot strength was very low and corrosion resistance decreased as alumina content increased.

To overcome the drawback of phosphate castable with lower HMOR strength, MgO-MA castable with SiO_2 fume addition was studied. Since a volume expansion occurs when MgO and Al_2O_3 react to form spinel, the proper choices of size distribution and Al_2O_3/MgO ratio become very critical. Bi et al [66] suggested the appropriate Al_2O_3/MgO ratio is between 1.1 and 1.8 with a total Al_2O_3 level around 10-15% in

castable, and a continuous particle size distribution in matrix portion does need to achieve good flowability at lower water addition in MgO-MA castable.

2.3.3.3 Other Bondings

The use of both SiO_2 and Al_2O_3 in MgO based castables have not been systematically studied. In a particular set of experiments, it has been found by Watanabe et al [78] that the simultaneous addition of medium grain fused silica and fine particle alumina is beneficial in improving slag penetration resistance and volume stability. By controlling the alumina-silicate reaction, it may be possible to form some mullite bonds, but of course any high amount addition of silica is not good idea for clean steel.

Zircon and zirconia additions have been tried in Japan [36,95,96]. Zirconia and MgO do not react together to form a new compound, but at sufficient temperature, zircon decomposes and a forsterite bond may form with MgO. Nakagawa et al [97] reported that, as for SiO_2, a 10% zircon addition to a magnesia-zircon mixture inhibited slag penetration, but any zircon addition increases the slag corrosion index. A magnesia-zirconia clinker as coarse grains and a magnesia clinker plus 5% zircon as the major components of the matrix have been developed to show the best wear index [97]. It was observed that magnesia-zirconia clinker absorbs slag composition and a coalescent texture is then formed between the clinker and matrix. This inhibits slag penetration and matrix corrosion.

A significant disadvantage for MgO-based basic castable is its poor penetration resistance to ferric oxide; the ultimate, to minimize slag penetration, would be to change

the wettability of the refractory surface by addition of carbons. Trials to use natural flake graphite are by now gaining some momentum. The poor water-dispersibility of graphite is an obstacle to overcome. Three solutions have been contemplated: 1) using of hydrophilic treatment by surface active agents [98,99,100]; 2) surface coating of graphite by plasma jet, flame coating or other techniques; 3) and finally a high speed impact method [101]. In this same line, by combining suitable additives. Mosser et al. [102] have created a castable, containing 85% magnesia grains, 7% SiO_2, and 7% carbon, using an aqueous system, avoiding magnesia hydration and achieving excellent strengths over the temperature range 20 to 1600°C. This slag corrosion resistance is as good as resin-bonded magnesia-graphite bricks for ladle slag line. Teranishi et al [45] also developed a MgO-C castable not with graphite, but combination with carbon black and pitch. They found that the slag corrosion resistance was significantly improved compared to Al_2O_3-MgO castable. The testing results show the durability of MgO-C castable at slag line of LF ladle was more than twice of conventional Al_2O_3-MgO castable.

2.4 Spinel Bonded, Al_2O_3-based Castables

2.4.1 Al_2O_3-MA Castables

Spinel bonded Al_2O_3-MA castables, which possess superior properties in terms of slag penetration and structural spalling, have been successfully used, as major lining materials in steel ladles. Al_2O_3-MA castables were mainly composed of alumina, pre-reacted spinel and high alumina calcium aluminate cement. Several papers have

discussed the importance of pre-reacted spinel addition [30,31,39]. They reported that around 20wt% of pre-reacted spinel is appropriate in Al_2O_3-MA castable [30,39,103]. At this level, both erosion and penetration indexes are the least. Figure 2.8 represents the effect of pre-reacted spinel content on indexes of slag corrosion and penetration of Al_2O_3-MA castable (Rotary test at slag composition of C/S=1:1).

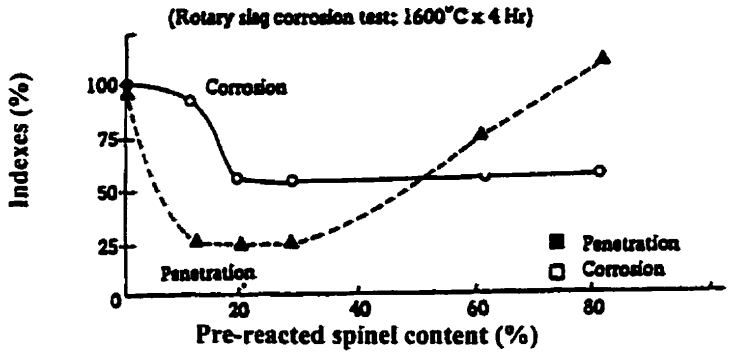

Figure 2.8 Pre-reacted Spinel Addition Amount vs. Slag Penetration and Corrosion Indexes of Al_2O_3-MA Castable [103]

The spinel grain size also significantly affects the slag corrosion resistance of Al_2O_3-MA castable. Fine grains are greatly beneficial to slag penetration resistance [30,39,104,105].

Yamamura et al. [17,106,107] demonstrated that the castable with addition of alumina-rich spinel at 90% Al_2O_3 content was better in terms of slag penetration than stoichiometric spinel or magnesia-rich spinel additions. The reason is that the Al_2O_3–

rich spinel has a strong capability to capture FeO, from slag, to form $(Mg,Fe)Al_2O_4$, and therefore, further prevents slag penetration. Figure 2.9 shows the slag penetration resistance as a function of spinel composition [17] for corrosion test performed in a horizontal rotary drum furnace, at 1650°C × 4hrs, using converter slag (C/S =3.6, Fe_2O_3 = 33.7%).

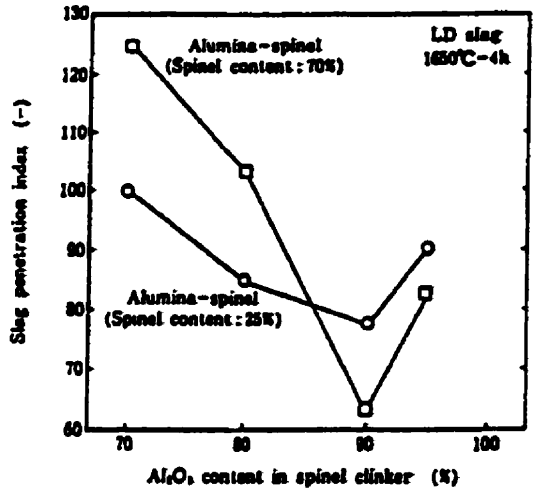

Figure 2.9 Relationship between Al_2O_3 Content in Spinel and Slag Penetration Indexes [17]

The mechanisms of slag penetration in Al_2O_3-MA castable was reported by A. Matsuo et al. [92,103,108] based on rotary slag tests, with two slag compositions of C/S=1.7, Fe_2O_3=0.7% and C/S=4.1, Fe_2O_3=15.0% respectively. The schematic representation is given in Figure 2.10.

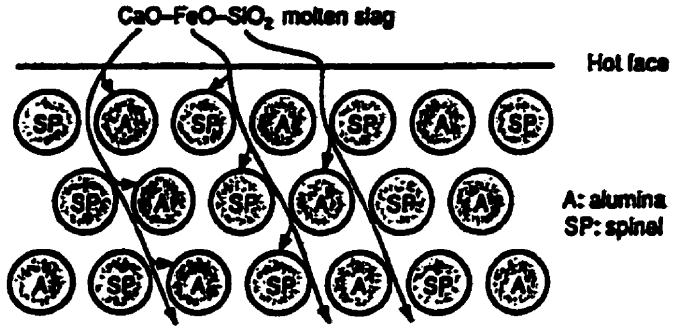

Figure 2.10 Schematic Representation of the Slag Penetration into the Al_2O_3-MA Castable [92]

In contact with CaO, FeO and SiO_2 from the slag, alumina firstly reacts with CaO to form $CaO.6Al_2O_3$. The growth of those CA_6 crystals densified castable texture. Then, SiO_2 in the slag can react with CA_6 to form gehlenite (having a low melting point).

$$\begin{array}{ccccc} CaO & & CaO & & SiO_2 \\ \downarrow & & \downarrow & & \downarrow \\ Al_2O_3 & \longrightarrow & CaO.6Al_2O_3 & \longrightarrow & CaO.2Al_2O_3 \longrightarrow 2CaO.Al_2O_3.SiO_2 \end{array}$$

Simultaneously, the spinel grains AR_{90} in castable may trapped FeO and MnO, from slag, to form an hercynitic spinel (Mg, Fe, Mn)$O.Al_2O_3$, the residual molten liquid due to SiO_2 -rich composition in the slag could be more viscous, those viscous liquid and densified texture by CA_6 do reduce slag penetration.

2.4.2 Al_2O_3-MgO Castables

Fine magnesia powders added into Al_2O_3-MgO castable instead of previous pre-reacted spinel addition are recently being viewed with keenest interest in Japan. Some reports [109,110,111] have indicated prolong durability of castables over Al_2O_3-MA castables. However, by adding MgO powders, the expansion from reaction of Al_2O_3 and MgO must be controlled well before the Al_2O_3-MgO castable can be put into practice.

Kobayashi et al. [42] determined the thermal expansion behaviors of Al_2O_3-MgO castable (Figure 2.11). They showed that the temperature at maximum thermal expansion for all samples is between 1300 and 1500°C. In case of MgO content at 10.0 or 15.0 wt%, the maximum expansion under 0.2Mpa load can reach 1.0% or 1.4%. Accordingly, he recommended that the proper magnesia content should be less than 7.5wt% in Al_2O_3-MgO castable .

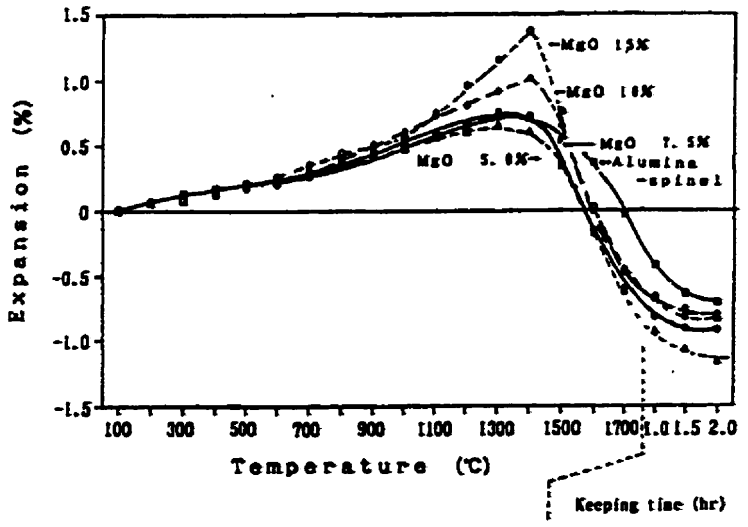

Figure 2.11 Thermal Expansion under Load (0.2MPa) of Al_2O_3-MA Castables (Three Different MgO Contents) after 1700°Cx2hrs [42]

M. Kobayashi et al. [42] carried out further tests with adding different amount of SiO_2 fume. The results for thermal expansion of castable with silica content >0.5% is larger than that of silica content <0.5% at 1300°C. but, the maximum thermal expansion does vary with different SiO_2 addition. The lowest maximum thermal expansion is at 0.5% (See Figure 2.12). They also concluded that SiO_2 in Al_2O_3-MgO castable could prompt the in-situ spinel formation.

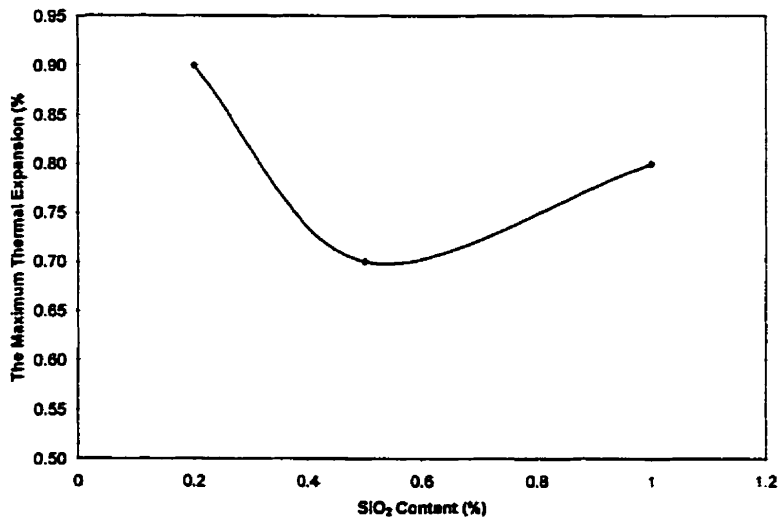

Figure 2.12 The Maximum Thermal Expansion of Al_2O_3-MgO Castable (under load 0.2MPa, 7.5% wt%) in Relationship with SiO_2 Addition after Firing at 1700°C×2hrs

M. Kobayashi et al [42] reported the effect of MgO/SiO_2 weight ratio in Al_2O_3-MgO castable on permanent linear change (PLC), their results demonstrated that, when the MgO/SiO_2 ratio exceeds 12, the PLC becomes too large (>2%), and castable peeling is significant. However, when the MgO/SiO_2 ratio is less than 3, there is a shrinkage effect

which also accelerates crack formation, therefore, an appropriate MgO/SiO_2 ratio is between 4 to 8 .

The corrosion behaviors of Al_2O_3-MgO castables in high frequency induction furnace was determined by Kobayashi and Tawara et al [42,111]. They found that the corrosion thickness and slag penetration depth are closely related to MgO fine grains content in the castable (Figure 2.13), the optimum MgO content being at 7.5-10.0 wt%.

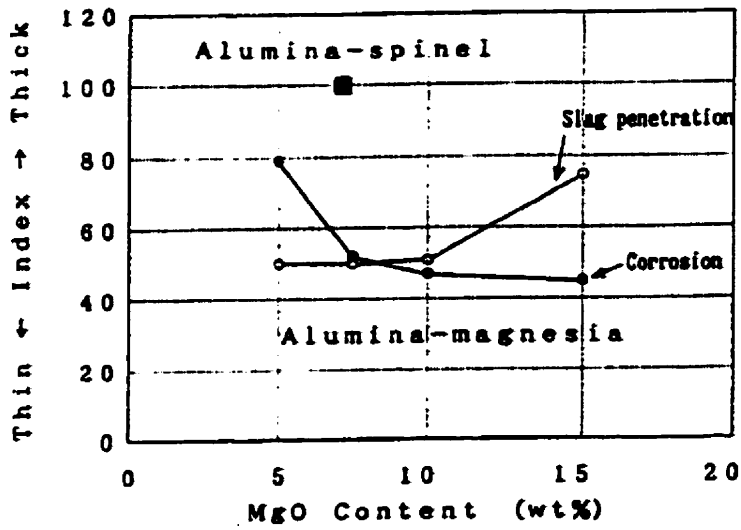

Figure 2.13 The Relative Corrosion Thickness and Slag Penetration for Al_2O_3-MgO and Al_2O_3-MA Castables [42]

Furthermore, from the fracture mechanics point of view, S. Itose et al. [112] confirmed that the optimum MgO content in Al_2O_3-MgO castable is indeed around 7.0 wt% (as [42]).

The castable life comparison tests were carried out at industrial trial stage by M. Kobayashi et al [42]. Chemical analysis for corroded samples shows CaO content in Al_2O_3-MgO castable, distance from hot face, was much less than that in Al_2O_3-MA castable; the erosion and penetration index being only half of the index for Al_2O_3-MA castable. Same results were confirmed in a steelmaking plant; the ladles lining lifes under the same industrial conditions were 180-200 heats for Al_2O_3-MgO castables, compared to 140-160 heats for Al_2O_3-MA castables.

Al_2O_3-MA, Al_2O_3-MgO castables applied in the side wall or bottom of steel ladles are by now commercially acceptable, obviously, their slag resistance to high basic slag is not to be expected and hence they cannot be used at slag lines, therefore, those castables have to be restrained to the barrels and bottoms of steel ladles.

2.5 Summary

Monolithics are now in use as refractory material in the steel industry. Alumina based castables with addition of fine spinel have successfully been used in steel ladle in bottoms and barrels. The modified Al_2O_3-MA castable with fine grains addition instead of the pre-reacted spinel in matrix portion, called Al_2O_3-MgO castables, have achieved better service performances than Al_2O_3-MA castables, but are not yet acceptable in slag line zone.

Drawing lessons from Al_2O_3-MA castables, magnesia based castables with spinel bonded are potentially perspective refractories to be used in the slag line. However, as reviewed, since the volume expansion during spinel formation, magnesia hydration,

pre-reacted spinel grades and addition, the MgO/Al_2O_3 ratio in the castable and the binder types greatly influence the properties of castables. Therefore further investigations on those factors have constituted the essential part of this thesis.

CHAPTER 3. FLOWABILIY OF MgO-Al_2O_3 CASTABLE MIXES

In general, a well designed castable has to present good flowability at low level of water addition to form a dense and consolidated product. Flow properties are influenced by a number of factors, such as raw material properties, type of binders, particle size, distribution and shapes etc. However, the most significant factors are particle size distributions and the appropriate deflocculant. With an appropriate continuous distribution of particles including a larger amount of fine particles, mixture may pack to the maximum density exceeding 80% theoretically [113]. Fines and ultrafines being distributed in interstices of larger particles do reduce the porosity of the packing body. Nevertheless, a proper deflocculant is needed to modify the interparticle forces, so as to prevent fine powders agglomeration, to minimize water demand, and to ensure good flowability of castable mix.

In this chapter, characterization of the flow properties of castables under study has been achieved using the extracting-matrix method. It helps to determine the effects of different deflocculant and additions and helps to select an appropriate deflocculant for MgO-Al_2O_3 castable mixes

3.1 Experimental Procedure

Flow property measurements have been made in two steps: firstly, "flow-time" was measured on the basis of three groups of slurry, MgO, Al_2O_3, and the mixture of MgO, Al_2O_3, pre-reacted spinel. The mixture is actually composed of the matrix part of the

castable. Four different deflocculants in each group, listed in Table 3.1, at the addition of 0.1, 0.5, 1.0, 5.0 and 10.0 wt% were respectively added, where the percentage is based on the dry mass of powders.

All the used materials have been defined already in terms of chemical composition and size distributions in Chapter 1. The "flow-time" experimental set up is shown in Figure 3.1.

Table 3.1 Deflocculants Studied

Denotation	Chemical Name
L	Lignosulphonate
O	Organic Salt
S	Sulphite
P	Phosphate

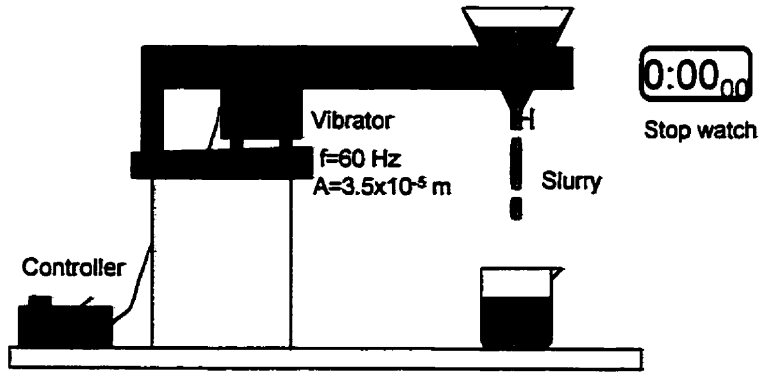

Figure 3.1 Schematic Representation of the Apparatus to Measure "Flow-Time"

Each tested slurry is composed of 80.00g fine powders and 18.67g water as well as of dispersant. After stirring for 5 minutes, the slurry is poured into the funnel. The knob on the funnel is turned at the same time as the vibrator is on. Time to empty out the funnel is recorded. The vibrator works at a frequency of 60Hz and amplitude of 3.5×10^{-5} m. The flow of the slurry is mainly driven by the vibrator and, of course, slurry mass itself, therefore, the shearing stress of the slurry may not significantly affect the measured flow-time, and it will not be specifically considered herein.

Based on the appropriate dispersant optimized from step one, the "flow-value" measurement of MgO-Al_2O_3 castable mixes were carried out by the flow cone method referring to ASTM C230-90 as the second step measurement. Batches weighing 1.5 kg were wet mixed for 5 minutes using a Hobart mixer. The castable mix was then consolidated into a flow cone by vibrating for 15 seconds on a Waker vibration table at frequency of 50 Hz and amplitude of 4.5×10^{-4} m. After leveling the surface on the top, the cone is carefully removed and vibrated for a further 15 seconds allowing the mix to spread. The diameter of castable spread is measured in six directions and the average base diameter is expressed as the "flow-value" of MgO-Al_2O_3 castable mix.

3.2 Results and Discussion

3.2.1 Effects of Different Deflocculants on Flow Time of MgO and Al_2O_3 Slurries

The "flow-time" measured for slurry of ball milled magnesia fine powders with water and different deflocculants are shown in Figures 3.2 (a) and (b).

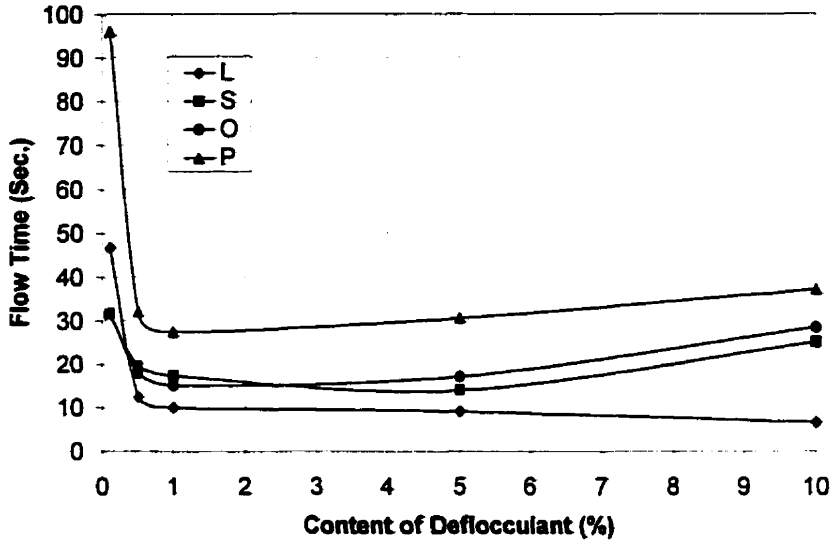

(a)

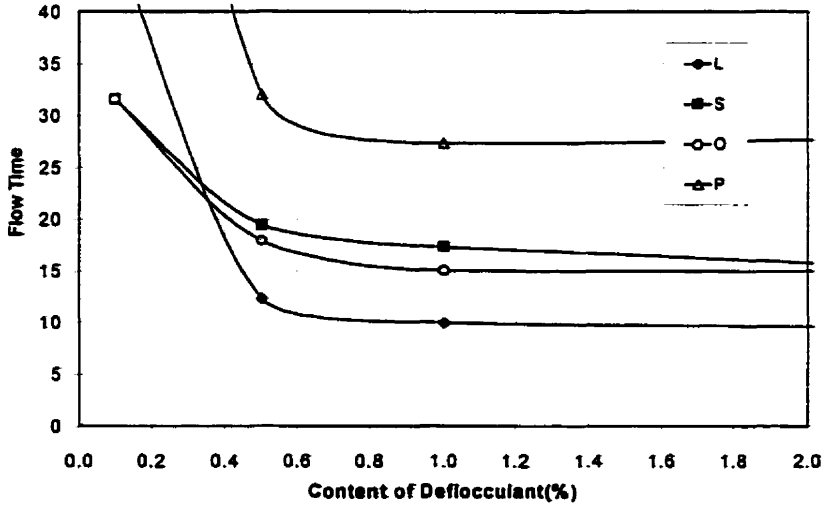

(b)

Figure 3.2 "Flow-Time" of MgO Slurry in Relationship with Deflocculant Type and Additions (Figure (b) is an enlargement of Figure (a) at 0-2% deflocculant addition)

The most efficient addition range, which significantly affects the flow time of MgO slurry, is located between 0.5 and 1.0% addition for all of deflocculants. Less than 0.5%, the slurry can't be well dispersed. Focusing on the specific range 0.5 – 1.0%, deflocculant L has the best dispersibility for MgO slurry, controversially, the worst deflocculant is phosphate P. With deflocculant addition more than 1%, "flow-times" in this experimental context are not affected significantly, although the order of dispersibility for each deflocculant remains the same as its in the range of 0.5-1.0%. At addition below 0.5%, the best deflocculants are O and S while P remains the worst. Therefore, not only the deflocculant type, but also the addition amount do play important role in the slurry.

As a comparison, "flow-time" tests of Al_2O_3 slurry, a mixture of UFA, FA, TA, HA and water, were also carried out. The results are shown in Figure 4.3. Again, the efficient addition range of deflocculants is still from 0.5 to 1.0%. However, in this case, P becomes the best deflocculant while the deflocculant L is the worst, totally in opposition with the results of the previous MgO slurry.

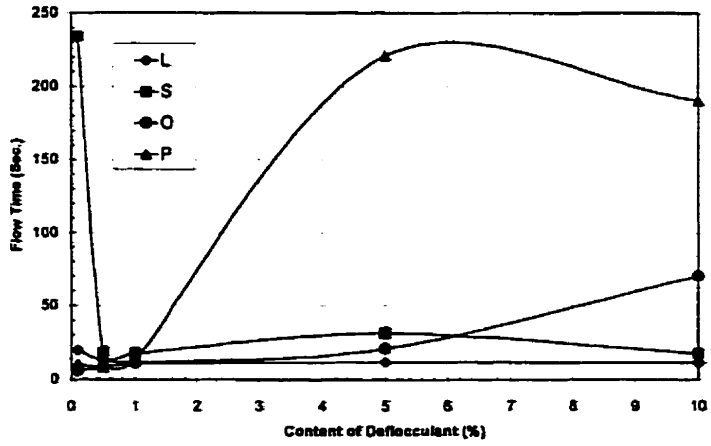

(a)

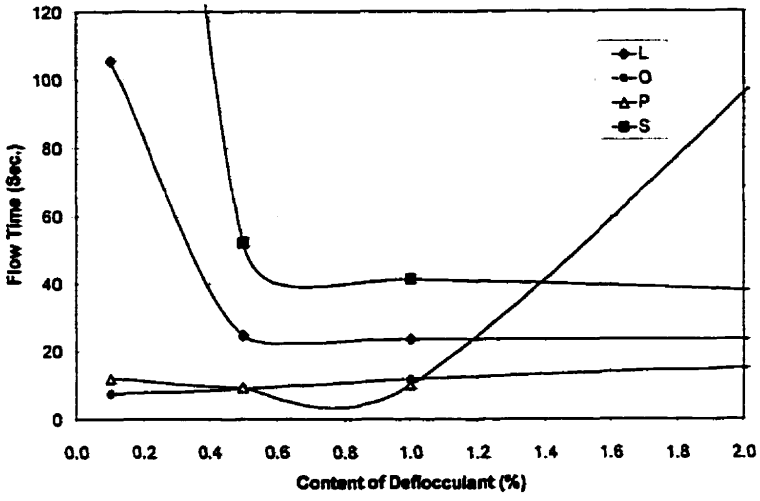

(b)

Figure 3.3 "Flow-Times" for Al_2O_3 Slurry in Relationship with Different Deflocculant and Additions (Figure (b) is an enlargement of Figure (a) at different addition of 0-2%)

The dispersing mechanisms of deflocculant used in MgO or Al_2O_3 slurry are highly related to the particle interactions which have been well described in DLVO theory.

3.2.2 Effects of Different Deflocculants on Flow Time of MgO-Al_2O_3 Mixture Slurry

The castable matrix is a mixture of alumina, magnesia and spinel AR_{78} fine powders, in the ratio 4:1:1. "Flow-Times" of matrix slurry versus different deflocculants are illustrated in Figure 3.4. Interestingly, the effects of the four kinds of deflocculant are in close agreement with the effects on flow time for Al_2O_3 slurry, but not for MgO slurry. The reasons may be regarded as two aspects, one is due to the significant amount of Al_2O_3 fine powders used controlling the properties of the slurry; or may be due to the

specific preparation technique to prepare the slurry. MgO particles are added into the dispersant solution first, then after stirring 2 minutes, alumina is added. This adding sequence could reduce the isoelectric point of MgO (pH=10.5-12) to close to that of the bare alumina particles (pH=8-9), because it helps the abundant dissociated multiple charged ions or polytelectrolyte chains to adsorb at the MgO particles/water interface and increase the negative surface charge [114], therefore, the afterward introduction of Al_2O_3 into the MgO slurry, does not cause strong electrostatic attractions between particles of different materials, ensure a homogeneous dispersion of both powders in the mixture slurry.

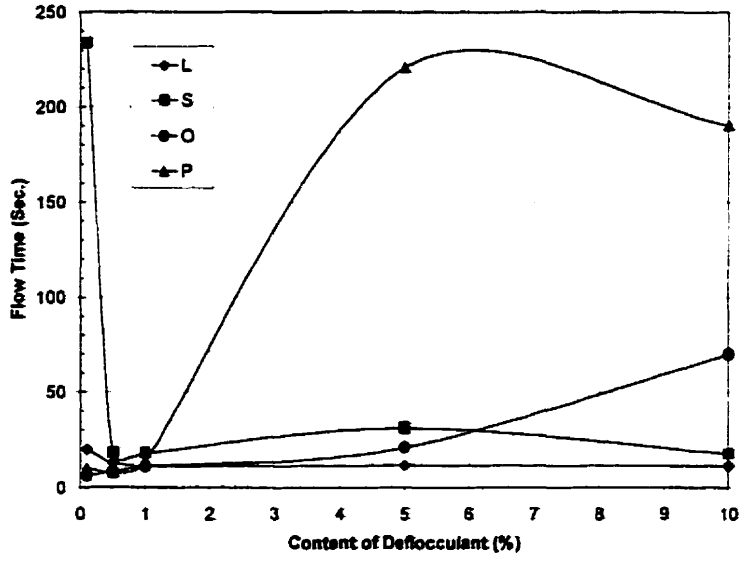

(a)

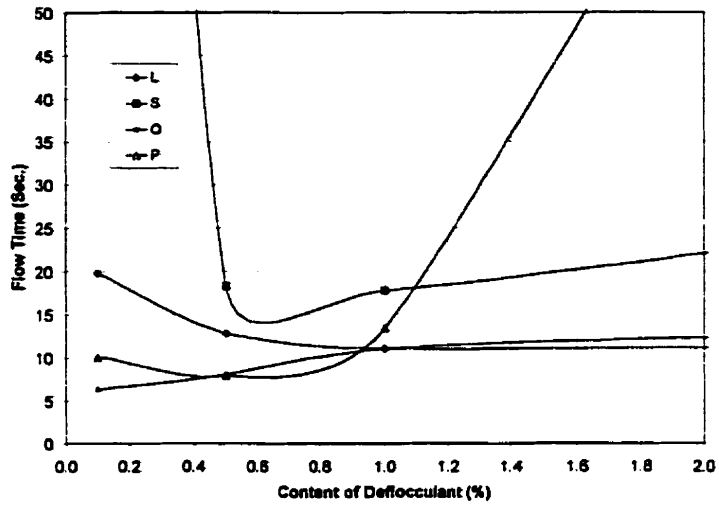

(b)

Figure 3.4 "Flow-Times" of Matrix Slurry in Relationship with Different Deflocculant and Additions (Figure (b) is an Enlargement of Figure (a) at Addition of 0-2%)

Results of 'Flow-times" as a function of "Setting-times", at level addition of 0.5% for each deflocculant are shown in Figure 3.5. "Setting-times" of matrix are not significantly changed during the first hour when adding deflocculants O, L or P.

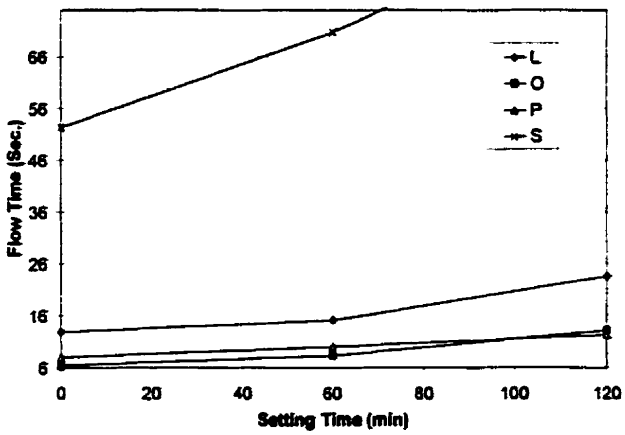

Figure 3.5 The Relationship Between Matrix Setting Time and Flow time with Different Deflocculant at addition of 0.5%

3.3 Correlation between Matrix "Flow-Time" and Castable "Flow-Value"

The "flow-value" was measured for $MgO-Al_2O_3$ castable mixes, composed of 70% MgO aggregates (6-170 mesh) and 30% matrix fine powders (-170 mesh), with addition of 0.5% of one of the three different deflocculants O, L or S respectively. Results are shown in Figure 3.6. For purpose of comparison, "flow–times" in castable with 30% matrix are also given in Figure 3.7.

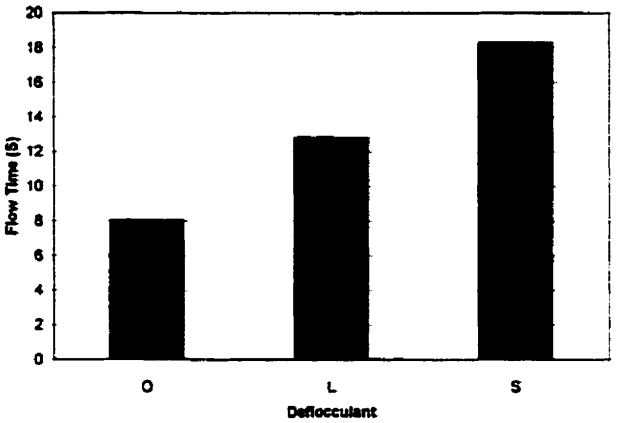

Figure 3.6 "Flow-Time" of Matrix at 0.5% Addition with Deflocculant O, L and S

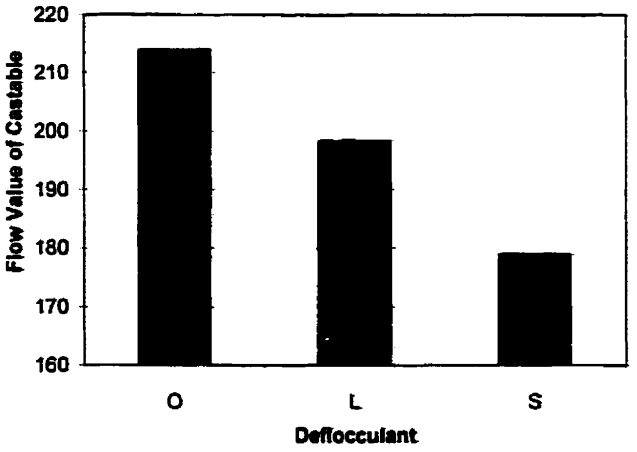

Figure 3.7 "Flow-Value" of Castable Mix at 0.5% Addition with Deflocculant O, L and S respectively

High correspondence appears between matrix "flow-times" and castable "flow-values" for the different deflocculant O, L, S. The smaller the "flow-time" of matrix is, the larger the "flow-value" of castable mix will be.

Furthermore, concentrating on the specified deflocculant O at four different additions, the same high correspondence between "flow-value" of castable and "flow-time" of matrix are clearly demonstrated in Figure 3.8. In conclusion of this section through this easy-to-do, so called "Extracting-Matrix", method measuring the "flow-time" of matrix does help to predict the flowability of the whole castable mix. Therefore, it is an efficient way to select the appropriate deflocculant type and appropriate addition in a new castable mix. Additionally, in our system, the flowability of castable will mainly depend on the matrix composition in castable mix. The reason may be due to the major factor, which remarkably affects the castable flowability of those fine powders in castable.

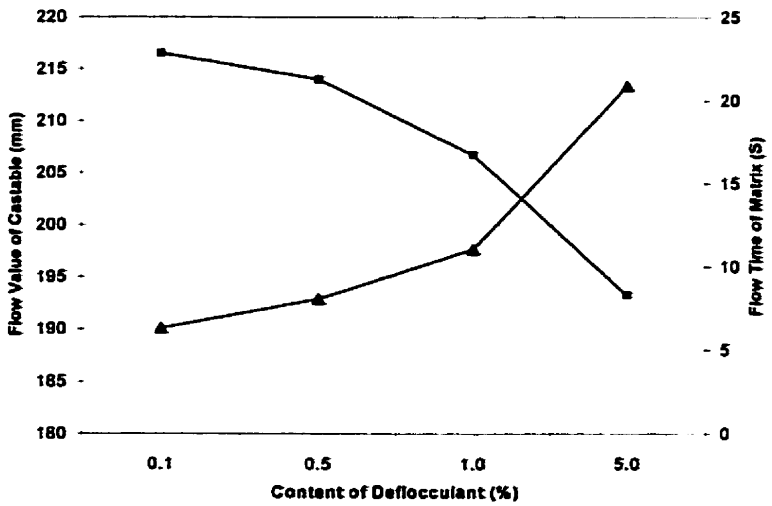

Figure 3.8 Flow Value of Castable and Flow Time of Matrix with Deflocculant O at four of Additions

3.4 Correlation of "Flow-Times" and "Flow-Values" with Physical and Mechanical Properties of $MgO-Al_2O_3$ Castable Mix

Based on the "extracting-matrix" method, the optimized deflocculant for $MgO-Al_2O_3$ castable is deflocculant "O" at 0.5% addition, meanwhile, the worst case is deflocculant L. Physical and mechanical properties of $MgO-Al_2O_3$ castables, with deflocculants L and O, at addition of 0.5%, were measured after curing, drying and firing respectively. Porosity, density and cold modulus of rupture etc. were also measured, and values are shown in Table 3.2. It gives that the higher density, higher CMOR and lower porosity were achieved with deflocculant O.

Table 3.2 Physical and Mechanical Properties of $MgO-Al_2O_3$ Castable with Deflocculant L and O

Castable		A	B
Deflocculant	Type	L	O
Water Addition	(wt%)	4.8	4.8
Flow Value of	Castable	198.4	214.0
Flow Time of	Matrix	8.05	12.94
Green Body (110°C×24hrs)	Bulk Density (g/cm^3)	3.01	3.04
	Porosity (%)	14.8	14.0
	MOR (MPa)	11.9	14.9
After firing at 1600°C	Bulk Density (g/cm^3)	2.88	2.89
	Porosity (%)	18	18
	MOR (MPa)	6.9	8.6
	PLC(%)	+0.9	+0.9

As a summary, "Extracting-Matrix" method can be used to optimize the deflocculant. The flowability of MgO-Al_2O_3 castable is predictable by measuring flow time measurement of matrix slurry. Meanwhile, the appropriate deflocculant for MgO-Al_2O_3 castable is the deflocculant O at the addition of 0.5%. This optimized properties for MgO-Al_2O_3 castable flowability will lay an important foundation in the following chapters.

CHAPTER 4 VOLUME STABILITY OF MgO-Al_2O_3 CASTABLE MIXES

The volume expansion, due to in-situ spinel formation from reaction of periclase and spinel [16,67] which has been documented in Chapter 2, is highly related to the properties of MgO-Al_2O_3 castable. A systematic experimental study on volume stability of MgO-Al_2O_3 castable mixes has been conducted to clarify the expansion characteristics and to control the expansion of MgO-Al_2O_3 castable mixes.

4.1 Experimental Plan

This part of the study is divided into two aspects: one is focussing on the study of different pre-reacted spinels on thermal expansion behavior, and the other on the silica addition. For the first part, thirty five mixes, divided into three series with different pre-reacted spinel AR_{90}, AR_{78} and MR_{66} respectively, are to be considered. The MgO aggregates in each castable mix of the three series have the same size distribution and weight percentage (75%). In the matrix, 5wt% hydratable alumina as a binder with additions of 0%, 5% or 10% pre-reacted spinel complement with MgO and Al_2O_3 fine powders. For the second part, silica fume was added from 0 to 3% into two series, with or without pre-reacted spinel AR_{78} addition, of MgO-Al_2O_3 castable mixes. The sample compositions in different series are given in Table 4.1 to 4.5 respectively.

Table 4.1 Composition of Tested Specimens of Series 1 in Part I

	Group 1					Group 2					Group 3				
Sample Number	A1	A2	A3	A4	A5	$A_{5}1$	$A_{5}2$	$A_{5}3$	$A_{5}4$	$A_{5}5$	$A_{10}1$	$A_{10}2$	$A_{10}3$	$A_{10}4$	$A_{10}5$
Magnesia	75	75	75	75	75	75	75	75	75	75	75	75	75	75	75
MgO Powder	0	5	10	15	20	0	3.75	7.5	11.25	15	0	2.5	5	7.5	10
Al_2O_3 Powder	20	15	10	5	0	15	11.25	7.5	3.75	0	10	7.5	5	2.5	0
AR_{90} Powder	0	0	0	0	0	5	5	5	5	5	10	10	10	10	10
Alumina Binder	5	5	5	5	5	5	5	5	5	5	5	5	5	5	5

Table 4.2 Composition of Tested Specimens of Series 2 in Part I

	Group 4					Group 5				
Sample Number	$M_{5}1$	$M_{5}2$	$M_{5}3$	$M_{5}4$	$M_{5}5$	$M_{10}1$	$M_{10}2$	$M_{10}3$	$M_{10}4$	$M_{10}5$
Magnesia	75	75	75	75	75	75	75	75	75	75
MgO Powder	0	3.75	7.5	11.25	15	0	2.5	5	7.5	10
Al_2O_3 Powder	15	11.25	7.5	3.75	0	10	7.5	5	2.5	0
MR_{66} Powder	5	5	5	5	5	10	10	10	10	10
Alumina Binder	5	5	5	5	5	5	5	5	5	5

Table 4.3 Composition of Tested Specimens of Series 3 in Part I

	Group 6					Group 7				
Sample Number	$R_5$1	$R_5$2	$R_5$3	$R_5$4	$R_5$5	R_{10}1	R_{10}2	R_{10}3	R_{10}4	R_{10}5
Magnesia	75	75	75	75	75	75	75	75	75	75
MgO Powder	0	3.75	7.5	11.25	15	0	2.5	5	7.5	10
Al_2O_3 Powder	15	11.25	7.5	3.75	0	10	7.5	5	2.5	0
AR_{78} Powder	5	5	5	5	5	10	10	10	10	10
Alumina Binder	5	5	5	5	5	5	5	5	5	5

Table 4.4 Composition of Tested Specimens of Series 1 in Part II

Sample Number	$N(SF)_{00}$	$N(SF)_{05}$	$N(SF)_{10}$	$N(SF)_{20}$
Magnesia Aggr.	70	70	70	70
MgO Powder	5	5	5	5
Al_2O_3 Powder	25	25	25	25
Spinel AR_{78}	0	0	0	0
Silica Fume	0	0.5	1.0	2.0

- For instance: $N(SF)_{10}$ ---- MgO-Al_2O_3 castable without pre-reacted spinel, but 0.10 wt% of SiO_2 Fume addition.
- (SF) --- SiO_2 Fume, N --- No pre-reacted spinel

Table 4.5 Composition of Tested Specimens of Serie 2 in Part II

Sample Number	$R_5(SF)_{00}$	$R_5(SF)_{05}$	$R_5(SF)_{10}$	$R_5(SF)_{15}$	$R_5(SF)_{20}$	$R_5(SF)_{30}$
Magnesia Aggr.	70	70	70	70	70	70
MgO Powder	5	5	5	5	5	5
Al_2O_3 Powder	20	20	20	20	20	20
Spinel AR_{78}	5	5	5	5	5	5
Silica Fume	0	0.5	1.0	1.5	2.0	3.0

- For instance: $R_5(SF)_{10}$ ---- MgO-Al_2O_3 castable with additions of 5 wt% pre-reacted spinel AR_{78} and 0.10 wt% of SiO_2 Fume.
- (SF) --- SiO_2 Fume, N --- No pre-reacted spinel, R--- Pre-reacted spinel AR_{78}

4.2 Sample Preparation

MgO-Al_2O_3 castable mixes are prepared from dead-burned seawater magnesia, which has been selected as both aggregates (denoted as MG afterwards, 3-170 mesh) and fine grains (BMF, -170 mesh); calcined and sintered alumina such as tabular alumina (TA, -325 mesh), fine ground alumina (FGA, d_{50}=4 μm), ultra fine ground alumina (UGA, d_{50}=0.4 μm) and hydratable alumina (HA, d_{50}=10 μm); pre-reacted spinel powders (AR_{90}, AR_{78}, MR_{66} , -325 mesh) as well as silica fume. The chemical and physical properties of those starting materials are all given in Tables 1.1 and 1.2 in Chapter 1.

All the mixes in nine groups, being carefully mixed in a Hobart mixer with water and deflocculant, were cast on a vibrating table in molds of 54 by 64 by 230 mm. To

prevent loss of moisture, the specimens were covered with polyethylene sheet, stored for 24hrs prior to demoulding, cured at ambient temperature for 2 days and dried at a temperature of 110°C×24hrs.

4.3 Experimental Methodology

4.3.1 Thermal Expansion Measurement

A high temperature vertical dilatometer (UNITHERM ™ MODEL 1161L) was used for measuring thermal expansion. Specimens of 15 by 15 by 60 mm were cut from the cast bar in longitudinal direction. Each sample was heated in the furnace chamber of dilatometer from room temperature to 1600°C at the rate 3°C/min and cooled down to 25°C at the same rate.

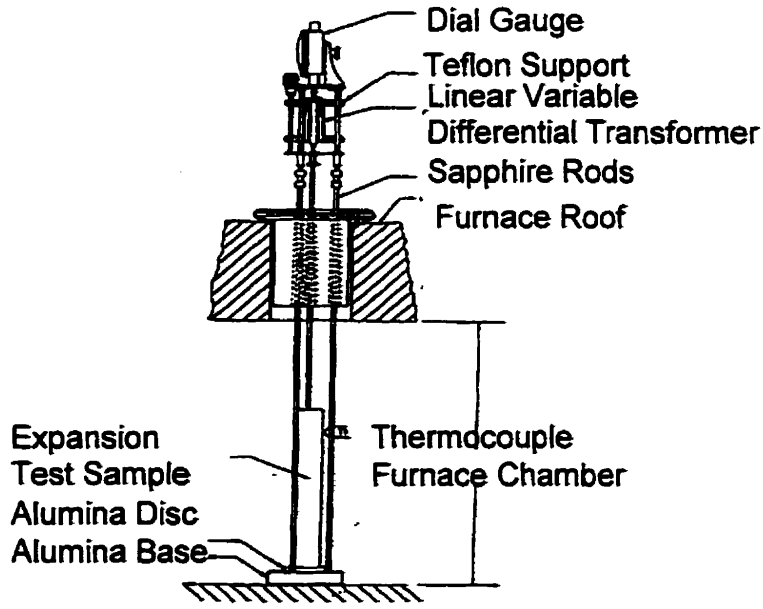

Figure 4.1 The Schematic Diagram of Dilatometer Assembly

4.3.2 Spinel Quantitative Analysis

An internal standard technique was applied to analyze the in-situ spinel formation amount. Samples, after thermal expansion tests, were individually crushed, ground and mixed homogeneously with 5% pure SiO_2 (99.6%) as a reference. A calibration test was established on five mixtures which are composed of pre-reacted spinel, MgO powders as well as 5% pure SiO_2. The weight fraction of pre-reacted spinel in each mixture is from 0 to 60% (at 15% intervals) with complement of MgO powders respectively. The ratio of x-ray diffraction intensity between I_{SP} and I_{SiO2} was calculated. And finally, the calibration curve was plotted with I_{SP}/I_{SiO2} and weight fraction of spinel added. Based on this curve and measured x-ray diffraction intensity of spinel and SiO_2, the amount of in-situ spinel in castable mix can be quantified.

4.4 Typical Thermal Expansion Characteristics of $MgO-Al_2O_3$ Castable Mixes

Figure 4.2 presents a typical plot of percent elongation as a function of temperature for a given $MgO-Al_2O_3$ castable (mix A3). The curve may be decomposed into four segments: for the first segment 25°C to 1100°C, the thermal expansion goes up linearly with temperature; at the second stage 1100°C to 1400°C, a sharp increase is observed up to a maximum temperature at 1410°C; afterward, the expansion drops while temperature still increases until it reaches 1600°C; during cooling down , i.e. the fourth segment represents shrinkage.

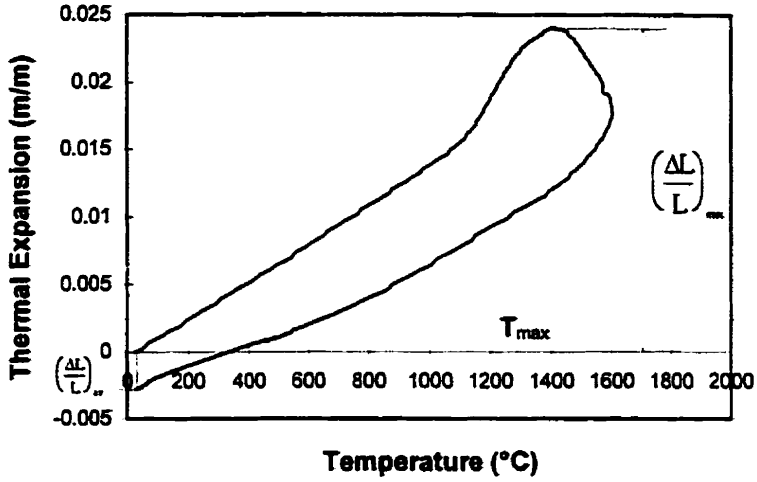

Figure 4.2 A Typical Thermal Expansion Curve for a MgO-Al_2O_3 Castable

A phenomenological model depicting the thermal expansion behavior of MgO-Al_2O_3 castable mix during the first heat-up can be plotted as shown in Figure 4.3.

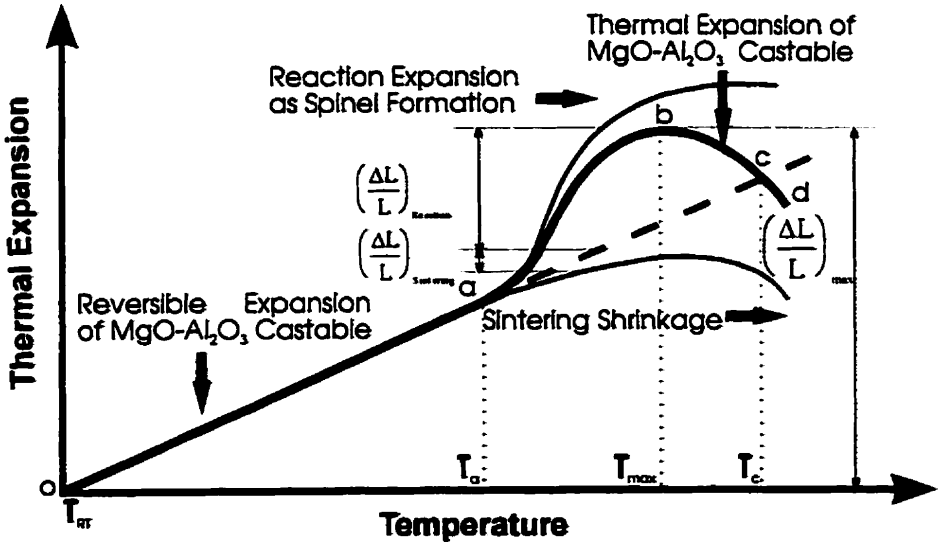

Figure 4.3 A Phenomenological Model of the Thermal Expansion of MgO-Al_2O_3 Castable Mixes

In this model, the first segment "$\overline{oa}$" corresponds to the reversible thermal expansion from MgO, Al_2O_3 and $MgAl_2O_4$ mixes; then the expansion "$\overline{ab}$" is due to the in-situ spinel formation as a result of the reaction between magnesia and alumina powders; finally the shrinkage behavior at "$\overline{bc}$" and "$\overline{cd}$" is from the sintering of components. For each step, the mathematical expressions of $\frac{\Delta L}{L}$ may be shown as:

$$\overline{oa}: \left(\frac{\Delta L}{L}\right)_{Castable} = \alpha_{castable}\,(T_i - T_{RT}) \qquad T_{RT} \le T_i < T_a$$

$$\overline{ab}: \left(\frac{\Delta L}{L}\right)_{Castable} = \left(\frac{\Delta L}{L}\right)_{Reaction} - \left(\frac{\Delta L}{L}\right)_{Sintering} + \alpha_{castable}\,(T_i - T_{RT})$$

$$T_a \le T_i < T_b$$

$$b: \left(\frac{\Delta L}{L}\right)_{Castable} = \left(\frac{\Delta L}{L}\right)_{Reaction} - \left(\frac{\Delta L}{L}\right)_{Sintering} + \alpha_{castable}\,(T_{max} - T_{RT})$$

$$T_i = T_b = T_{max}$$

$$\overline{bc}: \left(\frac{\Delta L}{L}\right)_{Castable} = \left(\frac{\Delta L}{L}\right)_{Reaction} - \left(\frac{\Delta L}{L}\right)_{Sintering} + \alpha_{castable}\,(T_i - T_{RT})$$

$$T_b \le T_i < T_c$$

$$c: \left(\frac{\Delta L}{L}\right)_{Reaction} = \left(\frac{\Delta L}{L}\right)_{Sintering} \qquad T_i = T_c$$

Where $\left(\frac{\Delta L}{L}\right)_{Castable}$ is the thermal expansion of castable mix. $\left(\frac{\Delta L}{L}\right)_{Reaction}$ is the expansion from the reaction of MgO and Al_2O_3, $\left(\frac{\Delta L}{L}\right)_{Sintering}$ is the shrinkage of castable mix due to the high temperature sintering, $\alpha_{castable}$ is the average thermal expansion coefficient of MgO-Al_2O_3 castable mixes, T_{RT} is room temperature, T_i is the temperature at any point i and T_{max} is the temperature at maximum thermal expansion.

Following this model, when T<Ta, the thermal expansion of castable mix presents the reversible linear expansion, however, while T>Ta, the overall expansion of MgO-Al_2O_3 castable is affected by both the $\left(\frac{\Delta L}{L}\right)_{Reaction}$ and $\left(\frac{\Delta L}{L}\right)_{Sintering}$. At point b, spinel formation has nearly ceased to progress, on the other hand, shrinkage due to the sintering of mix components begins to dominate, at point C, the expansion from spinel formation is equivalent to the sintering shrinkage from mix components.

4.5 Thermal Expansion Behaviors of MgO-Al_2O_3 Castable Mixes without SiO_2 Fume Addition

4.5.1 Thermal Expansion Behavior from 25°C to 1100°C

The thermal expansions versus temperatures are illustrated in Figure 4.4 through Figure 4.6 for the first three groups of castables defined in Table 4.1

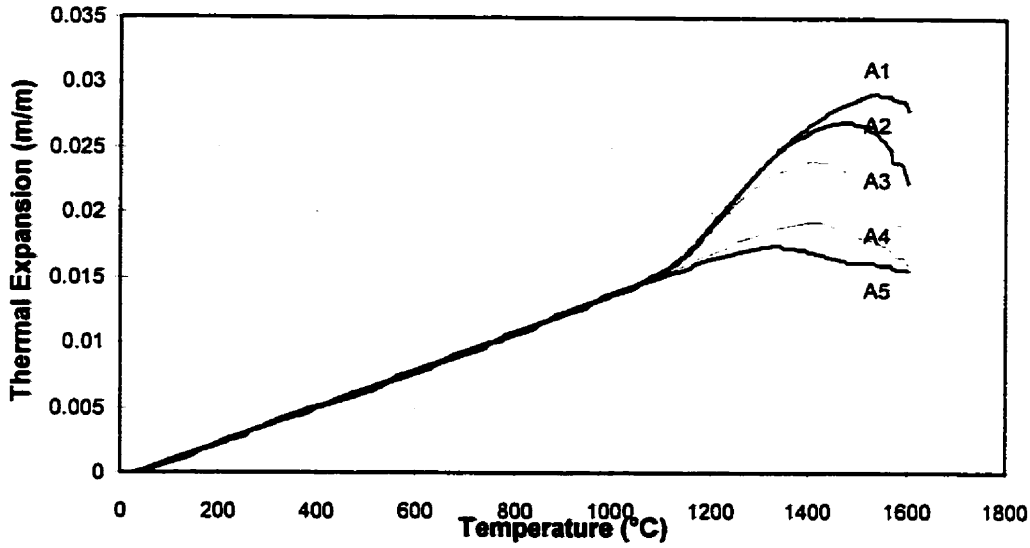

Figure 4.4 Thermal Expansion of $MgO-Al_2O_3$ Castables without Spinel Addition (A1-A5) versus Temperatures

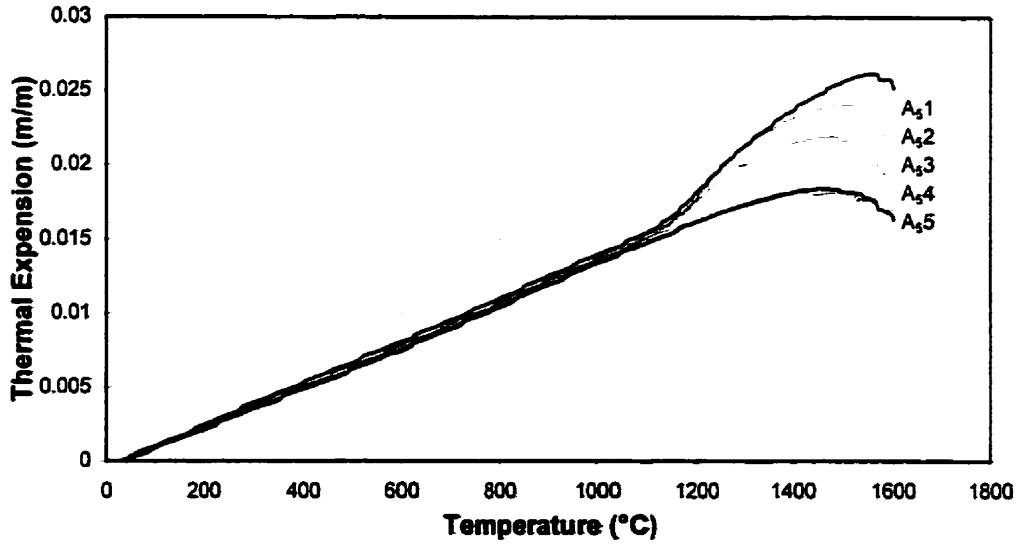

Figure 4.5 Thermal Expansion of $MgO-Al_2O_3$ Castables with 5% Spinel Addition ($A_5$1-$A_5$5) versus Temperatures

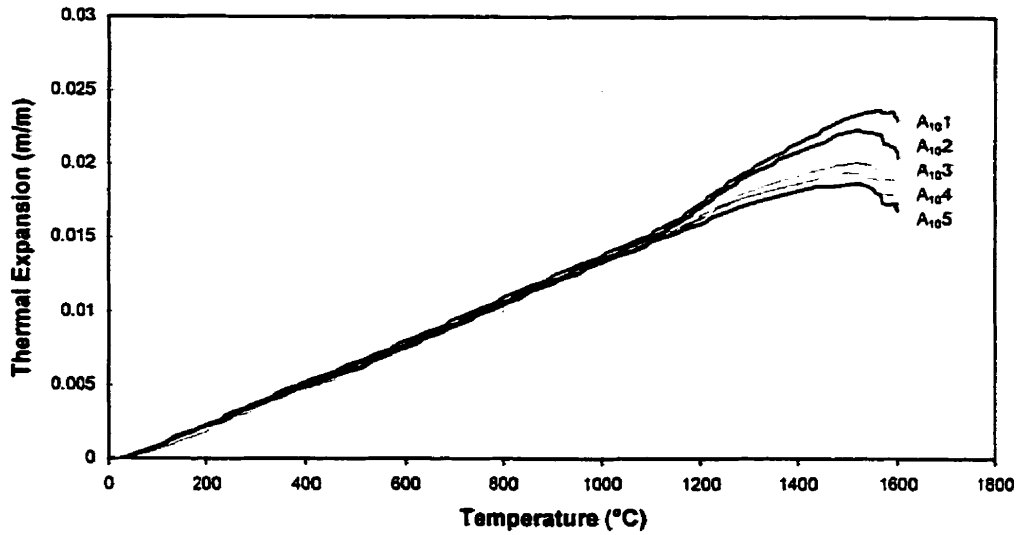

Figure 4.6 Thermal Expansion of $MgO-Al_2O_3$ Castables with 10% Spinel Addition ($A_{10}1$-$A_{10}5$) versus Temperatures

The thermal expansion of each castable, regardless of their compositions, exhibits a similar linear increase with increasing temperature up to 1100°C . It is thus deduced that the starting temperature of spinel formation is around 1100°C. Table 4.6 lists those thermal expansion coefficients of tested mixes between 25°C and 1100°C as calculated through a regression analysis. The correlation coefficient of R^2 for each regression is greater than 0.99.

Table 4.6 Thermal Expansion Coefficient of $MgO-Al_2O_3$ Castable Mix between 25°C and 1100°C through a Regression Analysis

Sample Number	Expansion Coefficient (1 /°C) (25-1100 °C)	Sample Number	Expansion Coefficient (1 /°C) (25-1100 °C)	Sample Number	Expansion Coefficient (1 /°C) (25-1100 °C)
A1	1.43×10^{-5}	A_51	1.43×10^{-5}	$A_{10}1$	1.43×10^{-5}
A2	1.41×10^{-5}	A_52	1.40×10^{-5}	$A_{10}2$	1.40×10^{-5}
A3	1.42×10^{-5}	A_53	1.42×10^{-5}	$A_{10}3$	1.39×10^{-5}
A4	1.41×10^{-5}	A_54	1.40×10^{-5}	$A_{10}4$	1.40×10^{-5}
A5	1.42×10^{-5}	A_55	1.40×10^{-5}	$A_{10}5$	1.38×10^{-5}

The average thermal expansion coefficient is $1.41\pm0.2\times10^{-5}$ $°C^{-1}$. It corresponds well to the α value for MgO coarse grain reported by Edwin Ran etc.[115], 1.51×10^{-5} $°C^{-1}$ for fused MgO's brick, and by Morrel [55], 1.40×10^{-5} $°C^{-1}$ for magnesia single crystal. In other words, the thermal expansion coefficient of $MgO-Al_2O_3$ castable mixes from 25°C to 1100°C actually depends on the expansion coefficient of MgO aggregates in the mix. All other fine grains do not significantly affect the overall expansion of the castable. Figure 4.7 shows the expansion and shrinkage behaviors of MgO coarse aggregate, Al_2O_3, spinel AR_{90} and MgO fine powders taken separately as well as castable A3.

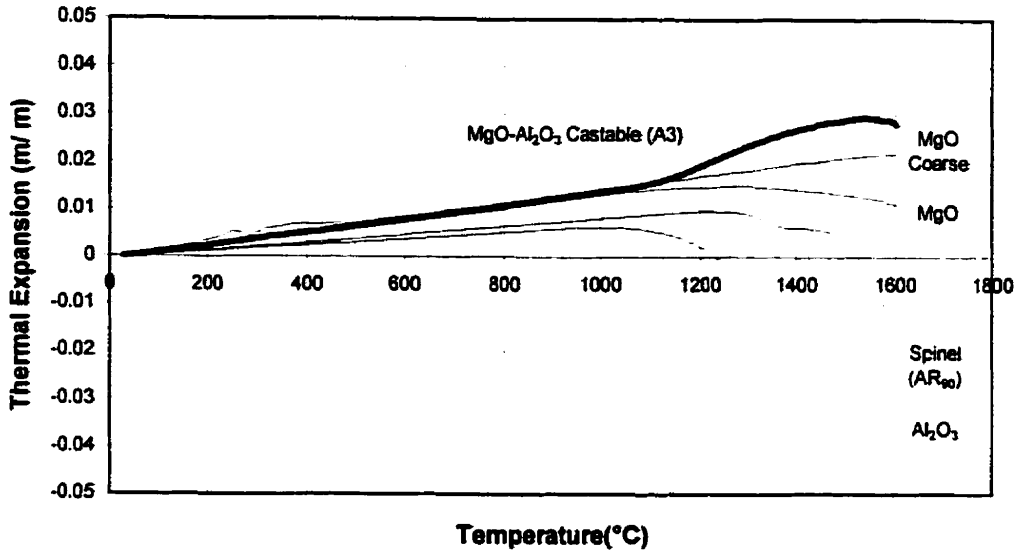

Figure 4.7 Thermal Behavior of MgO Aggregate, Al_2O_3, Spinel and MgO Fine Powders as well as of Castable A3

Obviously, the thermal expansion of MgO aggregate does overlap with the castable A3 at temperature range from 25°C to 1100°C, and also is predominant over those spinel and Al_2O_3 fine powders.

Additionally, the theoretical consideration from Turner's Equation [116] also agrees well with this conclusion. Turner assumed that each component in mixtures is constrained to change dimensions with temperature at the same rate as the aggregate with negligible shear stresses between particles, then

$$\alpha_m = \frac{\sum_{i=1}^{n}(\alpha_i W_i E_i / \rho_i)}{\sum_{i=1}^{n}(W_i E_i / \rho_i)} \qquad (4.1)$$

Where α_m and α_i are the overall and individual phase thermal expansion coefficient respectively, the E_i is Young's elastic moduli, and the W_i is weight fraction while ρ_i is density.

Through the calculations in Eq (4.1) for fifteen castable mixes defined in Table 4.1. with at least 75% MgO aggregates in the mix, the contribution for thermal expansion coefficient from those fine powders of Al_2O_3 and pre-reacted spinel can only vary the mix value α $\pm 0.07\times10^{-5}$/°C. Therefore, it can be concluded that the thermal expansion of MgO-Al_2O_3 castable mixes, at temperature below 1100°C, significantly depends on the magnesia aggregate expansion (1.38 to 1.43×10^{-5}/°C only).

4.5.2 Thermal Expansion Behavior from 1100°C to 1600°C

Table 4.7 gives the maximum thermal expansion $\left(\frac{\Delta L}{L}\right)_{max}$, the temperature at maximum thermal expansion (T_{max}) and the permanent linear change (PLC) for each mix. A regular variation with compositions in group 1, 2 and 3 can be clearly observed.

Table 4.7 The Temperature at Maximum Thermal Expansion, the Maximum Thermal Expansion and the Permanent Linear Change for $MgO-Al_2O_3$ Castable Mixes in Group 1 to 3 of Series 1

	(T_{max}) (°C)	$\left(\frac{\Delta L}{L}\right)_{max}$ (%)	$\left(\frac{\Delta L}{L}\right)_{RT}$ (%)
A1	1541	2.9	1.1
A2	1486	2.7	0.2
A3	1410	2.4	-0.3
A4	1408	1.9	-0.6
A5	1338	1.8	-0.9
$A_5$1	1556	2.6	0.8
$A_5$2	1501	2.4	0.1
$A_5$3	1464	2.2	-0.1
$A_5$4	1455	1.8	-0.4
$A_5$5	1429	1.8	-0.5
A_{10}1	1564	2.4	0.5
A_{10}2	1524	2.2	0.1
A_{10}3	1521	2.0	-0.2
A_{10}4	1501	2.0	-0.3
A_{10}5	1518	1.9	-0.3

To further analyze those results and establish their relationships, the amount of in-situ spinel formed in each specimen of A1-A5, after first cycle firing, was quantitatively measured through the internal standard technique of X-ray diffraction.

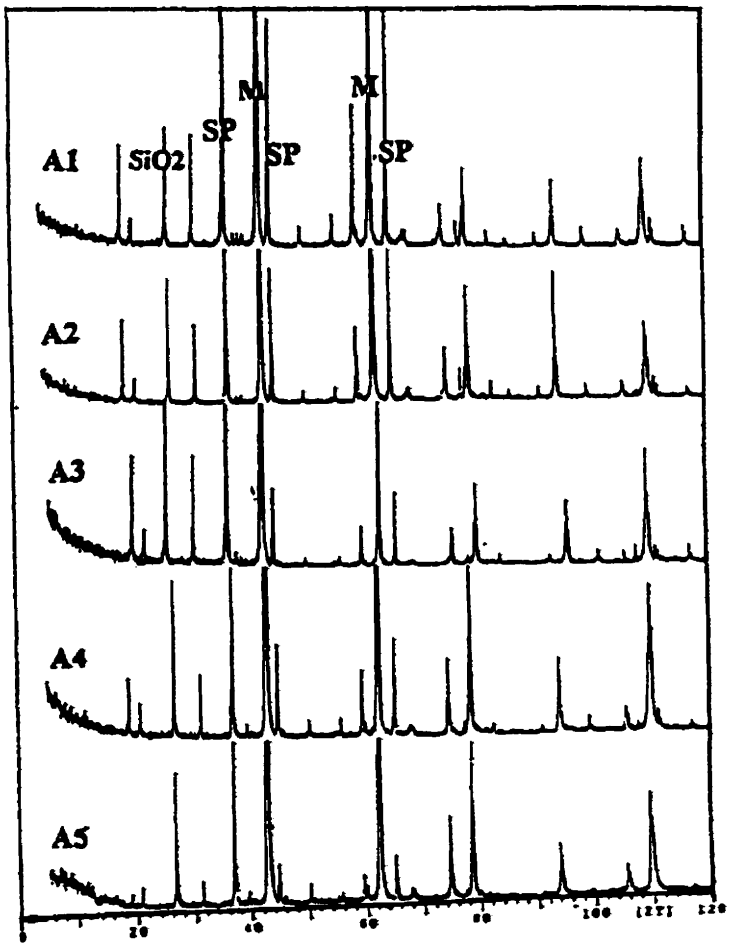

Figure 4.8 X-ray Diffraction Patterns for A1-A5

Figure 4.8 shows the x-ray diffraction patterns of sample A1-A5. On basis of those figures, the precise determination of lattice constant for each sample can be conducted. Since the systematic errors manifest a definite dependence upon differential angle θ, and also tend to a minimum as θ approaches 90° [117], plotting the calculated a_0's against $\cos^2\theta$, and extrapolating at $\cos^2\theta = 0$, yield a_0 values, listed in Table 4.8.

Table 4.8 The Lattice Constants for the In-situ Spinel Formed (A1-A5)

Sample	A1	A2	A3	A4	A5
a_0 (nm)	0.8083	0.8082	0.8080	0.8083	0.8085

Interestingly, regardless of the Al_2O_3 composition variation from sample A1 to A5, the lattice constant of each mix is quite close and the range locates in between 0.8082 ± 0.0003 nm. Compare to the value given in Chapter 2 by Nakagawa et al [14], this shows that the formed in-situ spinels are closed to the stoichiometric composition although the castable mix is a rich magnesia composition.

Since the lattice constant in sample A1-A5 is so similar to the pre-reacted spinel MR_{66} (a_0 = 0.8082 nm). MR_{66} was selected as the internal reference with 5% pure SiO_2 and complement of MgO fine powders. A calibration curve is shown in Figure 4.9.

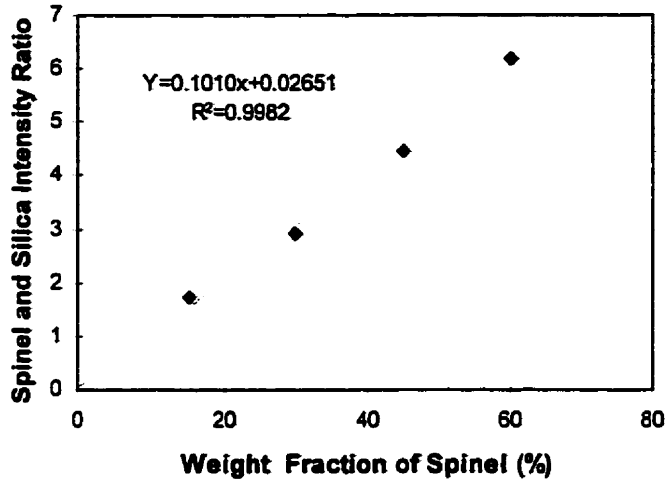

Figure 4.9 The Linearity of Typical Calibration Curve for In-situ Spinel Quantitative Analysis Using Silica (5%) and Pre-reacted Spinel as Internal Standard

Table 4.9 The Amount of In-situ Spinel Formed on the basis of Linearity of Typical Calibration Curve

Sample	A1	A2	A3	A4	A5
I_{spinel}/ I_{SiO2}	3.88	2.25	2.04	1.61	1.34
Amount of Spinel (wt%)	38	22	20	16	13

4.5.2.1 The Maximum Thermal Expansion

Figure 4.10 shows the relationship between thermal expansion and amount of in-situ spinel formation. It can be seen that the maximum thermal expansion is proportional to the amount of in-situ spinel formed.

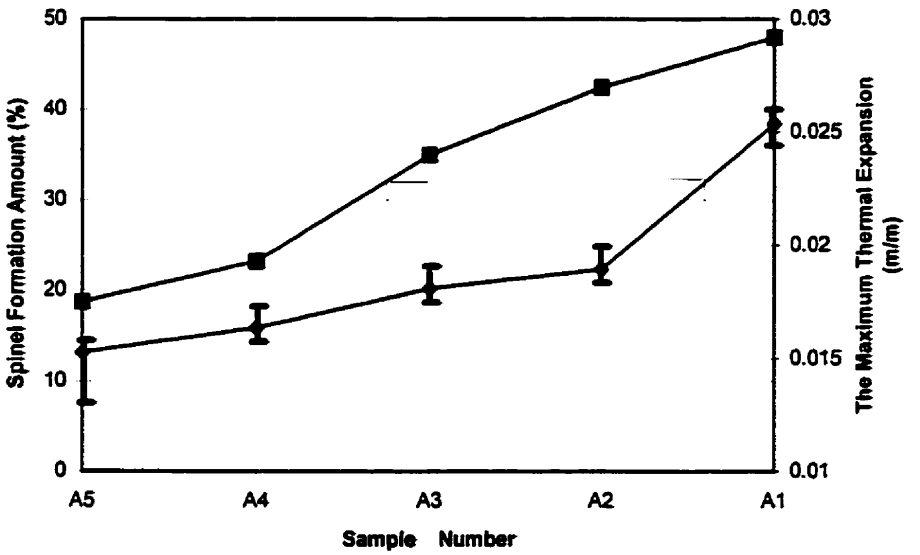

Figure 4.10 The Maximum Thermal Expansions versus the Amount of In-situ Spinel Formed for Sample A1-A5 (No pre-reacted spinel)

In this case, the expansion, obviously, depends on the ratio of Al_2O_3 to MgO in the mix, the higher the Al_2O_3 content, the more the in-situ spinel could be expected, and therefore the higher the maximum thermal expansion. If pre-reacted spinel AR_{90} is added instead of part of Al_2O_3 powders in the mix, the maximum thermal expansion is decreased, however, the direct proportional relation between maximum thermal expansion and in-situ spinel formation amount still follows the same rule as that of sample A1-A5.

With the aid of the phenomenological model given in Figure 4.3, the maximum thermal expansion can be considered as the function of the amount of in-situ spinel formed S_{in}, the shrinkage of fine powders S_s and the addition amount of pre-reacted spinel S_p.

As shown in Figure 4.10, it is already known that the maximum thermal expansion is proportional to the amount of in-situ spinel formed S_{in}, which is a direct function of the amount of alumina added.

$$(\frac{\Delta L}{L})_{max} \propto S_{in} \qquad (4.2)$$

On the other hand, the maximum thermal expansion decreases with pre-reacted spinel addition, because the in-situ spinel formation amount is reduced with the pre-reacted spinel addition instead of the same amount of Al_2O_3 powders, consequently, the inverse proportion relation between maximum thermal expansion and pre-reacted spinel addition is observed.

Figure 4.11 illustrates the differences brought by the use of the three levels of spinel grains AR_{90}. Hence

$$(\frac{\Delta L}{L})_{max} \propto \frac{1}{S_P} \qquad (4.3)$$

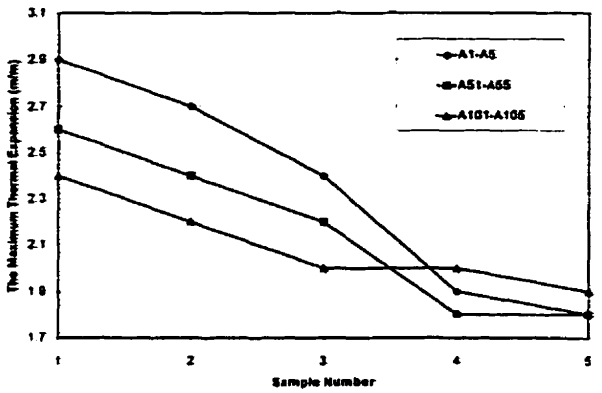

Figure 4.11 The Maximum Thermal Expansion versus Castable Mixes at 0%, 5% and 10% Levels of Spinel (AR_{90}) Addition Respectively.

To document the effect of shrinkage S_s, Al_2O_3 type and addition in the matrix have to be taken into consideration. Figure 4.12 presents the shrinkage of Al_2O_3 mixture in matrix for sample A1, A3, A5, A101 as well as MgO aggregate and fine powders as a function of temperatures.

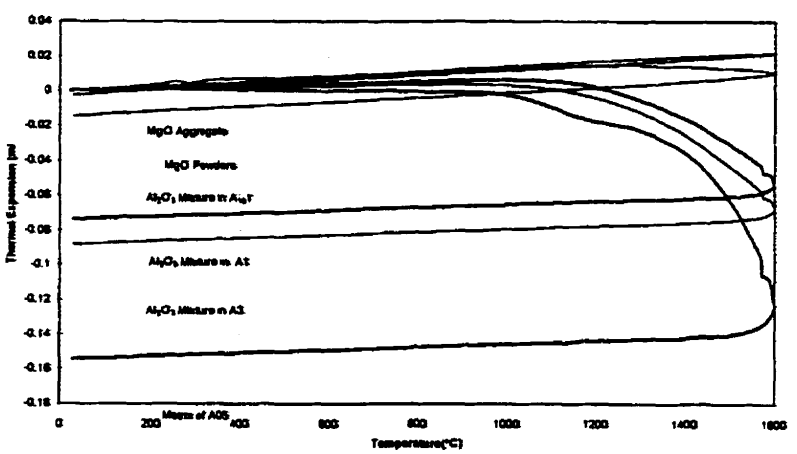

Figure 4.12 The Shrinkage of Al_2O_3 mixture in Matrix of Samples A1, A3, A5 and $A_{10}1$ as well as MgO Aggregate and Fine Grains vs. Temperature.

The shrinkage of MgO aggregate or fine powders is quite smaller than that of Al_2O_3 mixture in three different matrix compositions, in other words, the shrinkage of castable mix during heating and cooling will mainly depend on the Al_2O_3 addition and types in the matrix. Table 4.10 demonstrated the relationship between maximum thermal expansion and shrinkage of Al_2O_3 mixture in the matrix, it is evident that:

$$(\frac{\Delta L}{L})_{max} \propto \frac{1}{S_s} \qquad (4.4)$$

Table 4.10 The Maximum Thermal Expansion and PLC of Al_2O_3 Mixture in Castable Mix A1, A3 and A5

	$(\frac{\Delta L}{L})_{max}$ in Castable Mix (%)	PLC of Al_2O_3 Partition in Matrix (%)
A1	2.9	-7.4
A3	2.4	-8.8
A5	1.8	-15.5

Therefore, a formula to describe the maximum thermal expansion can be given as

$$(\frac{\Delta L}{L})_{max} = f(S_I, S_p, S_s), \quad (\frac{\Delta L}{L})_{max} \propto \frac{S_i}{S_p S_s} \qquad (4.5)$$

Where $(\frac{\Delta L}{L})_{max}$ is the maximum thermal expansion, S_i is the amount of in-situ spinel formed and highly related with Al_2O_3 content in castable mix, Ss is the shrinkage of fine powders and S_p is the addition amount of pre-reacted spinel.

4.5.2.2 The Temperature at Maximum Thermal Expansion

The temperatures at maximum thermal expansion with first three group 1-3 of samples is given in Figure 4.13

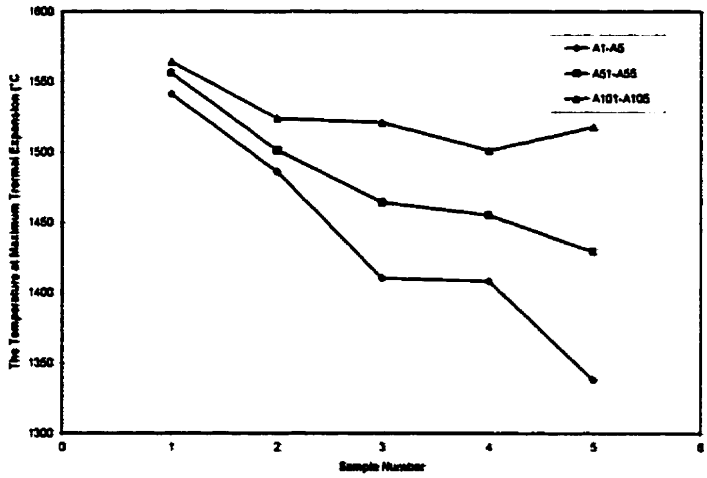

Figure 4.13 The Temperature at Maximum Thermal Expansion vs Spinel AR_{90} Addition of 0%, 5% and 10% respectively and Each Level with Five Compositions of MgO-Al_2O_3 Castable Mixes

Through the phenomenological model, T_{max} is still considered as the function of S_i, S_S and S_p.

From Figure 4.13, it has indicated that the relationships among the temperature at maximum thermal expansion and S_{in}, S_s are

$$T_{max} \propto S_i, \qquad (4.6)$$

$$T_{max} \propto \frac{1}{S_s} \qquad (4.7)$$

which are the exactly same as of $(\frac{\Delta L}{L})_{max}$. Normally T_{max} should be inversely proportional to S_p, however, in this specific case, since Al_2O_3-rich spinel AR_{90} was added into the castable mix, it will further react with MgO to change its spinel composition from Al_2O_3-rich to stoichiometric composition, and the reaction accompanies with volume expansion, hence

$$T_{max} \propto S_p \qquad (4.8)$$

Therefore, in case of alumina rich spinel AR_{90} addition, the temperature at maximum thermal expansion may be expressed as :

$$T_{max} = f(S_i, S_p, S_s), \quad T_{max} \propto \frac{S_i S_p}{S_s} \qquad (4.9)$$

Where S_i is the in-situ spinel formation amount, S_s is the sintering shrinkage of castable mix and S_p is the amount of pre-reacted spinel added.

In summary, based on the analyses of thermal expansion behavior and phenomenological expansion model of $MgO\text{-}Al_2O_3$ castable mixes, the following equation to represent the thermal expansion of the $MgO\text{-}Al_2O_3$ castable mixes:

$$\left(\frac{\Delta L}{L}\right)_T = \begin{cases} \alpha\,(T\text{-}T_0) & T_0 \le T < 1100°C \quad (4.10) \\ \alpha\,(1100\text{-}T_0)\left(\frac{T-T_{max}}{1100-T_{max}}\right)^2 + \left[1-\left(\frac{T-T_{max}}{1100-T_{max}}\right)^2\right]\left(\frac{\Delta L}{L}\right)_{max} & (4.11) \end{cases}$$

$$(\frac{\Delta L}{L})_{max} = f(Si, Sp, Ss), \quad (\frac{\Delta L}{L})_{max} \propto \frac{S_i}{S_p S_s} \qquad (4.12)$$

$$T_{max} = f(Si, Sp, Ss), \quad T_{max} \propto \frac{S_i S_p}{S_s} \quad (AR_{90}\text{ addition}) \qquad (4.13)$$

$$T_{max} = = f(Si, Sp, Ss), T_{max} \propto \frac{S_i}{S_s S_p} \quad (AR_{78}\text{ or }MR_{66}\text{ addition}) \qquad (4.14)$$

Where $\left(\frac{\Delta L}{L}\right)_T$ is the thermal expansion at temperature T, $(\frac{\Delta L}{L})_{max}$ is the maximum thermal expansion, T_{max} is the temperature at maximum thermal expansion, T_0 is the room temperature, α is the reversible average thermal expansion coefficient of $MgO\text{-}Al_2O_3$ castable, S_i is the in-situ spinel formation amount in the castable, S_s is the sintering shrinkage of castable mix and S_p is the amount of pre-reacted spinel added.

4.5.2.3 The Effects of Pre-reacted Spinel Addition (AR_{90}) on the Permanent Linear Change (PLC)

The measured values of shrinkage at room temperature after one cycle are shown in Table 4.11.

Table 4.11 The Effects of Pre-reacted Spinel Addition (AR_{90}) on PLC of $MgO-Al_2O_3$ Castables

	Pre-reacted Spinel Addition (%)	The Shrinkage at Room Temperature $(\Delta L/L)_{RT}$ (%)
A1	0	1.1
$A_5$1	5	0.8
A_{10}1	10	0.5
A2	0	0.2
$A_5$2	5	0.1
A_{10}2	10	0.1
A3	0	-0.3
$A_5$3	5	-0.1
A_{10}3	10	-0.2
A4	0	-0.6
$A_5$4	5	-0.4
A_{10}4	10	-0.3
A5	0	-0.9
$A_5$5	5	-0.5
A_{10}5	10	-0.3

The permanent linear changes are compensated by adding pre-reacted spinel AR_{90}. In the case of higher Al_2O_3 content, the permanent linear changes of castable mix are reduced with pre-reacted spinel addition instead of part of Al_2O_3 powders, for example, A1 and $A_{10}1$ or A2 and $A_{10}2$. On the other hand, PLC values increase with increasing spinel addition of higher MgO content, such as for A4 and $A_{10}4$ or for A5 and $A_{10}5$.

4.5.3 The Effect of Different Type of Pre-reacted Spinel Addition on Thermal Expansion

Adding pre-reacted spinel MR_{66} or AR_{78} instead of AR_{90} into MgO-Al_2O_3 castable mixes presents similar thermal expansion behaviors as for AR_{90} (see Figure 4.14 and 4.15). In other words, the maximum thermal expansion of MgO-Al_2O_3 castable mixes can be reduced with adding any composition of pre-reacted spinel.

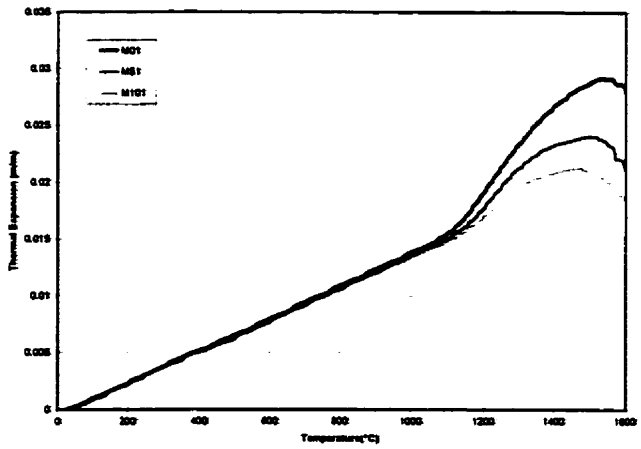

Figure 4.14 Thermal Expansion of MgO-Al_2O_3 Castable Mixes with Spinel MR_{66} Addition at 0, 5%, 10% respectively versus Temperatures

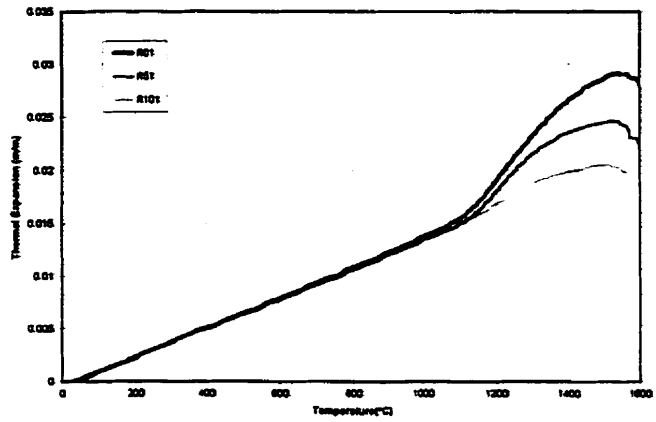

Figure 4.15 Thermal Expansion of MgO-Al_2O_3 Castable Mixes with Pre-reacted Spinel AR_{78} Addition at 0, 5, 10% Respectively versus Temperatures

However, a difference between AR_{90} and MR_{66} or AR_{78} is clearly demonstrated in Figures 4.16 and 4.17. At the same amount of pre-reacted spinel addition, the thermal expansion of castable mix with AR_{90} is much higher than that with MR_{66} or AR_{78}. It is attributed to the possibility of reaction occurring between Al_2O_3-rich spinel AR_{90} and MgO in the castable mix.

To confirm such a reaction, X-ray diffraction analysis has been performed on samples A1, $A_5$1, A_{10}1 as well as AR_{90} , results are shown in Figure 4.18. The precise calculation of lattice constant for each sample was conducted on the basis of the extrapolating method and the results are listed in Table 4.12. Based upon the values given by A. M. Lejus et al, [51], AR_{90} has been transformed to stoichiometric spinel (78% Al_2O_3 instead of 90%).

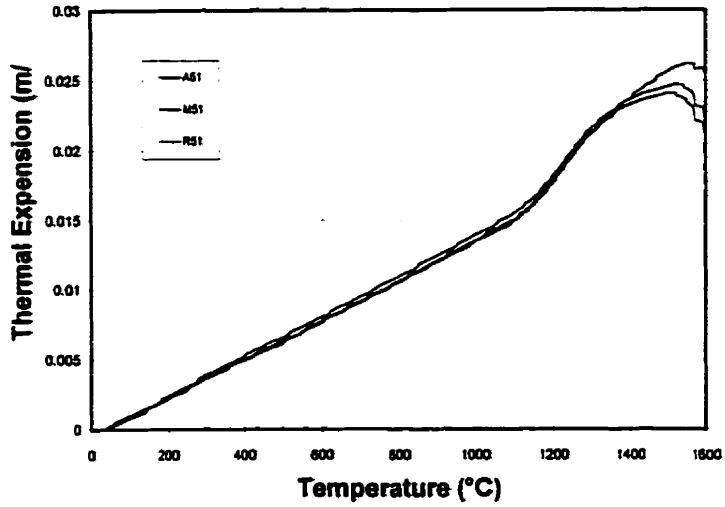

Figure 4.16 Thermal Expansion of $MgO-Al_2O_3$ Castable Mixes with 5% Pre-reacted Spinel AR_{90}, MR_{66} and AR_{78} respectively versus Temperatures

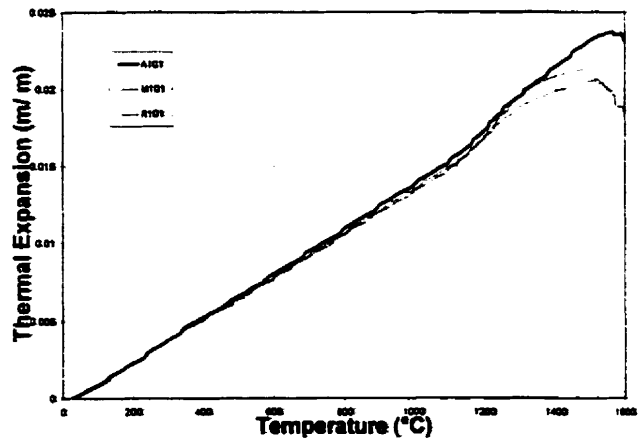

Figure 4.17 Thermal Expansion of $MgO-Al_2O_3$ Castable Mixes with 10% Pre-reacted Spinel AR_{90}, MR_{66} and AR_{78} respectively versus Temperatures

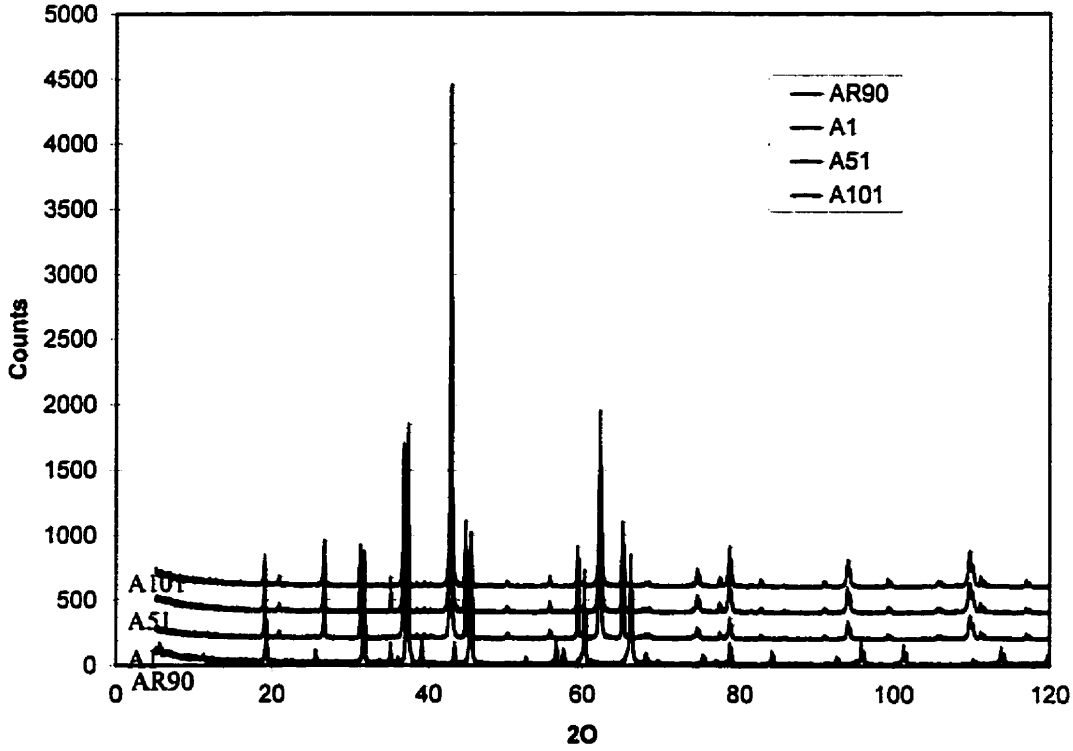

Figure 4.18 The X-ray Diffraction of Samples A1, $A_5$1, A_{10}1 and Pre-reacted Spinel AR_{90}

Table 4.12 The Lattice Constants of Samples A1, $A_5$1, A_{10}1, AR_{90} and Stoichiometric Spinel

Sample	A1	$A_5$1	A_{10}1	Pre-reacted Spinel AR_{90}	Stochiometric Spinel
a_0 (nm)	0.8083	0.8084	0.8083	0.7969	0.8081*

- From Anne-Marie Lejus [51].

4.6 Thermal Expansion Behaviour of MgO-Al_2O_3 Castable Mixes with SiO_2 as Additive

4.6.1 Thermal Expansion Behaviour from 25°C to 1100°C

The relationship between thermal expansion and heating temperature is given in Figure 4.19 and Figure 4.20 respectively.

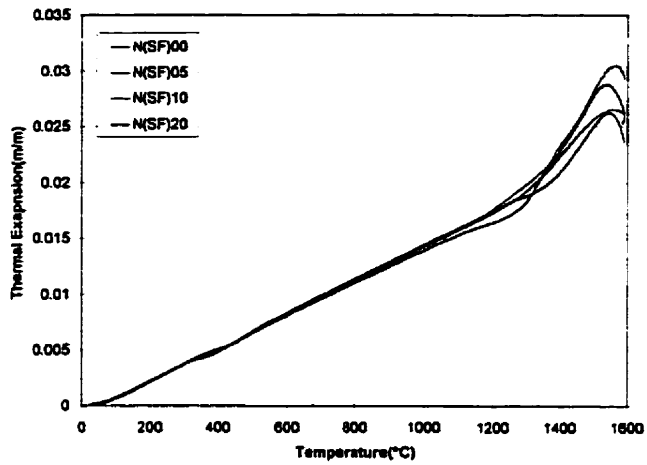

Figure 4.19 Thermal Expansion of $MgO\text{-}Al_2O_3$ Castable Mixes with SiO_2 Fume without Pre-reacted Spinel AR_{78} Addition versus Temperatures

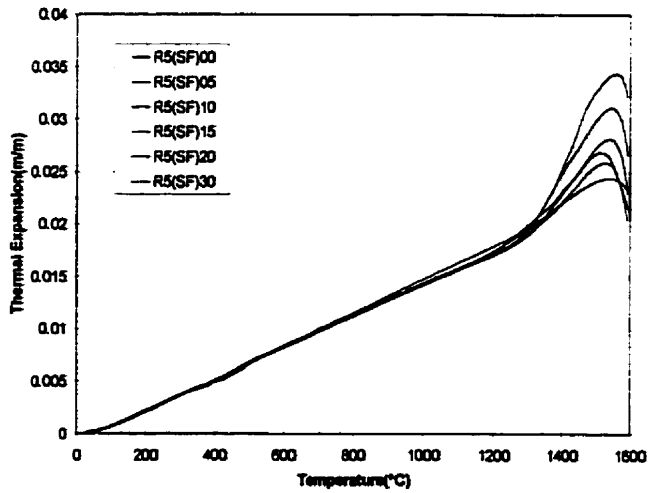

Figure 4.20 Thermal Expansion of $MgO\text{-}Al_2O_3$ Castable Mixes with SiO_2 Fume and Pre-reacted Spinel AR_{78} Added versus Temperatures

From room temperature to 1100°C, all samples present the linear relationship between thermal expansion and heating temperature, in other words, regardless of SiO_2 fume or AR_{78} addition, the thermal expansion coefficient is constant for each castable mix. The regression analysis results (R^2 ≥0.99 per each) are shown in Table 4.13. The average thermal expansion coefficient is $1.50\pm0.20\times10^{-5}$ / °C, slightly higher than the value quoted in Table 4.6.

Table 4.13 Thermal Expansion Coefficients between 25°C and 1100°C of $MgO-Al_2O_3$ Castable Mixes with SiO_2 Fume Addition through a Regression Analysis

Sample Number	Expansion Coefficient (1 /°C) (25-1100 °C)	Sample Number	Expansion Coefficient (1 /°C) (25-1100 °C)
$N(SF)_{00}$	1.51×10^{-5}	$R_5(SF)_{05}$	1.50×10^{-5}
$N(SF)_{05}$	1.52×10^{-5}	$R_5(SF)_{10}$	1.50×10^{-5}
$N(SF)_{10}$	1.51×10^{-5}	$R_5(SF)_{15}$	1.49×10^{-5}
$N(SF)_{20}$	1.46×10^{-5}	$R_5(SF)_{20}$	1.51×10^{-5}
$R_5(SF)_{00}$	1.56×10^{-5}	$R_5(SF)_{30}$	1.48×10^{-5}

4.6.2 Thermal Expansion Behaviour between 1100°C and 1600°C

4.6.2.1 The Maximum Thermal Expansion

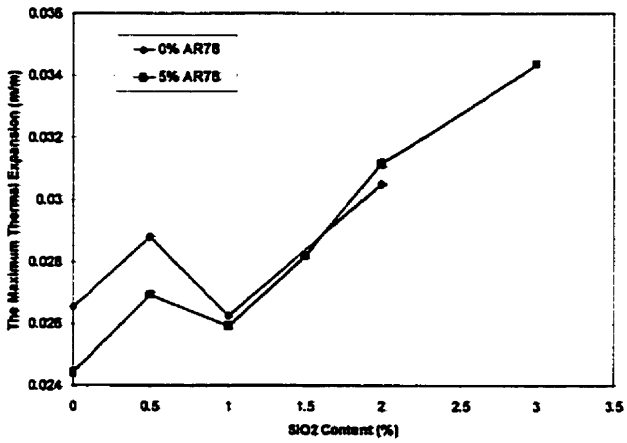

Figure 4.21 The Maximum Thermal Expansion versus SiO_2 Fume Amount in MgO-Al_2O_3 Castable Mixes with or without AR_{78} Addition

Figure 4.21 gives the maximum thermal expansions in relationship with SiO_2 fume addition showing the similarity between castable mixes with and without pre-reacted spinel AR_{78} addition. With an increase of SiO_2 fume, the maximum thermal expansion increases (except at 0.5% SiO_2).

Considering the discussion in previous section, with the SiO_2 fume addition, the maximum thermal expansion should still follow $(\frac{\Delta L}{L})_{max} \propto \frac{S_t}{S_p S_x}$, and be proportional to the in-situ spinel formation amount, therefore, the increase of maximum thermal expansion with SiO_2 fume addition, shown in Figure 4.21, can be considered as

the SiO_2 fume does prompt the in-situ spinel formation, which supports the finding of M. Kobayashi et al [62] discussed in Chapter 2. This is because SiO_2 will easily react with impurities from MgO, or Al_2O_3 raw materials to form liquid phases at high temperatures. This increase in the amount of liquid phase will facilitate the in-situ spinel formation, and of course, the more in-situ spinel formed with the more addition of SiO_2 fume, the higher the maximum thermal expansion will be.

As with AR_{90} grains, the maximum thermal expansion decreases with amount of the pre-reacted spinel AR_{78} added, and so $(\frac{\Delta L}{L})_{max} \propto \frac{1}{S_P}$ as in (4.3).

4.6.2.2 The Temperature at Maximum Thermal Expansion

The temperature at maximum thermal expansion varies with SiO_2 fume and pre-reacted spinel AR_{78} additions. Figure 4.22 shows the relationship between T_{max} and SiO_2 content. Again, $T_{max} \propto \frac{S_i}{S_s S_p}$. For example, at the same amount of SiO_2 fume addition, the T_{max} of castable mix with AR_{78} is smaller than of castable mix without AR_{78}. This is due to $T_{max} \propto \frac{1}{S_P}$, meanwhile, both curves perfectly present the similar trends. Taking one of the two curves, T_{max} at 0.5% of SiO_2 addition gives the smallest value, with further adding SiO_2, T_{max} goes up again.

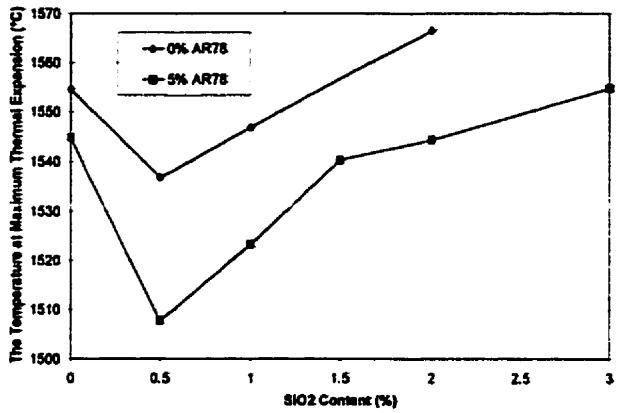

Figure 4.22 The Temperature at Maximum Thermal Expansion vs SiO_2 Addition in Castable Mixes

4.6.2.3 The Effect of SiO_2 Fume Added on the Permanent Linear Change (PLC)

The measured values of shrinkage at room temperature after first cycle heating and cooling are shown in Figure 4.23.

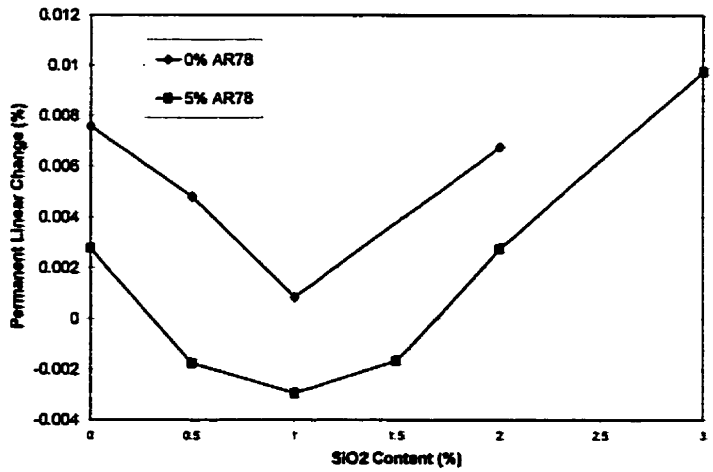

Figure 4.23 The Permanent Linear Change vs Silica Fume Addition

It presents that the PLC decreases with increasing of pre-reacted spinel AR_{78} addition which is the exactly same conclusion as in Section 4.5.2.3. Also, the lowest value of PLC is located at 1% SiO_2 fume addition, this may directly relate to the in-situ spinel formation amount, the liquid formation amount from SiO_2 contribution and the sintering shrinkage in the castable mix.

4.7 A Phenomenological Model of Shrinkage Behavior of $MgO-Al_2O_3$ Castable Mixes during first Cycle Cooling

As shown in previous Figure 4.2 for sample A3, during first cycle cooling, a significant shrinkage is observed. As temperature drops back to room temperature, $\frac{\Delta L}{L}$ decreases linearly with a change of slope at 850°C. This schematically represented in Fig.4.24.

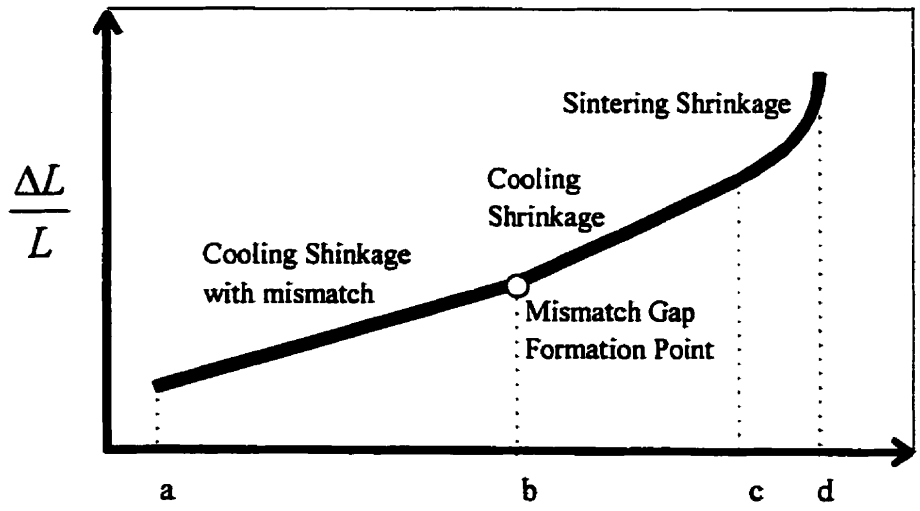

Figure 4.24 A Schematic Representation of Shrinkage Behavior of $MgO-Al_2O_3$ Castable Mixes during First Cycle Cooling

The figure shows that, at elevated temperature ($\overline{dc}$), a more rapid shrinkage occurred as if the sintering process is still active. In the interval ($\overline{cb}$), the relationship between shrinkage and temperature is linear. At point b, a change of slope does occur. This phenomenon is related to the formation of microcracking gaps during cooling. Since thermal expansion coefficients between magnesia and spinel are different [9], the shrinkage of MgO aggregate being larger than that of spinel, the residual stresses induced are so large that they lead to partial debonding and formation of microcracking gaps. Figures 4.25 and 4.26 demonstrate the mismatch gaps observed between aggregate MgO and spinel matrix in the sample A1 and the sample $A_5$5 respectively.

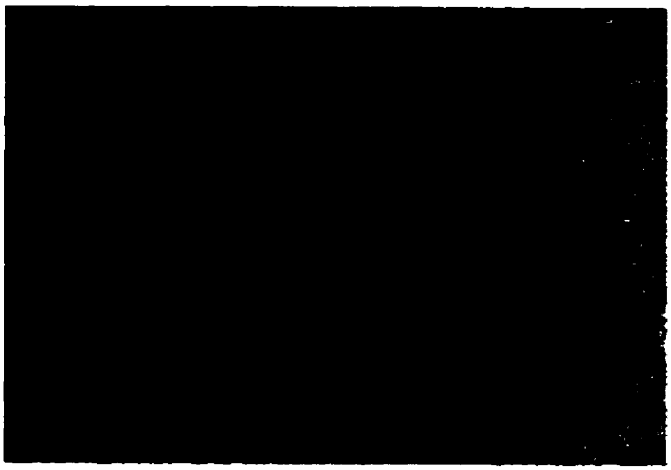

Figure 4.25 Microstructures of Sample A1 without AR_{90} after firing at 1600°C×4hrs . The mismatch gaps are clearly seen (OPM ×50)

Figure 4.26 Microstructure of Sample $A_5$5 with 5% AR_{90} addition after firing at 1600°C × 4hrs (OPM ×100)

4.8 The Shrinkage Behavior of Various MgO-Al_2O_3 Castable Mixes during Cooling from 1600° to 25°C

4.8.1 The Shrinkage Behavior with Pre-reacted Spinel Added

The shrinkage curves shown in Figure 4.27 through Figure 4.29 have the characteristics described in Figure 4.24. Each curve has been linearly fitted for the two linear segments corresponding to $\overline{cb}$ and $\overline{ba}$ in Figure 4.24. The intersection temperature, solution of both fitted linear equations, represents the temperature at which the gap formation (TG) is initiated. All correlation coefficients (R^2) have values higher than 0.997.

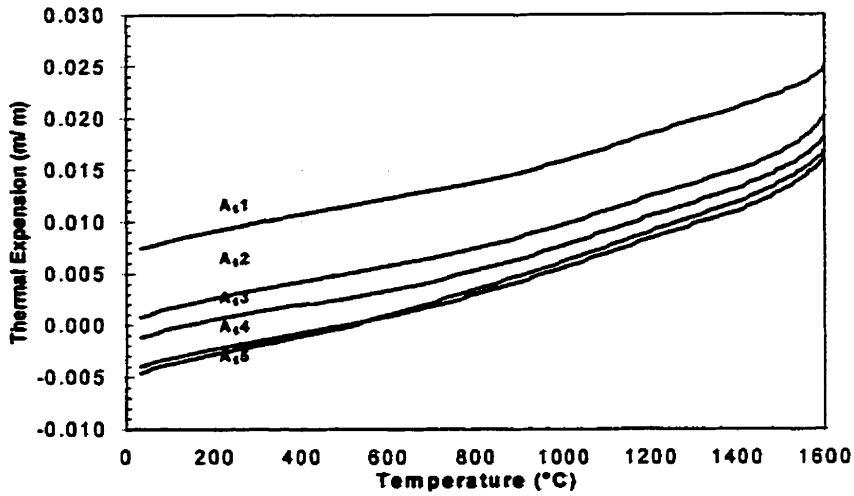

Figure 4.27 Shrinkage Plot for $MgO-Al_2O_3$ Castable without AR_{90} Added

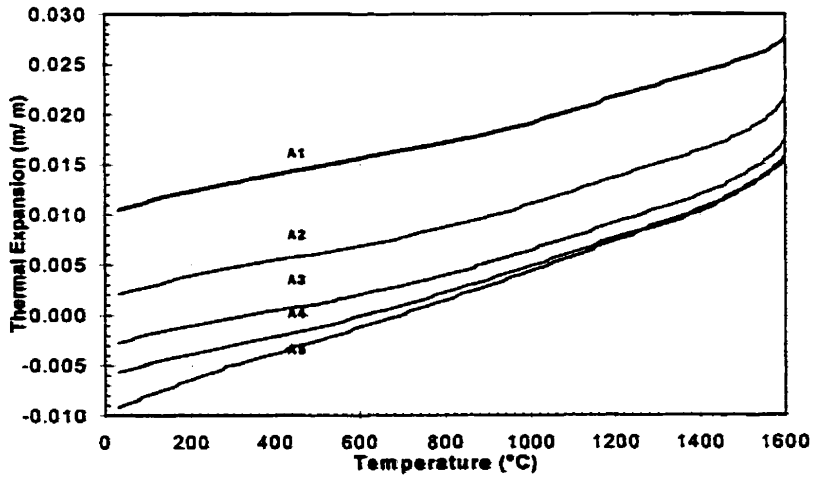

Figure 4.28 Shrinkage Plot for $MgO-Al_2O_3$ Castable with 5% AR_{90} Added

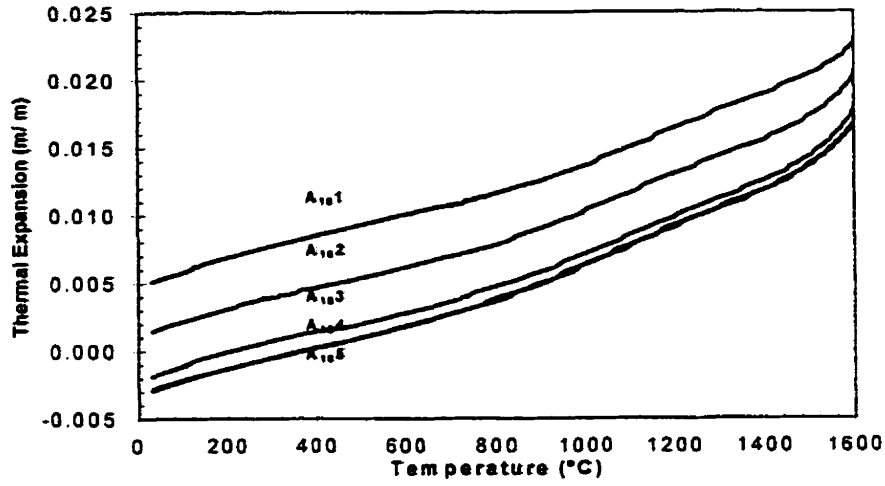

Figure 4.29 Shrinkage Plot for $MgO-Al_2O_3$ Castable with 10% Pre-reacted Spinel Added

Figure 4.30 illustrates the TGs in relation with alumina content and pre-reacted spinel addition in the $MgO-Al_2O_3$ castable mixes. It reveals that TGs significantly increase with the increase in the proportion of alumina and pre-reacted spinel additions. It may be associated with the "bonding ability" between MgO and spinel in the castable mix after sintering.

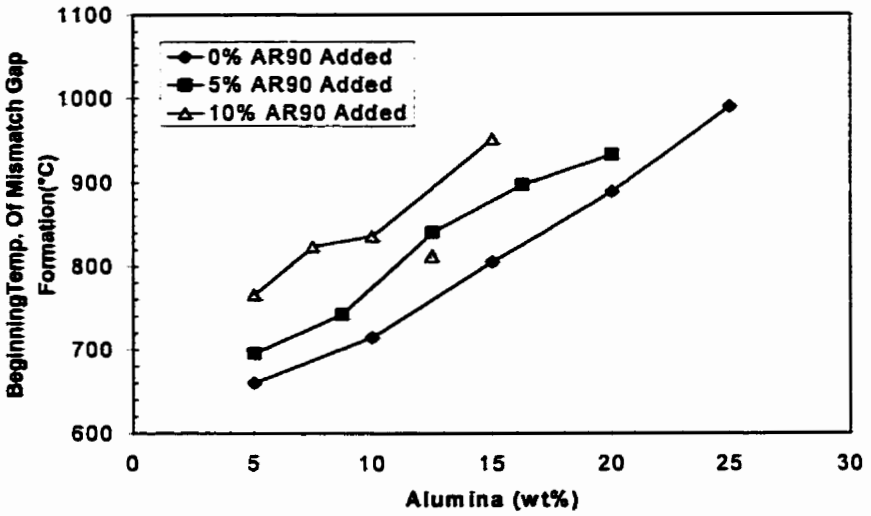

Figure 4.30 Temperature at which Gap Formations are Initiated as a Function of Alumina Content in the $MgO-Al_2O_3$ Castable Mixes

4.8.2 The Shrinkage Behavior with SiO_2 Fume Addition

The shrinkage as a function of cooling temperature at SiO_2 fume addition is given in Figures 4.31and 4.32 for two series of $MgO-Al_2O_3$ castable mixes.

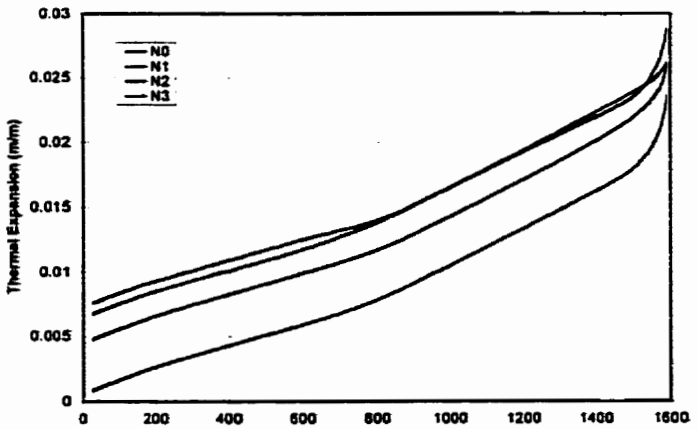

Figure 4.31 Shrinkage Plot for $MgO-Al_2O_3$ Castable Mixes with SiO_2 Fume, but without AR_{78} Added

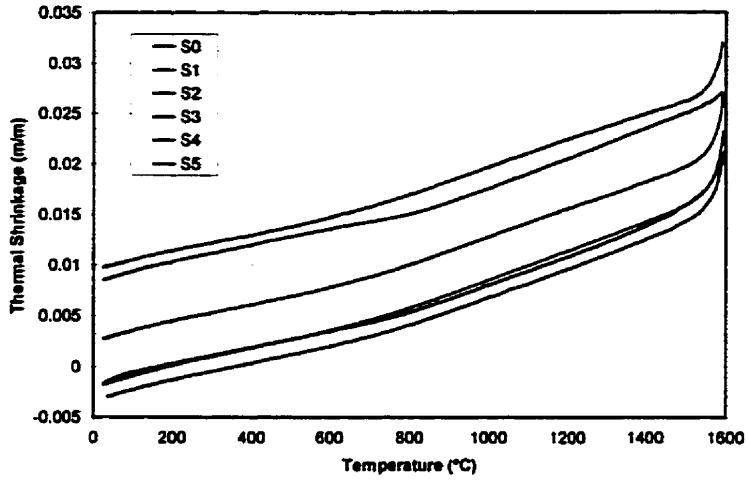

Figure 4.32 Shrinkage Plot for $MgO-Al_2O_3$ Castable Mixes with SiO_2 Fume and AR_{78} Added

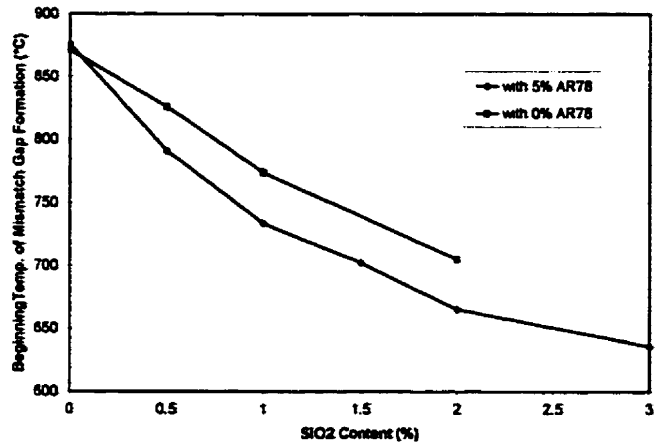

Figure 4.33 Temperatures at which Gap Formations are Initiated as a Function of SiO_2 Content in the $MgO-Al_2O_3$ Castable Mixes

Figure 4.33 demonstrated that TGs significantly depend on the SiO_2 fume addition, meanwhile, with the pre-reacted spinel AR_{78} added, the beginning temperature of mismatch gap formation is reduced. This result may still be due to the "bondability" between MgO aggregate and spinel matrix.

4.8.3 Repeated Temperature Cycles

The thermal expansion-shrinkage plots of $MgO-Al_2O_3$ castable mix ($A_5$1) during the initial, second and third cycle are given in Figure 4.34

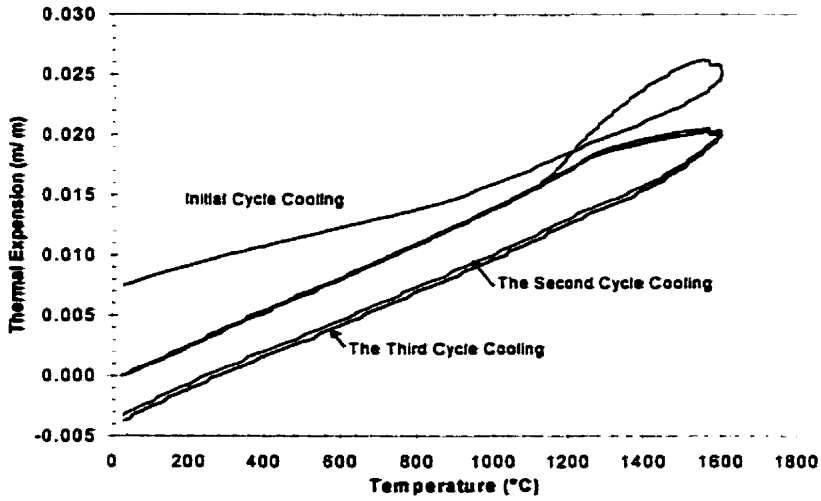

Figure 4.34 The Thermal Expansion-Shrinkage Plots of $MgO-Al_2O_3$ Castable Mix ($A_5$1) during the Initial, Second and Third Heating-Cooling Cycles

The residual permanent expansion or shrinkage after initial cycle heating can be regarded as internal disruption of the castable resulting from incompatible thermal strains between aggregate and matrix. Particularly, in case of $MgO-Al_2O_3$ castable mixes, the "internal disruption" also contributes to the mismatch gaps to be formed , in other words, a sudden relief of residual tensile stress between MgO aggregate and spinel matrix can occur. During the 2^{nd} and 3^{rd} thermal cycle, with same heating-cooling rate, the mismatch gap formation does not reappear .

CHAPTER 5 OPTIMIZATION OF PHYSICAL AND MECHANICAL PROPERTIES

For any castables, physical and mechanical properties are related to the performances in service. For instance, density and porosity of castable are closely relevant to the penetration and thermal shock resistance, meanwhile, the strength properties significantly affect the wear rate and impact resistance of castable. However, many factors will influence on castable properties. They not only depend on the mix composition, mix size and distribution, nature of raw materials, but also rely on selected binders, castable flowability, water addition, as well as the high temperature reaction process and reaction products.

This chapter is divided into two parts. Part I deals with physical and mechanical properties of MgO-Al_2O_3 castable mixes whose compositions were already used to determine thermal expansion behaviors in Chapter 4. The discussion will be focussed on the effects of different grades and additions of pre-reacted spinel. Part II involves those compositions which have been optimized after flowability and thermal expansion tests. The roles of pre-reacted spinel and SiO_2 fume addition on physical and mechanical properties are discussed in details.

5.1 Experimental Procedures

The compositions of tested samples in Part I are given in Tables 4.1 to 4.3, pp55-56, in Chapter 4. The optimized compositions of samples in Part II are shown in Table 5.1.

MgO-Al_2O_3 castable mixes were prepared with sea-water magnesia aggregates (3-170 mesh), magnesia fine powders (-170 mesh), Al_2O_3 powders (-325 mesh) including tabular alumina, fine ground alumina and ultrafine ground alumina, pre-reacted spinel AR_{90}, AR_{78}, MR_{66} as well as silica fume as additive.

Each mixture is firstly dry mixed in a Hobart mixer for 5 minutes. Afterwards, the pre-mixed slurry of magnesia fine powder with water and deflocculant is added and wet mixing is carried out for another 5 minutes. The homogenized mixture is cast into molds of 54 by 64 by 230mm onto a vibrating table. To prevent moisture loss, the samples are covered with polyethylene sheet, kept for 24 hrs before demoulding, then cured at room temperature for 2 days and dried at a temperature of 110°C×24hrs. The measurements of bulk density, porosity, cold modulus of rupture and hot modulus of rupture are done following ASTM standard C830-88, C133-94, C583-80 and C1198-91 respectively.

Table 5.1 Optimized Compositions of Test Samples

	MgO	Al_2O_3	$MgAl_2O_4$	Additive (SiO_2 Fume)
$1N(SF)_{00}$	75	25	0	0
$1M_5(SF)_{00}$	75	20	5	0
$1R_5(SF)_{00}$	75	20	5	0
$1A_5(SF)_{00}$	75	20	5	0
$1R_5(SF)_{10}$	75	20	5	1.0
$2N(SF)_{10}$	75	25	0	1.0
$2R_5(SF)_{10}$	75	20	5	1.0
$2R_{10}(SF)_{10}$	75	15	10	1.0
$2R_{20}(SF)_{10}$	75	5	20	1.0
$3R_5(SF)_{00}$	75	20	5	0
$3R_5(SF)_{05}$	75	20	5	0.5
$3R_5(SF)_{10}$	75	20	5	1.0
$3R_5(SF)_{20}$	75	20	5	2.0
ASP	1.9	96.3	1.9(CaO)	

- For instance: $1R_5(SF)_{10}$ ---- Batch 1, MgO-Al_2O_3 castable with additions of 5 wt% pre-reacted spinel AR_{78} and 0.10 wt% of SiO_2 Fume.
- (SF) --- SiO_2 Fume, N --- No pre-reacted spinel, M---Pre-reacted spinel MR_{66}, R--- Pre-reacted spinel AR_{78}, A--- Pre-reacted spinel AR_{90}
- ASP ---- Commercial product Al_2O_3-MA castable

5.2 Results and Discussion --- Part I

To obtain an idea of experimental error or variability, a repeatability test has been done. Two batches of the same samples in the series of A1 to A5 have been prepared at 15 days interval. The experimental procedures are maintained exactly the same as described in session 5.1 for both batches of castables. Table 5.2 and 5.3 respectively show the physical, mechanical properties and relative repeatability of the two batches.

Table 5.2 The Physical and Mechanical Properties of Two Batches of $MgO-Al_2O_3$ Castable Mixes

		A1		A2		A3		A4		A5	
		1	2	1	2	1	2	1	2	1	2
Apparent Porosity (%)	110°C×24h	14	14	14	15	15	16	16	17	17	18
	1000°C×4h	21		21							
	1600°C×4h	16	18	17	19	18	20	19	20	20	21
Bulk Density (g/cm^3)	110°C×24h	2.97	2.99	2.95	2.93	2.90	2.87	2.86	2.84	2.81	2.77
	1000°C×4h	2.81		2.78							
	1600°C×4h	2.94	2.87	2.91	2.86	2.88	2.83	2.84	2.82	2.79	2.79
Permanent Linear Change(%)	1000°C×4h	0.7	1.0	0.3	0.6	-0.5	-0.4	-0.1	-0.2	-0.3	-0.6
	1600°C×4h	2.5	1.2	2.0	1.2	1.2	0.6	0.4	0.3	0.1	-0.1
Cold Modulus of Rupture (MPa)	110°C×24h	11.2	11.1	8.5	8.3	7.2	6.4	6.1	6.8	4.6	4.7
	1000°C×4h	3.4	1.5	2.4	1.0	2.1	0.3	1.4	0	2.7	0.2
	1600°C×4h	7.7	6.2	5.8	5.7	4.1	3.4	3.9	3.5	4.9	5.8

Table 5.3 The Relative Repeatability of Two Batches of $MgO-Al_2O_3$ Castable Mixes

		Relative Repeatability (%)					Ave. Rel. Repeatability (%)
		A1	A2	A3	A4	A5	
Apparent Porosity (%)	110°C×24h	100	97	97	97	97	98
	1000°C×4h						
	1600°C×4h	94	94	95	95	98	95
Bulk Density (g/cm^3)	110°C×24h	99	99	99	100	99	99
	1000°C×4h						
	1600°C×4h	99	99	99	99	100	99
Permanent Linear Change (%)	1000°C×4h	82	67	89	67	67	74
	1600°C×4h	65	75	67	86	50	69
Cold Modulus of Rupture (MPa)	110°C×24h	100	100	94	95	99	98
	1000°C×4h	61	59	25	0	0	29
	1600°C×4h	89	99	91	95	92	93

The relative repeatability (%) is defined as $\frac{(|d_2 - d_1|)/2}{(d_2 + d_1)/2} \times 100\%$, where d_1 and d_2 are the measured values in batches 1 and 2 respectively. In series A1 to A5, the porosity, density and CMOR values are very close at temperatures of 110°C and 1600°C, however, not as good at intermediate temperature 1000°C. The repeatability of permanent linear changes is only around 70%.

The experimental results for the physical and mechanical properties of MgO-Al_2O_3 castable mixes at spinel additions of 0%, 5%, 10% with spinel grade AR_{90}, AR_{78}, or MR_{66} respectively are given in Tables 5.4 to 5.10.

Table 5.4 Physical and Mechanical Properties of MgO-Al_2O_3 Castable Mixes without Pre-reacted Spinel Addition (Group 1)

		A1	A2	A3	A4	A5
Apparent Porosity (%)	110°C×24h	14	14	15	16	17
	1000°C×4h	21	21			
	1600°C×4h	16	17	18	19	20
Bulk Density (g/cm^3)	110°C×24h	2.97	2.95	2.90	2.86	2.81
	1000°C×4h	2.81	2.78			
	1600°C×4h	2.94	2.91	2.88	2.84	2.79
Permanent Linear Change (%)	1000°C×4h	0.7	-0.03	-0.5	-0.1	-0.3
	1600°C×4h	2.5	2.0	1.2	0.4	0.1
Cold Modulus of Rupture (MPa)	110°C×24h	11.2	8.5	7.2	6.1	4.6
	1000°C×4h	3.4	2.4	2.1	1.4	2.7
	1600°C×4h	7.7	5.8	4.1	3.9	4.9

Table 5.5 Physical and Mechanical Properties of $MgO-Al_2O_3$ Castable Mixes with 5% of Pre-reacted Spinel AR_{90} Addition (Group 2)

		$A_5$1	$A_5$2	$A_5$3	$A_5$4	$A_5$5
Apparent Porosity (%)	110°C×24h	15	14	16	16	17
	1000°C×4h	23	21			
	1600°C×4h	19	18	19	20	21
Bulk Density (g/cm^3)	110°C×24h	2.95	2.94	2.89	2.86	2.80
	1000°C×4h	2.72	2.82			
	1600°C×4h	2.86	2.89	2.84	2.82	2.78
Permanent Linear Change (%)	1000°C×4h	0.3	0.3	0.03	-0.3	-0.3
	1600°C×4h	2.1	0.6	0.5	0.3	0.03
Cold Modulus of Rupture (MPa)	110°C×24h	8.2	6.2	5.0	6.1	5.0
	1000°C×4h	2.3	0.3	0	0.2	0.1
	1600°C×4h	6.7	5.2	4.1	3.6	3.3

Table 5.6 Physical and Mechanical Properties of $MgO-Al_2O_3$ Castable Mixes with 10% of Pre-reacted Spinel AR_{90} Addition (Group 3)

		A_{10}1	A_{10}2	A_{10}3	A_{10}4	A_{10}5
Apparent Porosity (%)	110°C×24h	15	16	17	17	17
	1000°C×4h	20	21			
	1600°C×4h	20	21	21	22	22
Bulk Density (g/cm^3)	110°C×24h	2.92	2.89	2.85	2.83	2.80
	1000°C×4h	2.83	2.80			
	1600°C×4h	2.81	2.80	2.78	2.76	2.75
Permanent Linear Change (%)	1000°C×4h	0.6	0.4	0.3	0.2	0.2
	1600°C×4h	0.51	0.50	0.4	0.3	0.1
Cold Modulus of Rupture (MPa)	110°C×24h	8.5	6.5	6.3	6.0	4.8
	1000°C×4h	0.5	0.1			
	1600°C×4h	5.8	4.9	3.8	3.6	2.6

Table 5.7 Physical and Mechanical Properties of $MgO-Al_2O_3$ Castable Mixes with 5% of Pre-reacted Spinel AR_{78} Addition (Group 4)

		R_51	R_52	R_53	R_54	R_55
Apparent Porosity (%)	110°C×24h	15	16	16	17	18
	1000°C×4h	21	22			
	1600°C×4h	19	20	20	21	22
Bulk Density (g/cm^3)	110°C×24h	2.94	2.89	2.86	2.83	2.78
	1000°C×4h	2.83	2.77			
	1600°C×4h	2.86	2.82	2.80	2.78	2.75
Permanent Linear Change (%)	1000°C×4h	0.6	0.5	0.4	0.2	-0.01
	1600°C×4h	0.4	-0.07	0.3	0.1	0.04
Cold Modulus of Rupture (MPa)	110°C×24h	6.5	5.6	5.3	4.6	3.7
	1000°C×4h	0.6	0.2			
	1600°C×4h	6.4	5.1	4.2	2.9	3.1

Table 5.8 Physical and Mechanical Properties of $MgO-Al_2O_3$ Castable Mixes with 10% of Pre-reacted Spinel AR_{78} Addition (Group 5)

		$R_{10}1$	$R_{10}2$	$R_{10}3$	$R_{10}4$	$R_{10}5$
Apparent Porosity (%)	110°C×24h	16	17	17	18	18
	1000°C×4h	21	22			
	1600°C×4h	17	21	21	22	22
Bulk Density (g/cm^3)	110°C×24h	2.89	2.85	2.84	2.80	2.77
	1000°C×4h	2.79	2.75			
	1600°C×4h	2.90	2.79	2.78	2.75	2.74
Permanent Linear Change (%)	1000°C×4h	0.4	0.5	0.4	0.3	0.1
	1600°C×4h	0.5	0.3	0.4	-0.1	-0.1
Cold Modulus of Rupture (MPa)	110°C×24h	5.7	5.2	5.1	4.3	3.6
	1000°C×4h					
	1600°C×4h	5.8	4.6	3.5	2.6	0.4

Table 5.9 Physical and Mechanical Properties of $MgO-Al_2O_3$ Castable Mixes with 5% of Pre-reacted Spinel MR_{66} Addition (Group 6)

		$M_5$1	$M_5$2	$M_5$3	$M_5$4	$M_5$5
Apparent Porosity (%)	110°C×24h	15	16	16	16	18
	1000°C×4h	20	21			
	1600°C×4h	19	19	20	20	21
Bulk Density (g/cm^3)	110°C×24h	2.93	2.89	2.87	2.85	2.78
	1000°C×4h	2.83	2.79			
	1600°C×4h	2.85	2.84	2.82	2.82	2.76
Permanent Linear Change (%)	1000°C×4h	0.6	0.6	0.5	0.2	0.1
	1600°C×4h	0.4	0.1	0	-0.1	-0.3
Cold Modulus of Rupture (MPa)	110°C×24h	10.2	8.7	7.9	8.3	4.0
	1000°C×4h	0.6	0.4	0.2	0.3	0.1
	1600°C×4h	7.0	5.2	3.9	2.8	2.5

Table 5.10 Physical and Mechanical Properties of $MgO-Al_2O_3$ Castable Mixes with 10% of Pre-reacted Spinel MR_{66} Addition (Group 7)

		M_{10}1	M_{10}2	M_{10}3	M_{10}4	M_{10}5
Apparent Porosity (%)	110°C×24h	16	16	16	17	18
	1000°C×4h	21	21			
	1600°C×4h	18	19	20	20	22
Bulk Density (g/cm^3)	110°C×24h	2.90	2.87	2.86	2.83	2.78
	1000°C×4h	2.80	2.77			
	1600°C×4h	2.87	2.83	2.82	2.81	2.74
Permanent Linear Change (%)	1000°C×4h	0.5	0.5	0.3	0.2	0.03
	1600°C×4h	0.1	0.1	-0.2	-0.3	-0.3
Cold Modulus of Rupture (MPa)	110°C×24h	9.0	7.8	6.6	6.2	3.8
	1000°C×4h	0.2	0.3	0.2	0.1	0.1
	1600°C×4h	5.2	4.0	3.2	2.8	2.3

5.2.1 The Effects of Al_2O_3 Content in Matrix

From the results shown in Tables 5.3 to 5.9, it can be noticed that, whichever group of MgO-Al_2O_3 castable mixes is considered, the variations of physical and mechanical properties with Al_2O_3 content in the matrix are similar Taking group one, without pre-reacted spinel addition as an example, the physical and mechanical properties at three different temperatures versus Al_2O_3 content in matrix are illustrated in Figures 5.1 and 5.2.

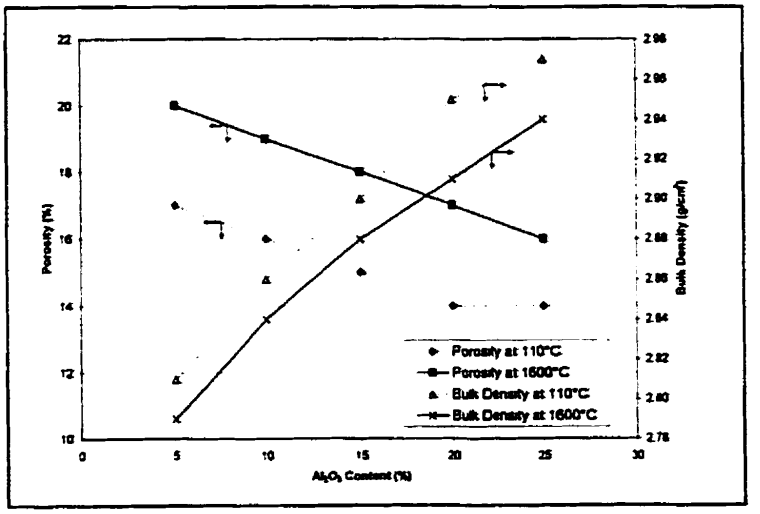

Figure 5.1 Porosity and bulk density as a function of Al_2O_3 content without pre-reacted spinel addition in the mix

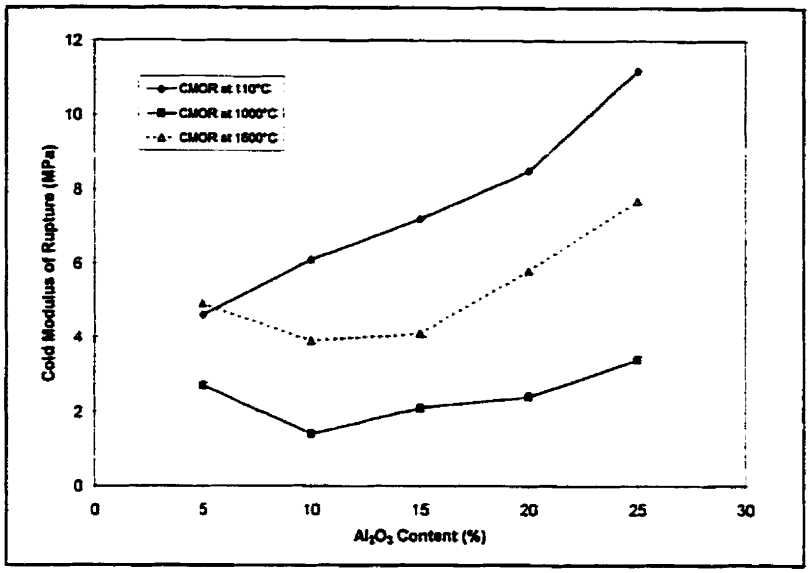

Figure 5.2 CMOR in relationship with Al_2O_3 content, without pre-reacted spinel addition in the mix

As shown in Figures 5.1 and 5.2, an increase of Al_2O_3 content results in an decrease of the castable porosity, while bulk density decreases. The reason is directly related to water addition. To meet the requirement of castable flowability, more water has to be added with the addition of MgO fine powders instead of Al_2O_3 powders into the mix, and therefore increase the porosity and decrease the density. Figure 5.3 shows the water addition with the variation of Al_2O_3 content in the first group of castable mixes.

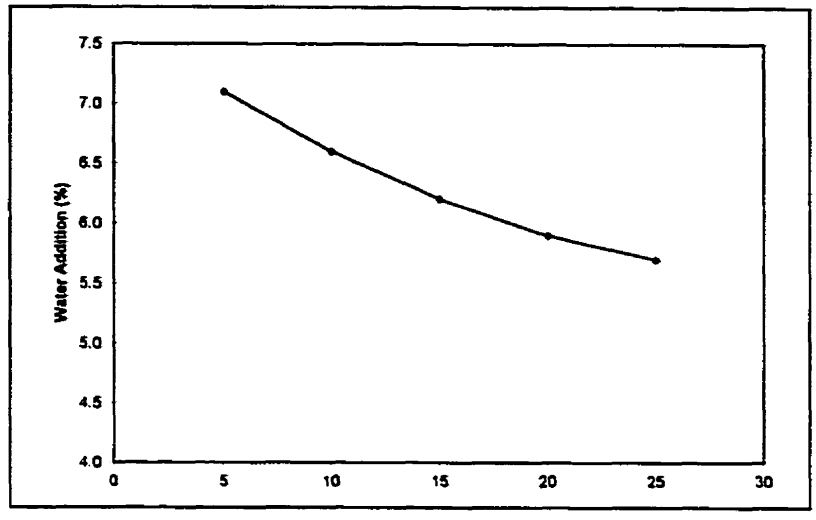

Figure 5.3 Water Addition vs. Al_2O_3 Content in MgO-Al_2O_3 Castable without Pre-reacted Spinel Addition

Nevertheless, a significant difference of porosity or density among sample A1 to A5 is observed only at more than 10wt% alumina intervals.

On the other hand, it also can be seen that the cold modulus of rupture after drying is significantly increased by increasing Al_2O_3 content in the matrix; this is obviously due to the reduction in water addition. After firing at 1600°C, when Al_2O_3 content is more than 15% in the castable, the cold modulus of rupture is still remarkably increased, however, below 15% Al_2O_3, the variation is not significant. As shown in previous section 4.5.2, less Al_2O_3 content will cause less in-situ spinel formed. Figures 5.4 and 5.5 present the microstructures of A1 and A5 mixes. At high alumina content, as in A1, the denser in-situ spinel network has been observed which creates higher bonding ability, meanwhile, at 5% Al_2O_3 as in A5, more pores and fewer in-situ spinel network

can be seen. Therefore, to obtain significant contribution on the strength value with the change of Al_2O_3 amount, more than 15% Al_2O_3 is needed in such MgO-Al_2O_3 castable.

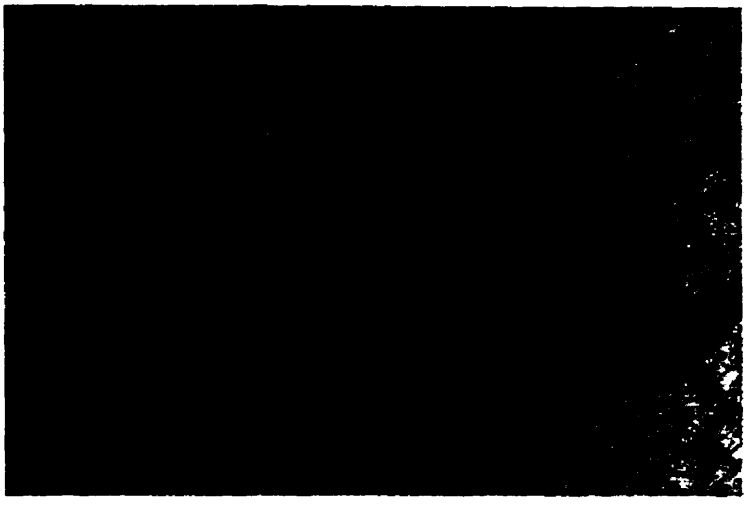

Figure 5.4 The Microstructure of MgO-Al_2O_3 Castable A1 after Firing at 1600°C×4hrs

Figure 5.5 The Microstructure of MgO-Al_2O_3 Castable A5 after Firing at 1600°C×4hrs

5.2.2 The Effects of Pre-reacted Spinel Addition Amount

Regardless of the nature of the pre-reacted spinel added (AR_{90}, AR_{78} or MR_{66}), similarities between physical and mechanical properties as a function of spinel addition amount, have been observed. In the first series, the differences of porosity, bulk density and cold modulus of rupture are significant between castables with and without pre-reacted spinel added at Al_2O_3 content greater than 15 wt %. At Al_2O_3 content less than 15wt%, those differences are not significant.

The microstructures of sample $R_5$1 with 5% AR_{78} is shown in Figure 5.6. More pores and less bonding are formed in $R_5$1 in comparison with A1 in Figure 5.4. This is because in adding pre-reacted spinel instead of fine alumina powders into the castable, more water is needed during casting and less in-situ spinel bonding is to be formed during heating, leading finally, to an increase in porosity and a decrease in cold modulus of rupture.

Figure 5.6 The Microstructure of MgO-Al_2O_3 Castable $R_5$1 with 5% AR_{78} Added after Firing at 1600°C×4hrs

5.2.3 Cold Modulus of Rupture at Intermediate Temperature

The strength ratio between high temperature and intermediate temperature can be used to evaluate the thermal spalling resistance of castable [92]. Obviously, the strength at intermediate temperature is one of the important parameters. Unfortunately, with the pre-reacted spinel AR_{90}, AR_{78} or MR_{66} addition, CMOR values at 1000°C are below 1.0 MPa, with one exception for the sample $A_5$1, while in the series without pre-reacted spinel CMOR values ≥ 3.4MPa.

At room temperature, Actibond reacts with water to form bayerite and bohemite gel [118, 119] and creates binding. However, those bohemite gels decompose and lose bondability around 250°C. The strength is not enhanced until 1000°C, before any sintering can take place. Figure 5.7 represents the cold modulus of rupture values for sample $M_5$1 at different temperatures. The lowest strength measured being at temperature around 1000°C.

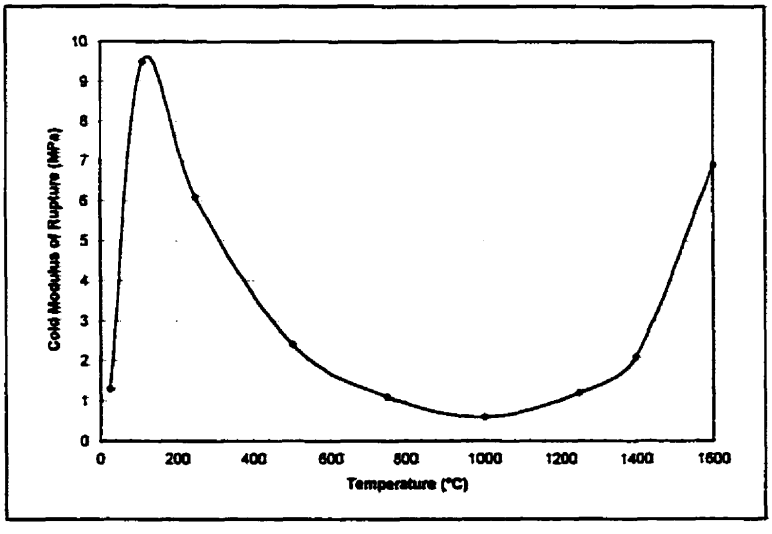

Figure 5.7 Cold Modulus of Ruptures as a Function of Firing Temperature for Sample $M_5$1.

To improve intermediate temperature strengths, 19 new $MgO-Al_2O_3$ castable mixes with 15 different additives have been prepared. The composition for each mix has remained the same except for small amounts of different additives. The experimental procedures remained the same as described in section 5.1. Tables 5.11 and 5.12 give compositions and results of tested samples ITS0 to ITS18 respectively.

Table 5.11 Compositions of Tested Samples with Different Additives

Sample Name	Base Composition			Additive		Remark
	MgO	Al_2O_3	$MgAl_2O_{4(AR_{78})}$	Name	Amount(%)	
ITS0	75	25	0	-	-	Reference
ITS1	75	25	5	-	-	Reference
ITS2	75	25	5	$Al(OH)_3$ Gel. 1	2	
ITS3	75	25	5	$Al(OH)_3$ Gel. 2	2	
ITS4	75	25	5	TiO_2	0.5	
ITS5	75	25	5	TiO_2	1.5	
ITS6	75	25	5	Nano-Al_2O_3	1	
ITS7	75	25	5	Nano-Al_2O_3	2	
ITS8	75	25	5	$AlH_2(PO4)$	0.5	
ITS9	75	25	5	ZrO_2	1	
ITS10	75	25	5	Superfine MgO	2	
ITS11	75	25	5	CA	2	80% Al_2O_3
ITS12	75	25	5	H_3BO_3	0.5	
ITS13	75	25	5	$MgCl_2$	1	
ITS14	75	25	5	$AlCl_3$	1	
ITS15	75	25	5	$Na_3(PO_4)$	2	
ITS16	75	25	5	SiO_2 (A)	0.5	
ITS17	75	25	5	SiO_2 (B)	1	
ITS18	75	25	5	Spinel-Gel	1.5	

Table 5.12 Physical and Mechanical Properties of $MgO-Al_2O_3$ Castables

Sample Name	Apparent Porosity (%)		Bulk Density (g/cm3)		CMOR (MPa)	
	110°C×24 hrs	1000°C×4 hrs	110°C×24 hrs	1000°C×4 hrs	110°C×24 hrs	1000°C× 4hrs
ITS0	14	17	3.03	2.98	12.9	0.9
ITS1	14	20	3.00	2.88	12.0	0.6
ITS2	16	22	2.94	2.81	10.7	0.7
ITS3	16	21	2.93	2.81	11.2	0.8
ITS4	14	20	3.01	2.87	12.8	0.8
ITS5	14	20	3.02	2.88	13.2	0.9
ITS6	12	20	3.01	2.08	14.0	0.8
ITS7	11	20	3.06	2.09	14.3	0.9
ITS8	23	27	2.67	2.59	8.7	0.6
ITS9	14	20	3.01	2.88	13.8	0.6
ITS10	14	17	3.05	2.98	10.2	0.9
ITS11	14	17	3.02	2.95	9.1	0.7
ITS12	15	18	2.95	2.81	6.3	0.6
ITS13	16	23	2.78	2.64	7.0	0.4
ITS14	16	17	3.00	2.97	5.4	1.1
ITS15	17	20	3.00	2.95	6.2	0.5
ITS16	12	20	3.05	2.86	13.9	1.7
ITS17	14	17	3.03	2.98	13.1	3.1
ITS18	14	17	3.04	2.99	14.1	1.0

Focusing on the cold modulus of ruptures at 1000°C, all the samples, except for the sample ITS17, show that the intermediate temperature strengths have not been improved at all, even some of them are worst than the reference sample ITS0. However, SiO_2 fume does play an important role in the increasing of strength. For example, with only 0.5% addition, it can significantly improve the intermediate temperature strength of castable up to 3 times of the sample ITS0 without SiO_2. Part II gives the effect of SiO_2 fume on properties of castable in detail.

5.3 Results and Discussion --- Part II

Values of the physical and mechanical properties of new optimized $MgO-Al_2O_3$ castable mixes (given in previous Table 5.1) are presented in Tables 5.13 to 5.15 respectively.

Table 5.13 Physical and Mechanical Properties of $MgO-Al_2O_3$ Castable Mixes with Pre-reacted Spinel and SiO_2 Addition

		$IN(SF)_{00}$	$IA_5(SF)_{00}$	$IR_5(SF)_{00}$	$IM_5(SF)_{00}$	$IR_5(SF)_{10}$
Apparent Porosity (%)	110°C×24h	14	13	13	14	14
	1000°C×4h	17	17	17	17	17
	1600°C×4h	16	16	16	16	15
Bulk Density (g/cm^3)	110°C×24h	3.06	3.05	3.04	3.04	3.03
	1000°C×4h	3.06	2.99	2.98	2.97	2.98
	1600°C×4h	2.96	2.97	2.97	2.98	3.02
Permanent Linear Change (%)	1000°C×4h	0.2	0.2	0.2	0.1	0.2
	1600°C×4h	0.7	0.5	0.5	0.5	-0.1
Cold Modulus of Rupture (MPa)	110°C×24h	12.9	12.5	13.5	12.5	13.1
	1000°C×4h	0.9	0.9	0.8	0.9	3.1
	1600°C×4h	9.7	9.3	8.6	8.9	12.3
HMOR (Mpa)	1400°C×1h	6.4		6.5		4.3

Table 5.14 Physical and Mechanical Properties of $MgO-Al_2O_3$ Castable Mixes at 1% SiO_2 Fume, but with Different AR_{78} Additions

		$2N(SF)_{10}$	$2R_5(SF)_{10}$	$2R_{10}(SF)_{10}$	$2R_{20}(SF)_{10}$
Apparent Porosity (%)	110°C×24hrs	14	14	14	15
	1000°C×4hrs	17	17	17	18
	1600°C×4hrs	15	14	14	16
Bulk Density (g/cm^3)	110°C×24hrs	3.03	3.00	3.00	2.94
	1000°C×4hrs	2.98	2.95	2.95	2.90
	1600°C×4hrs	3.02	3.03	3.03	2.97
Permanent Linear Change (%)	1000°C×4hrs	0.2	0.3	0.2	0.3
	1600°C×4hrs	-0.3	-0.5	-0.5	-0.5
Cold Modulus of Rupture (MPa)	110°C×24hrs	13.1	11.5	10.6	8.7
	1000°C×4hrs	3.1	3.1	2.6	2.0
	1600°C×4hrs	12.3	10.2	8.9	5.7

Table 5.15 Physical and Mechanical Properties of $MgO-Al_2O_3$ castable Mixes at 5% AR_{78}, but with Different SiO_2 Fume Additions

		$3R_5(SF)_{00}$	$3R_5(SF)_{05}$	$3R_5(SF)_{10}$	$3R_5(SF)_{20}$
Apparent Porosity (%)	110°C×24hrs	13	14	14	15
	1000°C×4hrs	17	17	17	17
	1600°C×4hrs	16	16	14	15
Bulk Density (g/cm^3)	110°C×24hrs	3.04	3.02	3.00	2.96
	1000°C×4hrs	2.98	2.96	2.95	2.93
	1600°C×4hrs	2.97	2.98	3.03	2.98
Permanent Linear Change (%)	1000°C×4hrs	0.2	0.1	0.3	0.2
	1600°C×4hrs	0.5	0.2	-0.5	-0.3
Cold Modulus of Rupture (MPa)	110°C×24hrs	13.5	13.4	11.5	13.3
	1000°C×4hrs	0.8	2.6	3.1	4.0
	1600°C×4hrs	8.6	8.9	10.2	10.5

5.3.1 Effects of Different Grades of Pre-reacted Spinel and SiO_2 Fume Additions

From Table 5.13, it can be noticed that no significant differences of physical and mechanical properties can be presented in the optimized compositions with whichever grade of pre-reacted spinel added, but the difference indeed existed between the castable with or without SiO_2 fume addition. The CMOR shows that the strength at 1000°C for sample $1R_5(SF)_{10}$ is nearly 3 times that of sample $1N(SF)_{00}$; this may be contributed to the sintering aid of SiO_2 fume. In addition, 4.3 MPa of HMOR is an acceptable value although HMOR has been reduced with addition of SiO_2 fume in comparison with that of $1N(SF)_{00}$. Therefore, in order to improve the strength at intermediate temperature, adding an appropriate amount of SiO_2 fume is a valid approach.

5.3.2 Effects of Different SiO_2 Addition on CMOR

The results shown in Table 5.12 illustrated that, the CMOR after drying and firing at 1600°C are almost not influenced by 0.5% SiO_2 addition, but the CMOR after firing at 1000°C is significantly increased. Meanwhile, with further addition SiO_2 up to 2.0%, the CMOR still increases, but slowly. Considering the properties at elevated temperature, the proper amount of SiO_2 addition may be between 0.5 to 1.0%.Furthermore, the intermediate temperature strength improvement due to SiO_2, in $MgO\text{-}Al_2O_3$ castable containing 5% AR_{78} is in agreement with the previous result, on $MgO\text{-}Al_2O_3$ castable, without pre-reacted spinel, meaning that SiO_2 does remarkably improve the intermediate temperature strength in such castable with or without pre-reacted spinel.

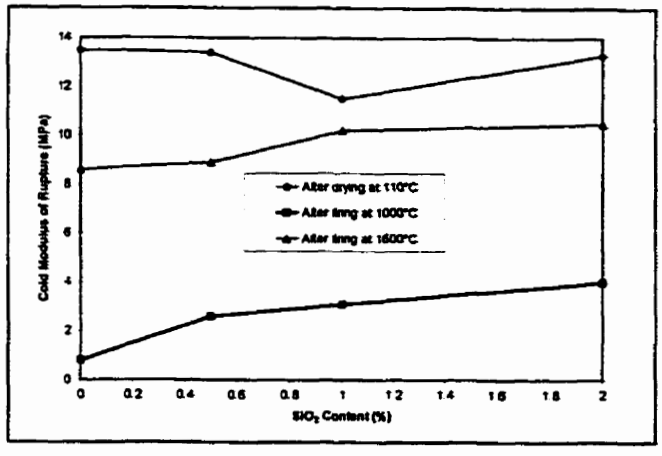

Figure 5.8 CMOR of $MgO-Al_2O_3$ Castable (with 5% AR_{78}) and Different Amounts of SiO_2 Addition

5.3.3 Effects of Pre-reacted AR_{78} Addition on Modulus of Rupture

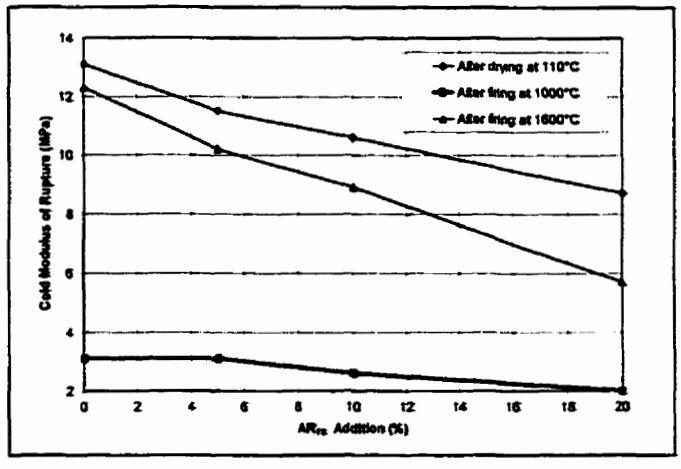

Figure 5.9 CMOR of $MgO-Al_2O_3$ Castable at 1.0% SiO_2 Fume and Different Amounts of AR_{78} Addition

Figure 5.9 shows the cold modulus of rupture as a function of AR_{78} additions from 0 to 20%. At 1.0% SiO_2 fume addition, a significant CMOR difference appears in castable with AR_{78} and without AR_{78} addition.

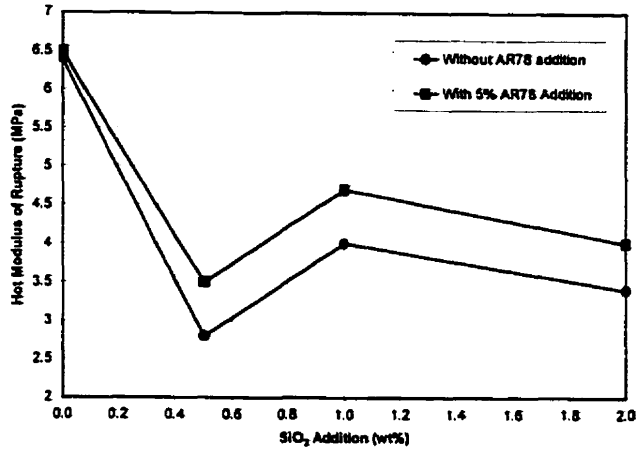

Figure 5.10 HMOR of $MgO-Al_2O_3$ Castable at Different Amounts of SiO_2 Fume and AR_{78} Additions

HMOR values for sample with or without 5% AR_{78} added at different SiO_2 additions are shown in Figure 5.10.

It can be seen that, due to the liquid phase formation, HMOR is reduced with adding SiO_2 into the compositions, however, the HMOR can be improved through addition of pre-reacted spinel AR_{78}. Also, at 0.5% SiO_2 level. The HMOR reaches the lowest value in both cases, with AR_{78} or without AR_{78} in castable, this is agreement with the results related to the maximum thermal expansion analyses discussed in Chapter 4.6.2. It may be related to the lowest liquid viscosity at 0.5% SiO_2 addition, therefore, from those physical and mechanical analysis, 1.0 % SiO_2 fume is recommended as the appropriate addition.

CHAPTER 6 CORROSION RESISTANCE

Corrosion of refractories is a complex phenomenon which involves chemical, physical and mechanical wear processes. Those processes do interact synergistically and promote refractories to be corroded progressively.

Typical corrosion tests for refractories include dipping test where a sample is held in the corrosive medium; induction furnace test where the corrosive medium is melted in a refractory-lined induction furnace; crucible test in which the corrosive medium is melted in a cored-out brick; and rotary slag test where the corrosive medium is melted with an oxy-acetylene flame in a rotating drum, which is lined with sections of refractory.

Corrosion resistance in rotary slag test is evaluated on the basis of corroded refractory thickness or area loss from the original surface. Benefits of this particular method include that multiple samples can be tested at the same time; thermal gradients in samples help to simulate the practical service conditions; and the slag, being renewed, gives a dynamic abrasion component.

In the following study, a rotary slag test has been used to determine the erosion and penetration behaviors of MgO-Al_2O_3 castable.

6.1 Experimental Procedure

The compositions of tested sample are already defined in previous Table 5.1. For the purpose of comparisons, sample $1M_5(SF)_{00}$, $1R_5(SF)_{00}$ and $1A_5(SF)_{00}$ with 5% pre-reacted spinel AR_{90}, AR_{78} and MR_{66} respectively, are considered at first to detect the

effect of adding different grade of pre-reacted spinels. Those samples are also to be compared with the reference sample $1N(SF)_{00}$ to attain the difference between castables with and without spinel addition. Focussing on AR_{78}, the influence of pre-reacted spinel addition level, varying from 5 to 20%, on erosion and penetration indexes of castable is also considered in samples $2N(SF)_{10}$, $2R_5(SF)_{10}$, $2R_{10}(SF)_{10}$ and $2R_{20}(SF)_{10}$.

Meanwhile, SiO_2 fume as an additive has been introduced into castable. Sample $3R_5(SF)_{00}$, $3R_5(SF)_{05}$, $3R_5(SF)_{10}$ and $3R_5(SF)_{20}$ adding with 0, 0.5, 1.0 and 2.0% SiO_2 respectively will show the corrosion difference from SiO_2 addition amount. Finally, the relative comparison of corrosion test results are to be carried out between the developed MgO-Al_2O_3 castable ($1R_5(SF)_{10}$) and commercial Al_2O_3-MA castable (ASP).

MgO-Al_2O_3 castable mixes are prepared from dead-burned seawater magnesia (-3 mesh), calcined or sintered alumina (-325 mesh), hydratable alumina (d_{50}=10 μm), pre-reacted spinel powders (AR_{90}, AR_{78}, MR_{66} , -325 mesh) and silica fume. The chemical and physical properties of those starting materials are given in Tables 1.1 and 1.2 in Chapter 1.

Each mixture is processed sequentially as dry mixing in Hobart mixer for 5 minutes, after adding 4.8% water, wet mixing for another 5 minutes, casting into moulds of 160×40×40mm and finally vibrating on the flow table for 3 minutes. To prevent moisture loss, the samples are covered with polyethylene sheet, kept for 24 hrs before demoulding, then cured at room temperature for 2 days and dried at a temperature of 110°C×24hrs.

For the rotary slag test, the ASTM practice C874-85 has been adopted. The apparatus is schematically shown in Figure 6.1. The nominal dimensions of the sample are 230×80×40mm. In each operation, six samples are bundle up together and lined into an hexagonal shape in the furnace. Insulating grains of alumina are used to fill the gap between samples and steel shell. All the samples are heated up to 1600°C and maintained 2 hours before adding slag. Amount of 0.2 kg slag is added at half hour intervals. The testing temperature is held at 1600°C±15°C for 6-8hrs, measured with a non-contact infra-red radiation pyrometer (Minolta/Land Cyclops 152).

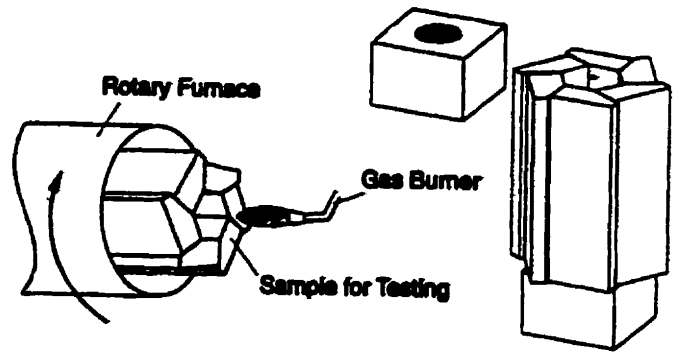

Figure 6.1 Schematic View of Rotary Slag Test Set-up

As reviewed in Chapter 2, the disadvantage of MgO-based refractory is its poor penetration resistance, causing the structural spalling of the material in science. However, for the purpose of attaining the most significant results, a highly ferric basic slag has been selected for the rotary slag tests. The slag composition is given in Table 6.1.

Table 6.1 Chemical Composition of Slag

CaO	SiO_2	Fe_2O_3	MgO	Al_2O_3	MnO	TiO_2	K_2O	Na_2O
36.4	16.5	29.2	12.2	4.96	1.51	0.65	0.01	0.10

The areas of slag erosion and penetration (including the coloration area) are schematically defined in Figure 6.2. Each area is calculated by an approximate integral method, based upon measured depths, in multiple points. The erosion depth is determined by the difference between initial and final remaining depth of the tested sample (d_0-d_1), where the remaining depth does not count the depth of the attached slag layer. The penetration depth represents the depth of the altered layer (d_1-d_3), observed microscopically and partially confirmed by optical microscopy. Additionally, within altered layer, the colored depth, which is easily seen by macro-observation, is calculated by d_1-d_2. The erosion or penetration index is defined as I_s (%) = $\frac{S_i}{S_{ref}}$. Where I_s is the erosion or penetration index based on the erosion or penetration area; S_i and S_{ref} are the eroded or penetrated areas of the i^{th} sample and reference sample respectively.

For post-mortem microstructure examination, the eroded samples are cut in piece, impregnated with epoxy resin, ground and polished using standard ceramographic techniques; an optical microscope and a scanning electron microscope (SEM) with an energy dispersive spectrometer (EDS) detector are used for microstructure analysis. Some samples etched by acid are under the conditions of etch time: 1 min. and acid concentration: 30% H_3PO_4.

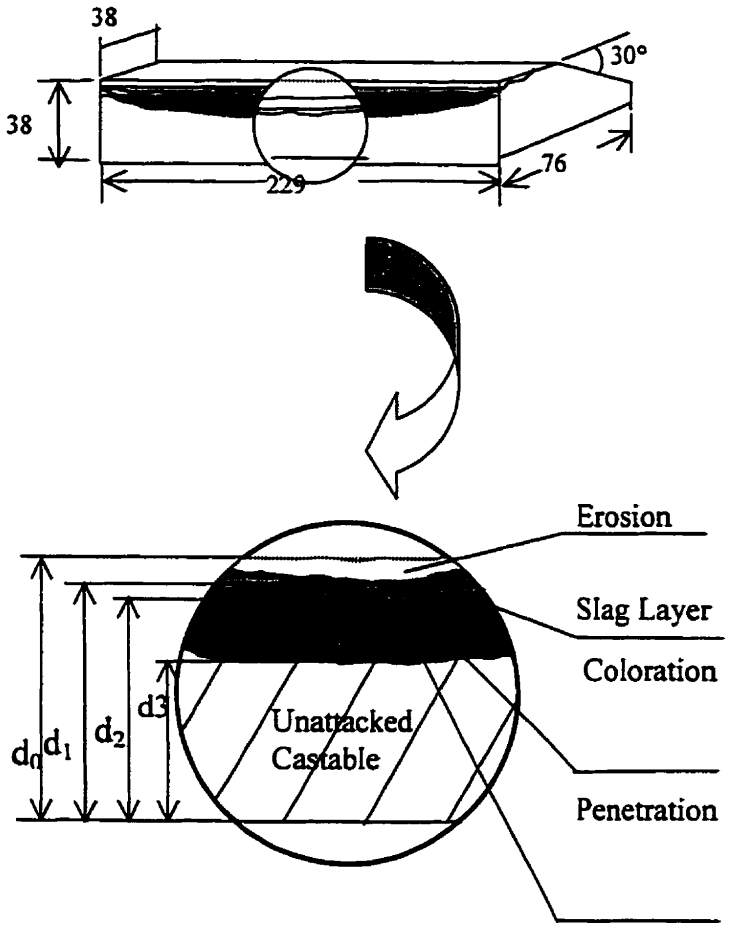

Figure 6.2 Schematic Representation of the Sample after Slag Testing

6.2 Experimental Results

6.2.1 Validation Tests

In order to validate the amount of work done in this thesis, it seems worthwhile first to compare the corrosion resistance of so far developed cement-free, magnesia based castable and a commercially available alumina-spinel based castable. The erosion,

penetration indexes and cross sections of $MgO-Al_2O_3$ castables with or without silica addition and Al_2O_3-MA castable, are shown in Figures 6.3 and 6.4. The numeric values are to be found in Tables 6.2 and 6.3.

Table 6.2 The Erosion, Coloration and Penetration Values of Samples after Rotary Slag Tests (1)

Name	Max. Depth (mm)			Min. Depth (mm)		
	Erosion (d0-d1)	Coloration (d1-d2)	Penetration (d1-d3)	Erosion (d0-d1)	Coloration (d1-d2)	Penetration (d1-d3)
$1N(SF)_{00}$	5.19	11.1	19.19	1.41	6.8	10.06
$1M_5(SF)_{00}$	5.39	10.8	18.59	2.06	6.9	10.51
$1R_5(SF)_{00}$	3.79	11.3	19.79	0.78	7.8	9.63
$1A_5(SF)_{00}$	4.75	14.3	19.25	2.71	8.3	12.33
$1R_5(SF)_{10}$	4.29	11.6	18.87	0.8	6.4	10.5
$2N(SF)_{10}$	3.27	16.0	16.58	1.63	5.0	10.35
$2R_5(SF)_{10}$	4.40	15.3	19.04	1.36	5.3	12.6
$2R_{10}(SF)_{10}$	5.00	12.2	19.63	1.69	5.4	9.91
$2R_{20}(SF)_{10}$	5.07	12.6	18.87	0.88	6.6	9.63
$3R_5(SF)_{00}$	4.70	10.0	16.70	1.14	6.6	9.06
$3R_5(SF)_{05}$	3.88	12.4	12.40	1.23	6.7	10.70
$3R_5(SF)_{10}$	3.67	10.3	18.27	1.51	3.9	8.52
$3R_5(SF)_{20}$	4.21	10.1	18.29	1.68	6.3	9.64
ASP	15.96	0	18	9.13	0	13.55

* d_0, d_1, d_2, d_3 are given in Figure 6.2

Table 6.3 The Erosion, Coloration and Penetration Values of Samples after Rotary Slag Tests (2)

Name	Areas (mm^2)			Average Depth (mm)		
	Ero.	Color.	Pene.	Ero.	Color.	Pene.
$1N(SF)_{00}$	640	1730	2276	3.5	9.5	15.9
$1M_5(SF)_{00}$	651	2100	2124	3.5	9.7	15.21
$1R_5(SF)_{00}$	463	1774	2326	2.5	9.8	15.19
$1A_5(SF)_{00}$	702	1768	2312	3.9	11.8	16.54
$1R_5(SF)_{10}$	525	1750	2350	2.8	9.5	15.61
$2N(SF)_{10}$	481	1403	2029	2.6	7.7	13.78
$2R_5(SF)_{10}$	451	1810	2384	2.7	9.9	16.20
$2R_{10}(SF)_{10}$	554	1757	2351	3.1	9.6	15.92
$2R_{20}(SF)_{10}$	636	1844	2223	3.5	10.1	15.64
$3R_5(SF)_{00}$	580	1675	1981	3.2	9.1	13.98
$3R_5(SF)_{05}$	455	1652	2106	2.5	9.0	14.00
$3R_5(SF)_{10}$	507	1480	2171	2.8	8.0	14.59
$3R_5(SF)_{20}$	548	1589	2169	3.0	8.7	14.82
ASP	2486	2865	379	13.3	0	15.53

* d_0, d_1, d_2, d_3 are given in Figure 6.2

It is clearly seen that the erosion index of Al_2O_3-MA castable is significantly larger than that of MgO-Al_2O_3 castable. The dissolution rate of Al_2O_3-based castable is extremely higher than that of MgO in contact with the highly ferric basic slag, used for testing. However, the magnesia based castable is less resistant to penetration.

Adding SiO_2 fume into MgO-Al_2O_3 castable not only improves castable physical and mechanical properties as discussed in Chapter 5, but do not make the erosion and penetration resistance worst. It means that adding appropriate SiO_2 into MgO-Al_2O_3 castable could be an efficient way to optimize castable properties.

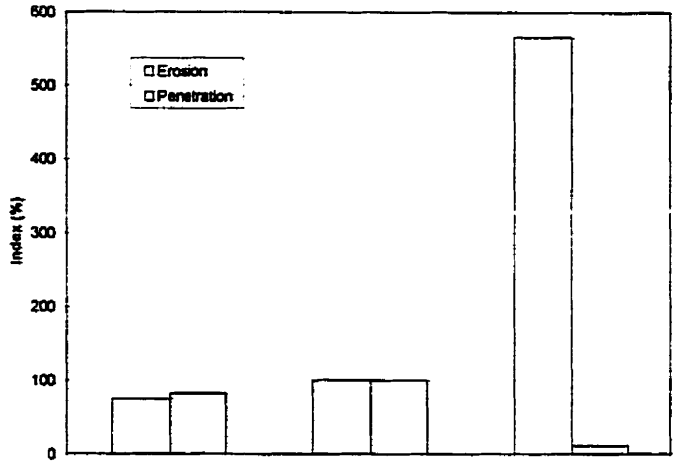

Figure 6.3 The Erosion and Penetration Indexes of Samples after Rotary Slag Test at 1600°C×6hrs

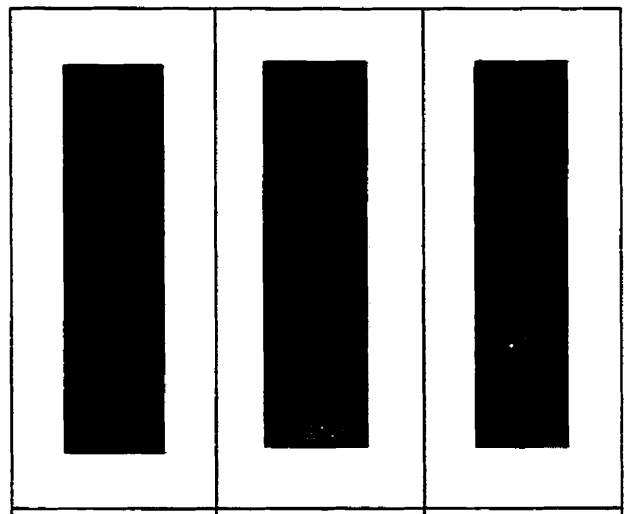

ASP	$1N(SF)_{00}$	$1R_5(SF)_{10}$
Erosion (mm^2) ± 50		
2490	440	330
Penetration (mm^2) ± 100		
380	3480	2850

Figure 6.4 Corroded Areas and Cross Sections of Samples after Rotary Slag Test at 1600°C×6hrs

The repeatability of corrosion tests has been estimated with two compositions $2R_5(SF)_{10}$ and $3R_5(SF)_{10}$ produced in batch 2 and 3 respectively. The experiment results are given in Table 6.4. The difference between the two trials is to be considered as an index of repeatability.

Table 6.4 Repeatability of Rotary Slag Test Results

Batch	Sample	Erosion Area(mm^2)	Erosion Depth (mm)	Penetration Area (mm^2)	Penetration Depth (mm)
1	$2R_5(SF)_{10}$	450	4.4	2400	19.0
2	$3R_5(SF)_{10}$	510	3.7	2200	18.3
Deviation		±50	±0.5	±100	±1.0

On the basis of the above results, it is suggested that, to differentiate between values on erosion, numbers have to differ by ±50 mm^2, an erosion depth by ±0.5 mm, on penetration area by ±100 mm^2 and or penetration depth by ±1.0 mm. The following discussions will be based on those estimates of errors.

6.2.2 Microstructure Characteristics of $MgO-Al_2O_3$ Castable

The microstructure of the unattacked $MgO-Al_2O_3$ castable after firing at 1600°C×4hrs (take sample A1 as an example) is shown in Figures 6.5 and 6.6. It can be noticed that the castable is composed of large discrete aggregate and continuous matrix with entrapped pores. Two major interlocking phases, periclase and spinel, with direct bonding, are clearly seen. The periclase clusters are mostly joined by solid spinel bridges to form spinel "network", which is easily observed in the enlarged SEM photo shown in

Figure 6.6. The "network" in matrix do affect the properties of physical, mechanical and corrosion resistance. Additionally, inter- and intra-granular pores, with variable sizes and irregular shapes, are also present in Figure 6.5.

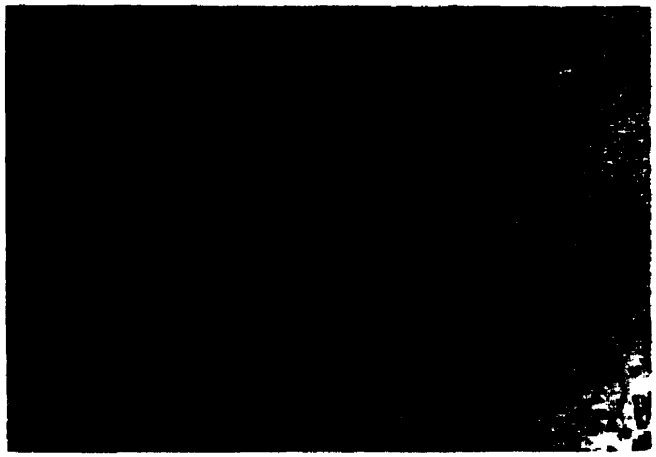

Figure 6.5 A Typical Microstructure of $MgO\text{-}Al_2O_3$ Castable (Sample A1 after Firing at 1600°C×4hrs, OPM×100)

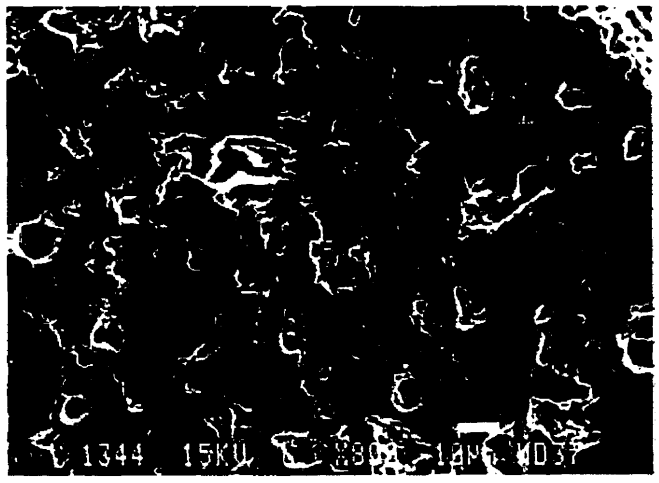

Figure 6.6 Spinel Networks in the Matrix of $MgO\text{-}Al_2O_3$ Castable (Sample $1N(SF)_{00}$ after firing at 1600°C×4hrs, SEM × 800)

Due to the difference of thermal expansion coefficients, which has been discussed in chapter 2 and 4, the mismatch gap between periclase and spinel phases, has been observed in high magnitude SEM photo of Figure 6.7. It shows that the acid etched MgO aggregate, located in the center, partially connects with spinel matrix on the left side, and forms a right side narrow gap. The gap width is 2 to 5μm.

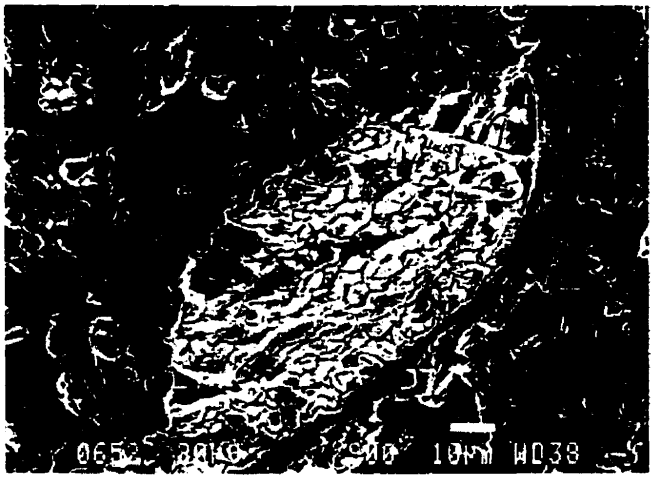

Figure 6.7 Mismatch Gaps between MgO Aggregate and Spinel Matrix (Sample 1N$(SF)_{00}$ after Firing at 1600°C×4hrs)

Meanwhile, focusing on a MgO aggregate, SEM analysis shown in Figure 6.8 presents a continuous grain boundary net, which encloses and separates small grains in a big aggregate. Further EDS analysis, given in Figure 6.9, illustrates the existance of silicates at grain boundary.

Figure 6.8 The Grain Boundary Net Existed in MgO Aggregate (Sample $1N(SF)_{00}$ after Firing at 1600°C×4hrs, Acid Etched)

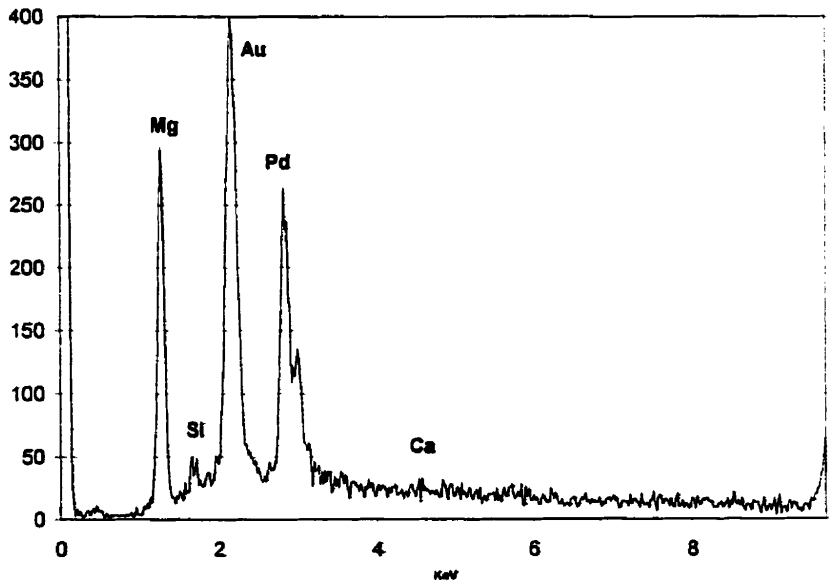

Figure 6.9 EDS Analysis at the Grain Boundary of MgO Aggregate (Point A)

The microstructure characteristic of corroded $MgO-Al_2O_3$ castable by rotary slag is schematically illustrated in Figure 6.10. It shows that three different layers: slag layer, penetration layer and unattacked original castable layer, are present in the diagram. The slag layer is always attached to the castable surface and followed by penetration layer. In penetration layer, the colored and uncolored sublayers are clearly seen even through macroscopic observation. Interestingly, in within penetration layer, the colored dense, colored porous and uncolored dense again texture are observed by Optical Microscopy.

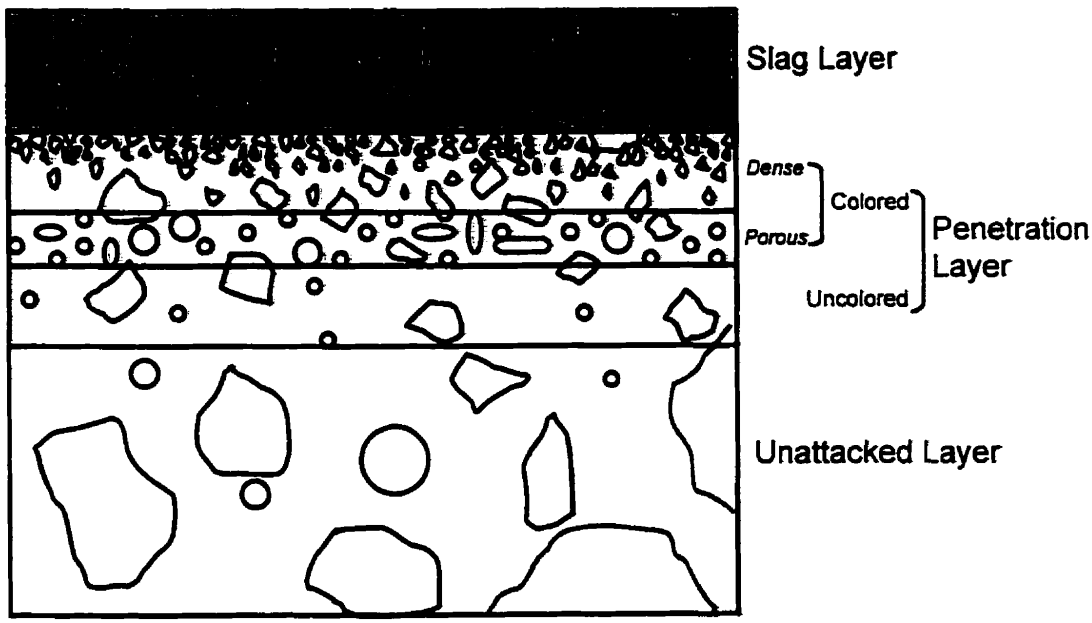

Figure 6.10 Schematic Diagram of the General Patterns of $MgO-Al_2O_3$ Castable after Slag Corrosion

The schematic representation is based on the microstructure observations of corroded $MgO-Al_2O_3$ castables. For example, Figure 6.11 shows the interface between slag layer and penetration layer of sample $2R_5(SF)_{10}$. It reveals that a lot of needle crystals are formed in the slag layer. Further SEM, EDS analyses given in Figure 6.12 indicates that those like-needle crystals correspond to a C_2S phases. Additionally, with the highly ferric slag attack, both MgO grains and spinel matrix will be dissolved into slag to cause dissolution of castable. Those dissolved MgO and spinel are also easily seen in Figure 6.11.

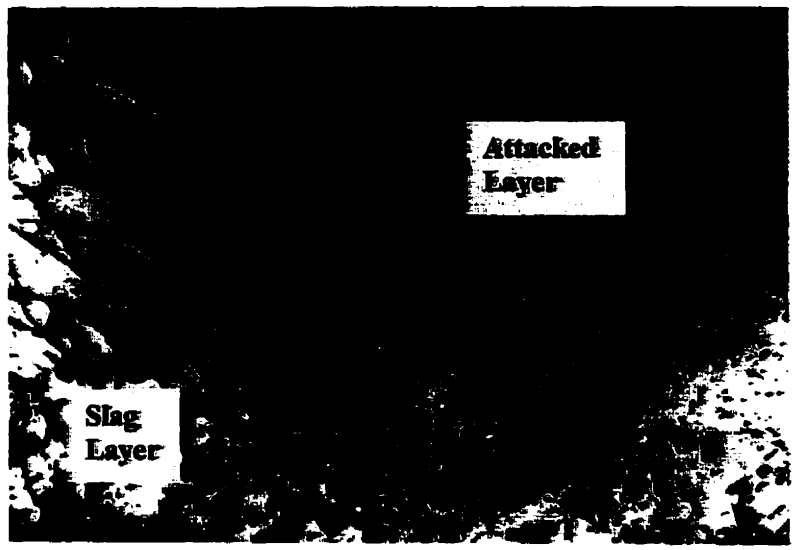

Figure 6.11 The Interface between Slag Layer and Attacked Layer (Sample $2R_5(SF)_{10}$ after Rotary Slag Test at 1600°C×6hrs)

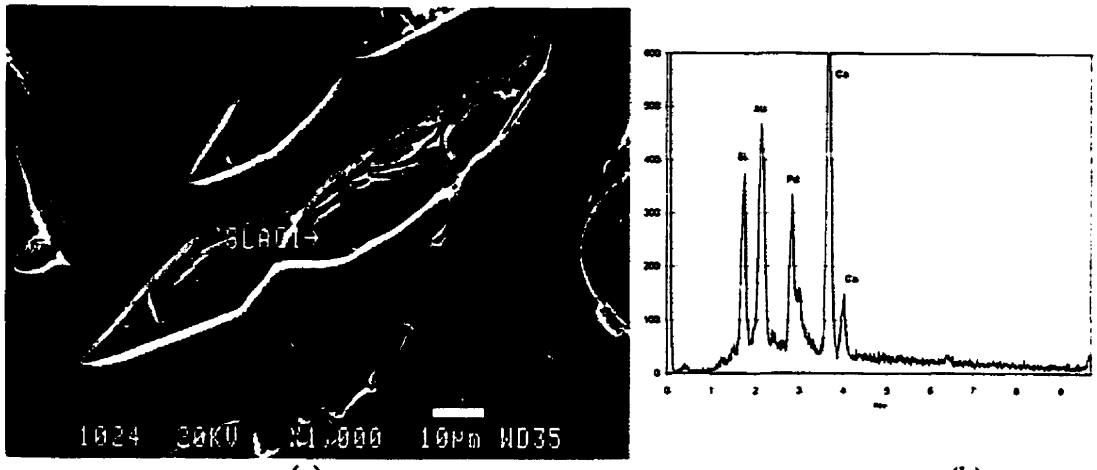

(a) (b)

Figure 6.12 (a) The C_2S formed in the Slag Layer (Sample $2R_5(SF)_{10}$ after Rotary Slag Test at 1600°C×6hrs); (b) EDS Analysis of Point A

Considering the sample $2N(SF)_{10}$ in detail, after corrosion test at 1600°C×6hrs, in the penetration layer, the interface between brown colored and uncolored layer is visible through macro- or micro-observations. Element Fe does exist in brown colored layer, but no more Fe can be found in uncolored layer via EDS analysis. It is believed that the formed "color" is due to the penetration of Fe_xO from slag, and the Fe_xO penetration is to be stopped at the interface of colored and uncolored layer. Meanwhile, by the optical microscopy, the variation of porosity can be seen in colored layer while the sublayer near the uncolored layer is more porous than the sublayer near the slag layer. Figures 6.13 and 6.14 give the microstructure observation in different colored sublayers. Interestingly, following the porous colored layer, the uncolored layer appears denser again as shown in Figure 6.15.

Figure 6.13 The Interface between Slag Layer and Dense Colored Layer (Sample $2N(SF)_{10}$, after Rotary Slag Test at 1600°C×6hrs)

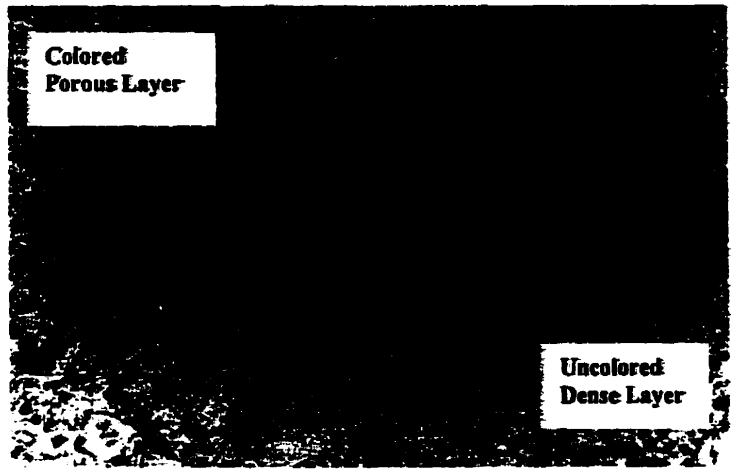

Figure 6.14 The Interface between Colored Porous Layer and Uncolored Dense Layer (Sample $2N(SF)_{10}$, after Rotary Slag Test at 1600°C×6hrs)

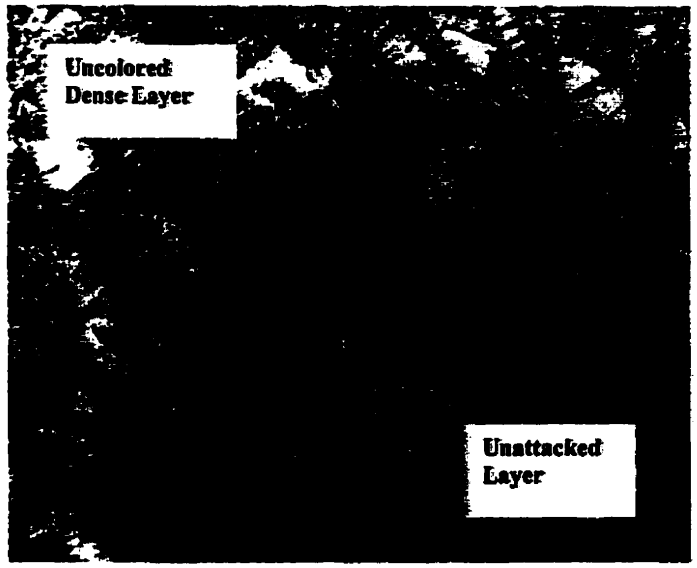

Figure 6.15 The Interface between Uncolored Dense Layer and Unaffected Castable (Sample $2N(SF)_{10}$, after Rotary Slag Test at 1600°C×6hrs)

6.2.3 The Effects of the Nature of Pre-reacted Spinel Used

Comparison between three grades of pre-reacted spinel AR_{90}, AR_{78} and MR_{66} is now to be made at addition level of 5 wt% in each case. Sample $1N(SF)_{00}$ is selected as reference. All the samples are tested at 1600°C for 8hrs.

The maximum erosion and penetration depth, the calculated erosion and penetration areas, the cross section of corroded samples are given in Figure 6.16. The relative changes at erosion and penetration indexes in comparison with reference sample are shown in Figure 6.17.

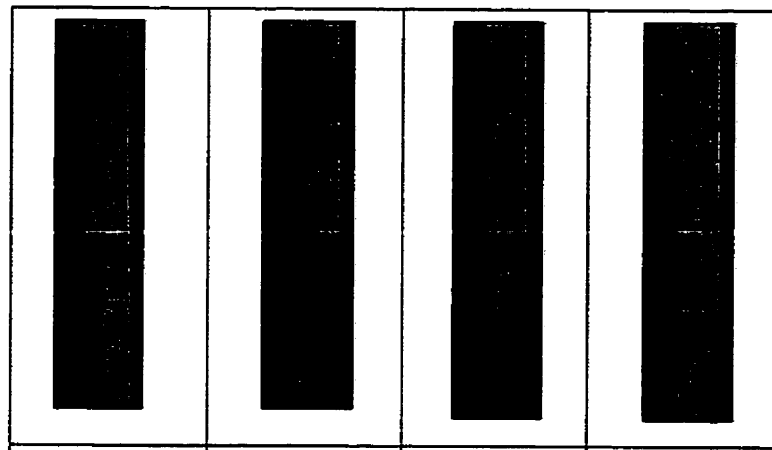

$1N(SF)_{00}$	$1A_5(SF)_{00}$	$1R_5(SF)_{00}$	$1M_5(SF)_{10}$
Erosion (mm^2) ± 50			
640	700	460	650
Maximum Erosion Depth (mm) ± 0.5			
5.2	4.8	3.8	5.4
Penetration (mm^2) ± 100			
2280	2310	2330	2120
Maximum Penetration Depth (mm) ± 1.0			
19.2	19.3	19.8	18.6

Figure 6.16 Corroded Areas and Cross Sections of Samples after Rotary Slag Test at 1600°C×6hrs

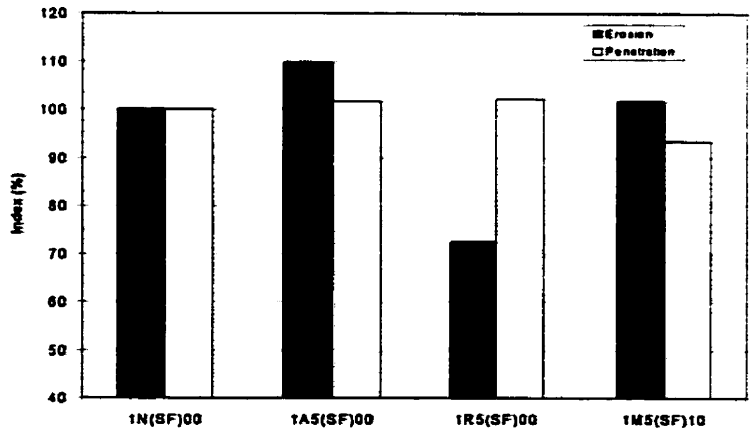

Figure 6.17 The Erosion and Penetration Indexes of the Samples after Rotary Slag Test at 1600°C×8hrs

Comparing with $1N(SF)_{00}$, addition of 5wt% AR_{78} ($1R_5(SF)_{00}$) improves the erosion resistance significantly, but not the penetration resistance. In the cases of MR_{66} and AR_{90} ($1A_5(SF)_{00}$, $1M_5(SF)_{00}$), the erosion and penetration resistance values do not differ from the ORS value, but the dissolution of castable is less with adding AR_{90} and penetration is less with adding MR_{66} , while they are compared to the castable with AR_{78} addition.

6.2.4 Effects of Silica Fume Addition

Results from samples $3R_5(SF)_{00}$ without SiO_2 fume addition and $3R_5(SF)_{05}$, $3R_5(SF)_{10}$ and $3R_5(SF)_{20}$ with 0.5%, 1.0% and 2.0% SiO_2 fume respectively are to be compared. Each castable mix contains 5% AR_{78}. The corrosion and penetration differences are illustrated in Figures 6.18 and 6.19, again, the numerical values are to be found in Appendix 6.2.

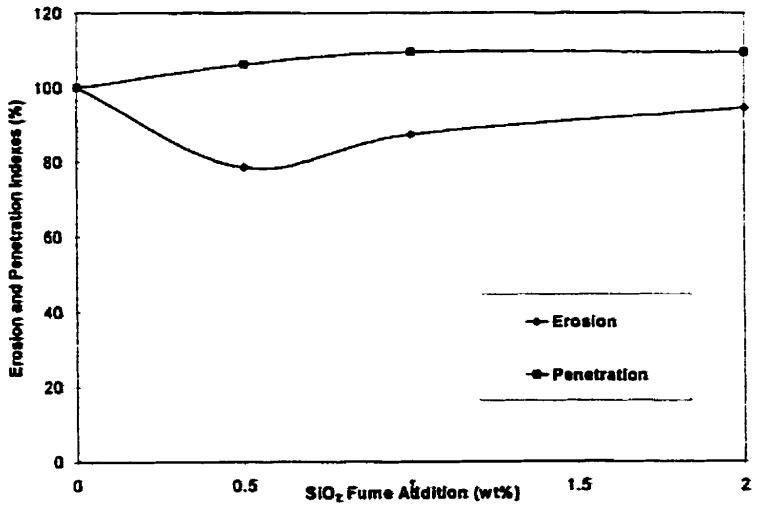

Figure 6.18 The Erosion and Penetration Indexes of the Samples after Rotary Slag Test at 1600°C×6hrs

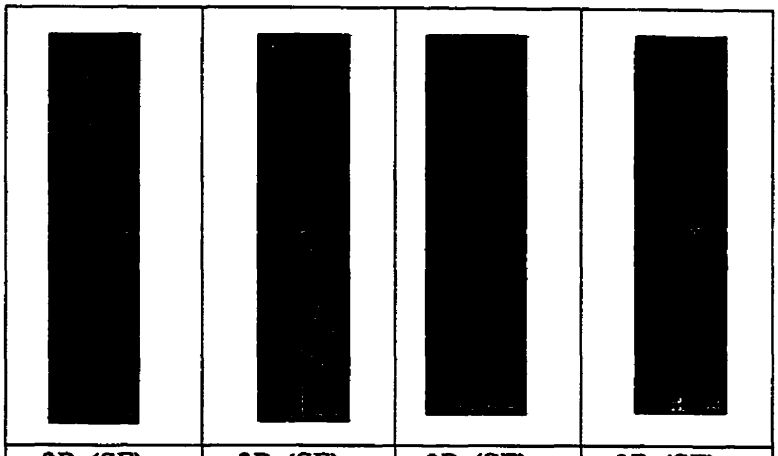

$3R_5(SF)_{00}$	$3R_5(SF)_{05}$	$3R_5(SF)_{10}$	$3R_5(SF)_{20}$
Erosion (mm^2) ± 50			
580	460	510	550
Maximum Erosion Depth (mm) ± 0.5			
4.7	3.9	3.7	4.2
Penetration (mm^2) ± 100			
1980	2110	2170	2170
Maximum Penetration Depth (mm) ± 1.0			
16.7	12.4	18.3	18.3

Figure 6.19 Cross Section of Corroded Samples after Rotary Slag Test at 1600°C×6hrs

Compared to the reference sample $3R_5(SF)_{00}$, with the introduction of 0.5 - 1.0% SiO_2 fume, the erosion resistance is improved. This positive effect disappears using more than 1.0% SiO_2 addition. Meanwhile, regardless of SiO_2 fume added or not, the penetration resistance of all samples are not significantly different.

Microstructure analysis of sample $1R_5(SF)_{10}$ with 1% SiO_2 fume addition after firing at 1600°C×4hrs is given in Figure 6.20. It shows the well connected network

between spinel and spinel, spinel and MgO. This may be attributed to a better sintering due to SiO_2 addition. Furthermore, this is clearer when ones observe such a sample as $1N(SF)_{00}$, without SiO_2 fume addition (Figure 6.22). The SEM photo of $1N(SF)_{00}$ shows that more gaps and pores exist between spinel and spinel, spinel and magnesia. Therefore, the enhanced direct bonding due to SiO_2 in sample $1R_5(SF)_{10}$, helps to improve its erosion resistance.

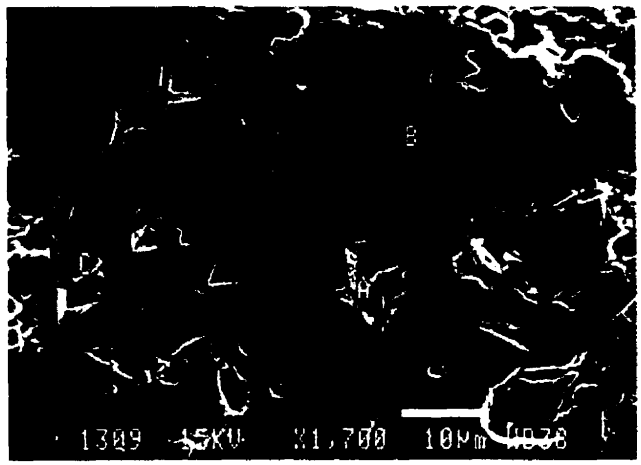

Figure 6.20 Microstructure of Sample $1R_5(SF)_{10}$ after firing at 1600°C×4hrs

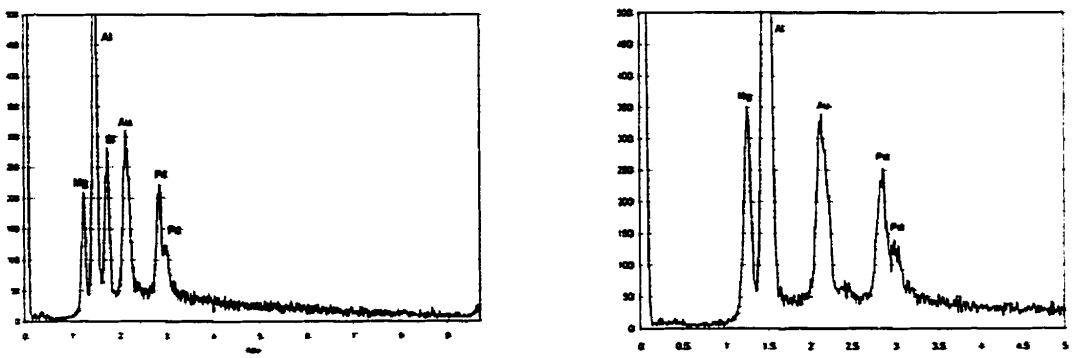

Figure 6.21 EDS Analyses of Points A and B in Sample $1R_5(SF)_{10}$ of Figure 6.20

Figure 6.22 Microstructure of Sample $1N(SF)_{00}$after Firing at 1600°C×4hrs

Meanwhile, the added silica fume can further react with MgO to form M_2S. This has been seen in sample $1R_5(SF)_{10}$, as shown in Figures 6.20 and 6.22. With 0.5 – 1.0% SiO_2 fume addition, M_2S is mostly limited in triple junctions and is enveloped by in-situ spinel. However, with an increase of SiO_2, more M_2S are expected to be formed. Those forsterites, previously distributed in spinel triple junctions at 0.5 – 1.0% of SiO_2 addition, now can spread to the interface and reduce the direct bonding between spinel and MgO, therefore, it can be easily attacked by slag through the "interface" to form lower melting phases. Actually, with 1% SiO_2 addition, some of M_2S located on the interface have been observed.

6.2.5 Effects of Pre-reacted Spinel AR_{78} Addition Amount

It has been concluded from Section 6.2.3, that the erosion resistance of MgO-Al_2O_3 castable can be improved by adding pre-reacted spinel AR_{78}. Further experiments are now to be done to attain the appropriate amount. The corrosion and penetration indexes in relationship with AR_{78} addition amounts and macrophotoes of sections are given in Figures 6.23 and 6.24 respectively. The numerical values can be found in Appendix 6.2.

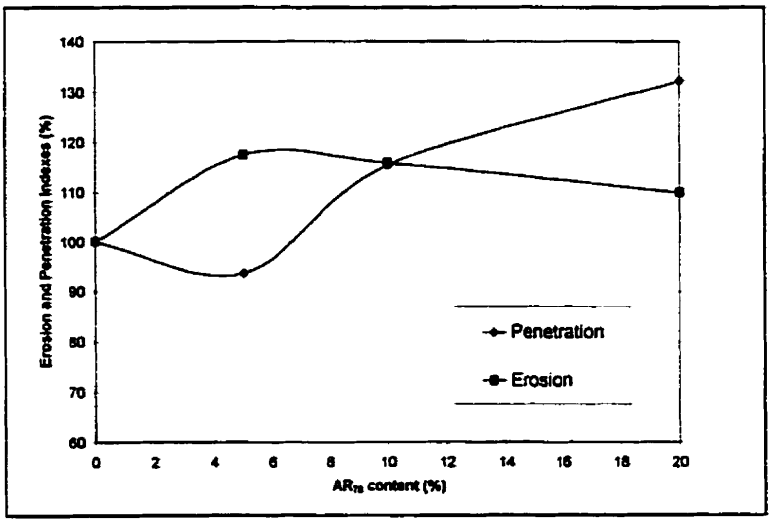

Figure 6.23 The Erosion and Penetration Indexes of the Samples after Rotary Slag Test at 1600°C×6hrs

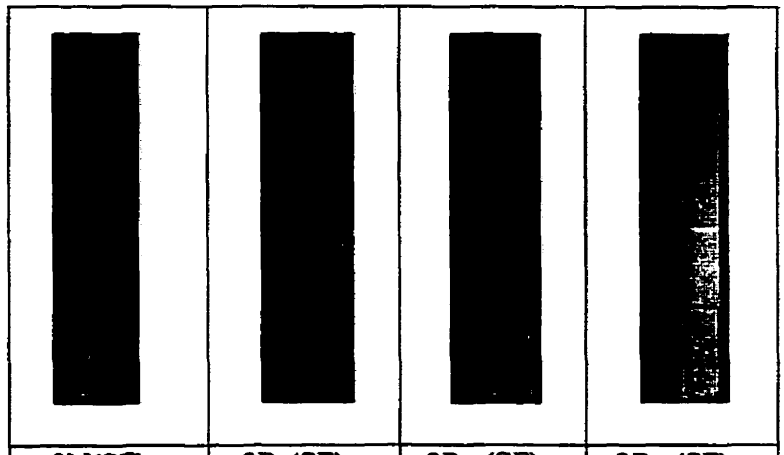

$2N(SF)_{10}$	$2R_5(SF)_{10}$	$2R_{10}(SF)_{10}$	$2R_{20}(SF)_{10}$
Erosion (mm^2) ± 50			
480	450	550	640
Maximum Erosion Depth (mm) ± 0.5			
3.3	4.4	5.0	5.1
Penetration (mm^2) ± 100			
2030	2380	2350	2220
Maximum Penetration Depth (mm) ± 1.0			
16.6	19.0	19.6	18.9

Figure 6.24 Cross Section of Corroded Samples after Rotary Slag Test at 1600°C×6hrs

By adding AR_{78} into castable in comparison with the sample $2N(SF)_{10}$ without AR_{78} addition, the penetration resistance is reduced, however, at 5% level, the erosion resistance has been improved. With more than 7% addition, this predominance disappears.

Since the pre-reacted spinel grains have higher erosion resistance than the formed in-situ spinel as discussed in Section 6.2.3, all of samples with AR_{78} addition should

present higher corrosion resistance than the one for sample $2N(SF)_{10}$ without AR_{78}. However, on the other hand, adding more than 5% synthetic spinel into castable instead of same amount of fine alumina, leads to in-situ spinel formed and hence less in-situ bonding which weakens the castable (see the MOR values in Chapter 5).

6.3 Microstructure Analysis of Corroded MgO-Al_2O_3 Castable

In general, castable corrosion may occur by mechanisms like penetration of liquid slag and dissolution of the refractory. Both penetration and dissolution processes are interactive and synergistic. The corrosion characteristic will now be discussed based on a microstructural analysis.

The mineralogical composition of the slag used, in corrosion tests, can be calculated from its chemical composition, as containing: 47% Ca_2SiO_4 (C_2S di-Calcium-Silicate); 12% Ca_2AlFeO_5 (C_4AF Brownmillerite); 38% (Mg, Fe)(Fe, $Al)_2O_4$ (Complex spinel) and 3% glassy phases. In spite of the relatively high content of iron oxides, the slag could be considered as only mildly aggressive against basic refractories, because it is MgO-saturated and all of the mineral-components of the slag are coexistent with MgO.

The fluid slag does penetrate into pores and interacts with components of the refractory castable. MgO grains have the ability to dissolve unlimited portion of FeO forming solid solutions in the whole range of binary compositions (Figure 6.25). The solubility of Fe_2O_3 in MgO is similarly very high, approximately 70% at 1700°C, forming Magnesio-Wustite. The ratio of FeO/Fe_2O_3 that will be present in real systems,

like the slag-refractory interface during the corrosion test, will depend on the temperature and the partial pressure of oxygen. Based on the literature review [30, 39, 103, 104, 105] and the stronger aggressive ability of FeO for magnesia-based material, the effects of FeO on corrosion resistance of $MgO-Al_2O_3$ castable will be mainly considered as the following.

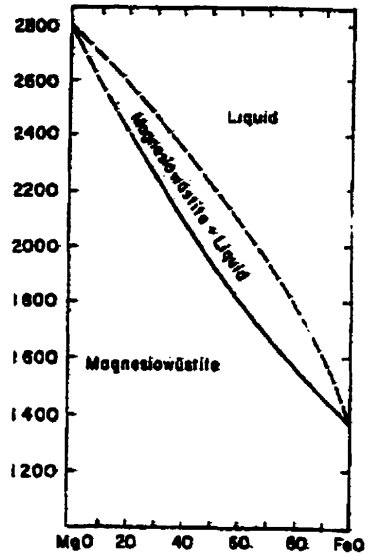

Figure 6.25 Phase Diagram of MgO-FeO System

(R.E.Johnson and Arnulf Muan, J. Ame. Ceram. Soc., 48 [7], 1965, pp361)

$(Mg, Fe)_xO$ solid solutions are easily detectable in the corroded $MgO-Al_2O_3$ castables, for example in sample $1N(SF)_{00}$, as shown in Figures 6.26 and 6.27, the solid solutions existed in both dissolved MgO grains of the slag layer, and the big aggregate located in the front of penetration layer.

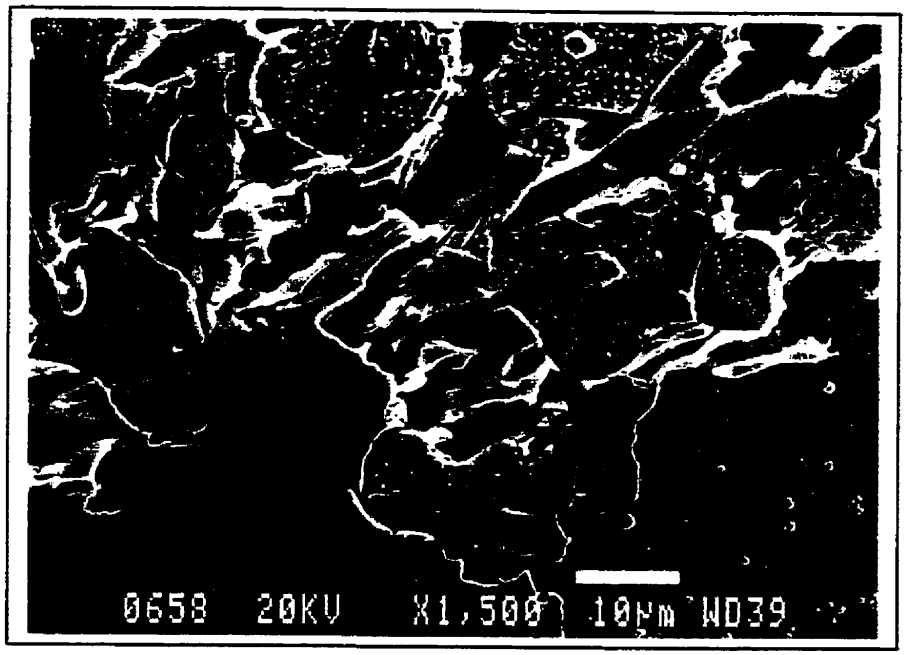

Figure 6.26 The Dissolved Spinel in Matrix (Sample $1N(SF)_{00}$ after Rotary Slag Test at 1600°C×8hrs)

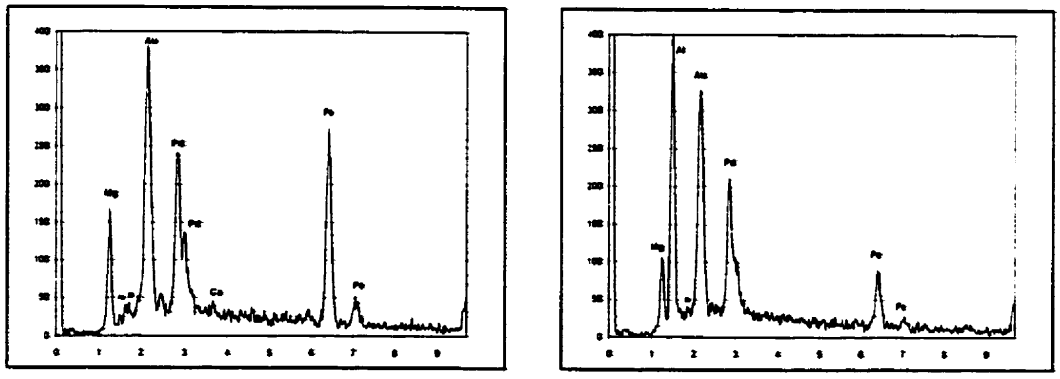

(A) (B)

Figure 6.27 EDS Analyses of Point A and B in Sample $1N(SF)_{00}$ of Figure 6.26

Figure 6.28 gives semi-quantitatively the element distributions in an MgO grain. It shows that Fe even can be founded under 300μm from the surface of MgO aggregate

(indicated in Figure 6.26 by an arrow). The Fe amount decreases with distance into the center of MgO aggregate, this would indicate that the solid solution of FeO in MgO was formed by solid phase diffusion during the corrosion test.

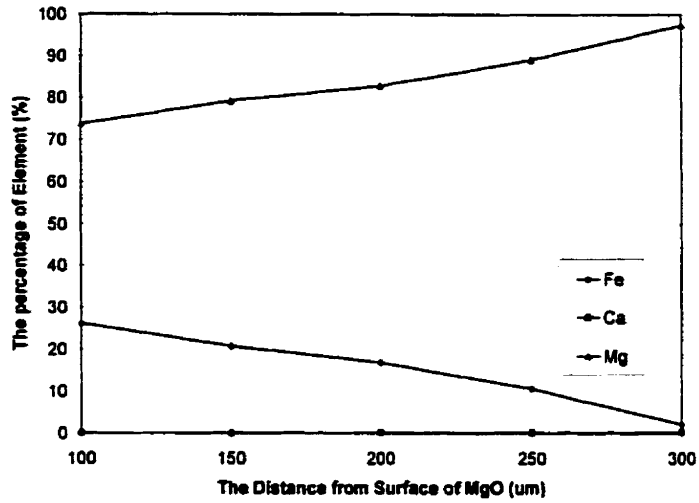

Figure 6.28 The Distribution of Elements Fe, Ca and Mg from the Surface of Eroded MgO Aggregate

On the other hand, besides MgO aggregates, FeO can be easily solubilized into spinel matrix to form solid solutions. In fact, Figures 6.26 (A) and (B) indicated the presence of (Mg, Fe)(Fe, $Al)_2O_4$ in the penetrated layer, while Figures 6.29 and 6.30 represent the dissolved spinel in the slag layer which also captured FeO.

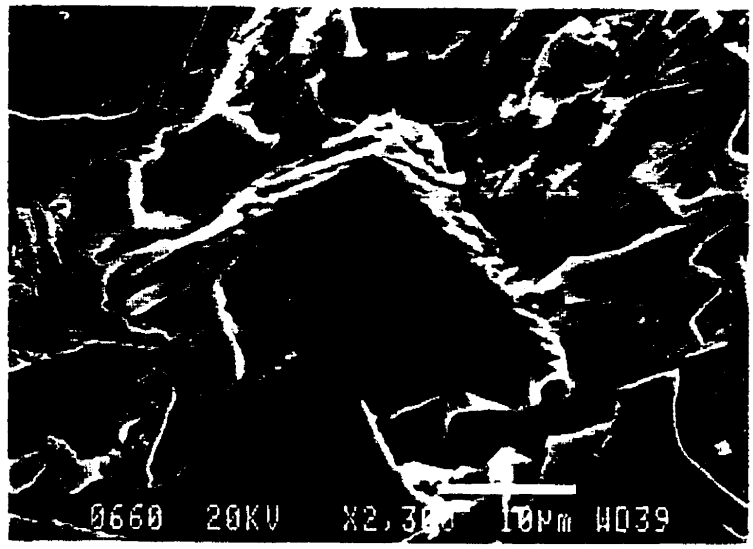

Figure 6.29 The Dissolved Spinel (Sample $1N(SF)_{00}$ after Rotary Slag Test at 1600°C×8hrs)

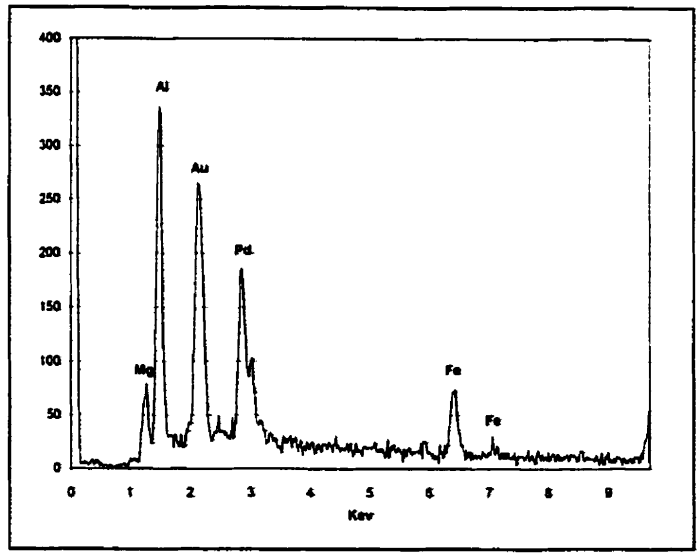

Figure 6.30 Point A EDS Analysis of Sample $1N(SF)_{00}$ in Figure 6.29

Interactions between the slag and the refractory castable will cause local changes in the composition of both the slag and the refractory material, in a narrow contact zone. MgO aggregates in the castable can be attacked by liquid slag through the grain boundaries that are mostly formed by Ca-Mg-Silicates (See Figure 6.8). The individual crystals of MgO, without being actually dissolved, are then released from the aggregate and can be simply washed into the slag. Figures 6.31 and 6.32 show the microstructure and the corresponding EDS analysis of the attacked $(Mg, Fe)_xO$ aggregate located on the interface between penetration layer and slag layer. Getting into contact with fresh slag, MgO particles can be, at least partially, dissolved. The slag becomes more MgO saturated and that will lead to the precipitation of more spinel.

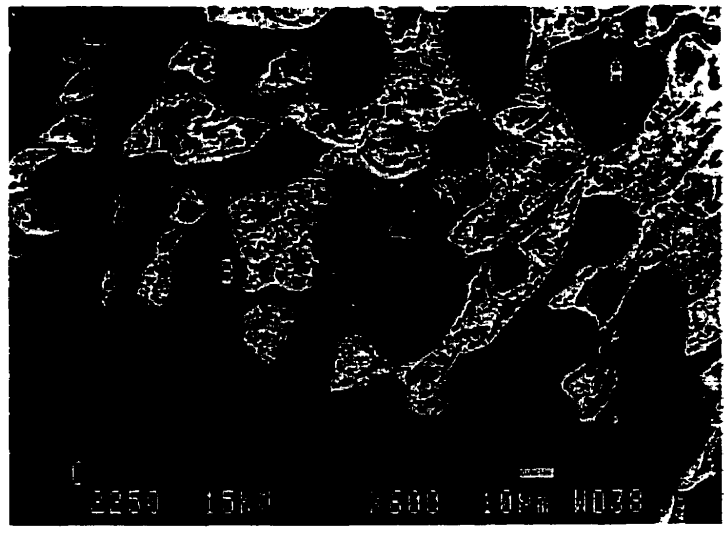

Figure 6.31 The Dissolving (Mg, Fe)O Aggregate on the Interface between Penetration and Slag Layer (Sample $2N(SF)_{10}$ after Rotary Slag Test at 1600°C×6hrs)

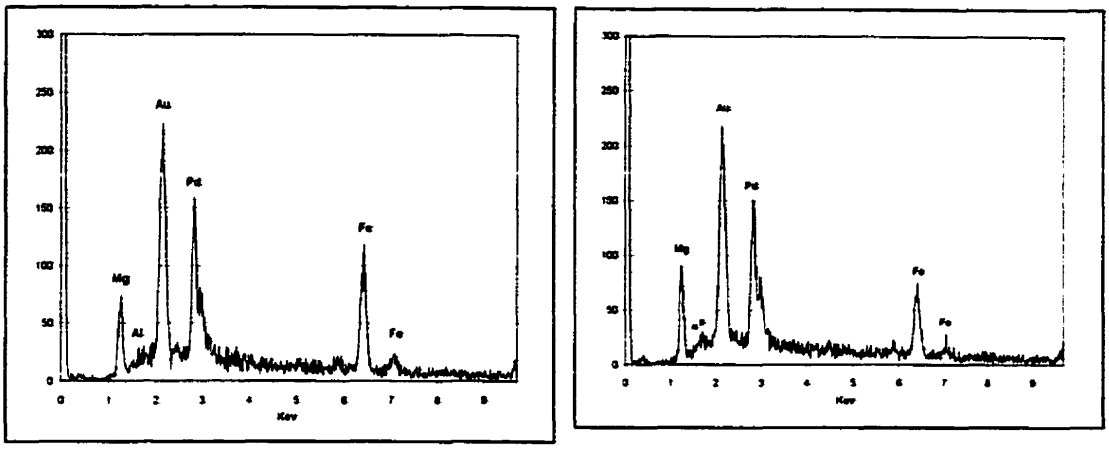

(a) (b)

Figure 6.32 EDS Analyses of Point A (a) and Point C (b) for Sample $2N(SF)_{10}$ in Figure 6.31

Those precipitated secondary spinels, netted with in-situ formed spinel together, do form a protective layer to prevent the further attack from slag. Considering the colored layer shown in schematic diagram Figure 6.10, the secondary spinels fill the pores and increase the density of the colored sublayer near the slag as compared with the sublayer close to the unattacked castable. Actually, a protecting layer with angular secondary spinels have been observed as shown in Figures 6.33 and 6.34 respectively.

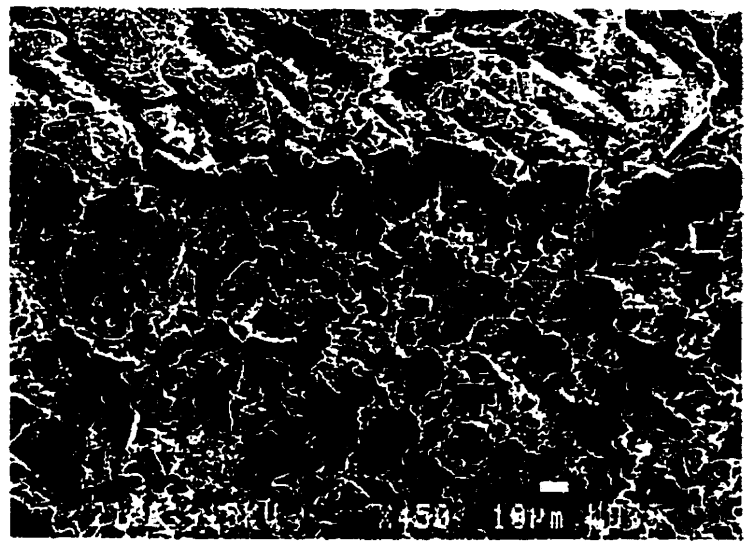

Figure 6.33 The Spinel Protective Layer (Sample $1N(SF)_{00}$ after Rotary Slag Test at 1600°C×6hrs

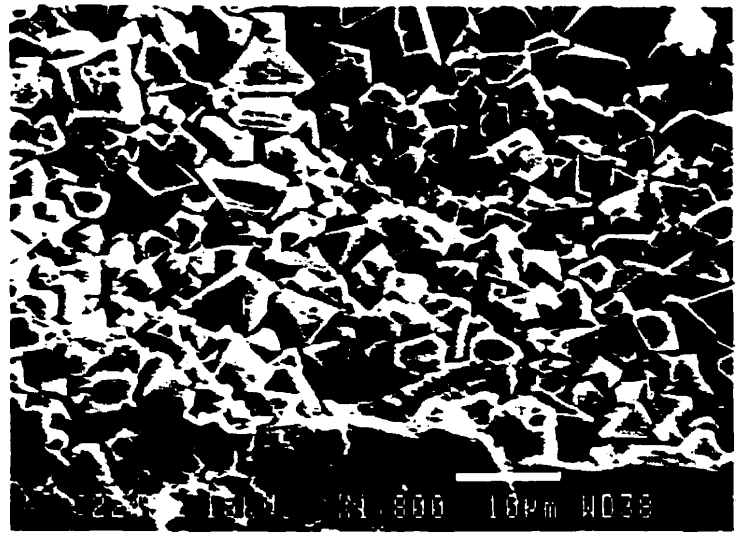

Figure 6.34 The Angular Secondary Spinel (Sample $2N(SF)_{10}$ after Rotary Slag Test at 1600°C×6hrs

The precipitation of spinel will leave a remaining liquid phase enriched in CaO-SiO_2. This silicate phase, in the system CaO-MgO-SiO_2 - (Fe_xO-MnO-TiO_2), will penetrate deeper into the structure of castable. This will accelerate the sintering and recrystalization processes, subsequently reducing the porosity in the uncolored layer as shown in previous Figure 6.10).

The schematic representation of slag penetration in MgO-Al_2O_3 castable is illustrated in Figure 6.35.

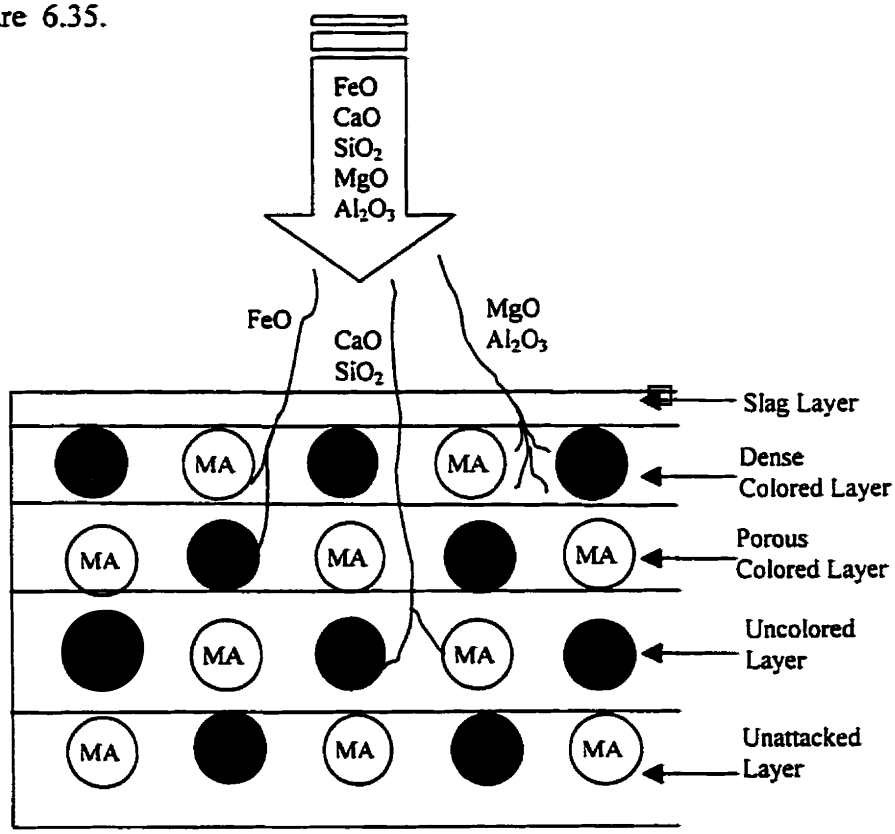

Figure 6.35 A Schematic Representation of Slag Penetration

As a summary, during the corrosion of MgO-Al_2O_3 castable, MgO and MA will capture nearly all of FeO-Fe_2O_3 from the penetrated slag to form (Mg, Fe)$_x$O and (Mg,

Fe)$(Fe,Al)_2O_4$ solid solutions. The dissolution of (Mg, Fe)O and (Mg, Fe).$(Fe,Al)_2O_4$ leads to the precipitation of secondary spinel that together with the in-situ spinel will form a densified spinel layer, which does protect $MgO-Al_2O_3$ castable from further slag attack. The composition of liquid slag is relatively enriched by $CaO-SiO_2$ can further penetrate into the uncolored layer and form low melting phases in the system $CaO-MgO-SiO_2-(Fe_xO-MnO-TiO_2)$.

CHAPTER 7 SUMMARY AND CONCLUSIONS

Magnesia based, cement-free, spinel bonded MgO-Al_2O_3 castables have been developed and optimized to be conferred with stronger resistance to basic ferritic slag attack. This new type of truly basic castable holds potential to be used as monolithic lining in slag zone of steel ladles.

Optimization of such castables has been achieved by

1) using hydratable alumina as binder to enable advantageous CaO-free system;
2) selecting suitable deflocculant for a good workability;
3) incorporating silica fume to improve intermediate temperature strength; and
4) properly controlling of in-situ and pre-reacted spinel in terms of level and type to achieve good volume stability.

This work has reached the objectives set in Chapter 1 and experimentally confirmed that:

1) It is possible to produce MgO based truly basic castables without hydration concern;
2) Spinel is an effective bonding agent, engendering good strength and high refractoriness;
3) Hydratable alumina is an applicable impurity-free hydraulic binder, though leading to insufficient strength after firing around 1000°C, however, by incorporating small amount, up to 1%, of SiO_2 fume, it can be remarkably improved;
4) Slag resistance of such castables, documented by rotary slag test, has been found to be much superior to that of commercially available Al_2O_3-MgO castable.

The optimized $MgO-Al_2O_3$ castable consists of 74% magnesia aggregates with properly controlled grain size distribution, 5% hydratable alumina, 15% alumina, 5% AR_{78} pre-reacted spinel and 1% SiO_2 fume, requiring 4.8% mixing water and a specific organic acid salt as deflocculant for good placement. This optimized composition results in the following physical and mechanical properties:

- Bulk Density: 3.0 g/cm^3 (110°C)
- Apparent Porosity: 14 % (110°C) and 15 %(1600°C)
- CMOR: 13.1 MPa (110°C), 3.1 MPa (1000°C) and 12.3 MPa (1600°C)
- HMOR: 4.3 MPa at 1400°C × 1hr.

Moreover, the developed $MgO-Al_2O_3$ castable shows much better resistance to ferritic basic slag's attack than commercial Al_2O_3-MgO castable.

Flowability tests have been carried out to select appropriate deflocculant type and addition level. An "extracting-matrix" method has been adopted to optimize the flowability of the $MgO-Al_2O_3$ castables. The measured "flow-time" values on matrix slurry are well correlated to the "flow-values" of the castable. The flowability of the $MgO-Al_2O_3$ castables is thus predictable by "flow-time" of their matrix. Optimization done by this approach allows to improve physical and mechanical properties of the castables as well.

For mixes with at least 74% MgO, the starting temperature for in-situ spinel to form in the $MgO-Al_2O_3$ castables is around 1100°C. Below this temperature, variation in the matrix composition has little effect on thermal expansion of the castables, as the expansion is predominantly derived from the magnesia aggregates. Phenomenological

and mathematical models demonstrates and reveals that the net expansion above 1100°C is the consequence of reversible expansion of magnesia aggregates, the in-situ spinel reaction and the sintering shrinkage which mainly takes place in the fine portion of the matrix. The maximum thermal expansion, however, is proportional to the amount of in-situ spinel formed, and the temperature at maximum thermal expansion is strongly dependent on the ratio of MgO to Al_2O_3. Since the in-situ spinel reaction between MgO and Al_2O_3 may give rise to a volume expansion of 8 % theoretically, it is important to control the volume stability of the MgO-Al_2O_3 castable. Thermal expansion tests have shown that, regardless of Al_2O_3-rich, MgO-rich or close to the stoichiometric composition, adding a proper amount of pre-reacted spinel is beneficial, not only to control the maximum linear expansion to less than 2% on first heat-up, but also to compensate for the permanent linear change of the castable. However, the thermal expansion behavior of AR_{90} in the castable is different from that of MR_{66} and AR_{78}, owing to the further reaction between AR_{90} and MgO in the castable mix. XRD analyses confirmed that the Al_2O_3-rich spinel actually has been converted to stoichiometric special after firing at 1600°C.

Adding silica fume into the castable enhances in-situ spinel formation. Below 1100°C, thermal expansion of magnesia is still dominant, and a small addition of SiO_2 fume doesn't have any influence. However, at elevated temperatures, the maximum thermal expansion is directly related to SiO_2 amount. With an increase of silica fume addition, the maximum thermal expansion tends to increase and PLC to decrease, except for at the addition of 0.5%.

Due to the significant difference of thermal expansion coefficient between magnesia and spinel, the residual stress induced by thermal shrinkage on cooling may lead to partially debonding, and micro-cracks or micro-gaps may occur between those two phases. It is beneficial to toughness enhancement and thermal shock resistance under temperature cycling (heating-cooling). The temperature, at which gaps are initiated, is a function of alumina, silica and pre-reacted spinel amount in the mix. With addition of pre-reacted spinel, it increases, whereas it decreases with addition of silica fume. These behaviors are closely associated with the "bonding ability" between MgO and spinel. Meanwhile, the "internal disruption" occurs once, and will not change in intensity after the first heating and cooling cycle.

Physical and mechanical properties of the MgO-Al_2O_3 castables are significantly affected by Al_2O_3 content or MgO/Al_2O_3 ratio in the mix and, of course, pre-reacted spinel addition. The cold modulus of rupture, after drying or firing at 1600°C, decreases with an increase of the MgO/Al_2O_3 ratio. More than 15% alumina is required to reach appreciable MOR values.

Thermal expansion can be controlled using pre-reacted spinel addition. Substitution of alumina by spinel leads to a decrease in physical and mechanical properties at room temperature, but an increase in modulus of rupture at high temperature. The optimal spinel addition, irrespective of the grade used, is 5 wt% in all cases.

Low intermediate temperature strength, attributed to the hydratable alumina as binder, can be significantly improved by adding small amount of silica fume, despite a

slight reduction in hot strength. As a compromise, the appropriate SiO_2 addition should be limited to less than 1.0%.

Dynamic slag test is conducted in a rotary furnace, using a steel making slag with high ferrite content. The microstructure of the corroded MgO-Al_2O_3 castables is characterized by two different penetration layers under the slag, one is colored, Fe_xO enriched zone and the other is uncolored, CaO and SiO_2 penetrated zone.

Both MgO and MA can capture FeO/Fe_2O_3 from the slag to form $(Mg, Fe)_xO$ and $(Mg, Fe)(Fe,Al)_2O_4$ solid solutions. The continuous dissolution of $(Mg, Fe)_xO$ and $(Mg, Fe)(Fe,Al)_2O_4$ leads to the local saturation of liquid phases and therefore precipitates secondary spinel, which is netted with in-situ spinel to form a densified spinel layer. Simultaneously, the CaO and SiO_2 components penetrate further and react with the refractory components to form low melting silicate phases, as detected in the uncolored zone.

In regard to slag resistance, at 5wt% spinel addition, AR_{78} is superior to AR_{90} in slag erosion resistance, whereas MR_{66} is more beneficial to penetration resistance. In addition, with a proper amount of SiO_2 fume, not only can the intermediate temperature strength be remarkably improved, but the erosion and penetration resistance as well.

Although the above encouraging results have been achieved in this thesis work, further efforts, focusing on improving slag penetration, still need to be exerted, as the penetration resistance of the developed MgO-Al_2O_3 castable is thought to be still weak, due to the inherent nature of MgO. The "ultimate solution" could be to incorporate carbon into the mix, because carbon is expected to be the most effective inhibitor to slag

penetration, if one can well cope with its lack of hydration. As well known, carbon is not wettable by water, the castable has to demand more mixing water for workability with all the consequences attached to this, nevertheless, it still should be a worthwhile approach. Furthermore, to pursue the work on $MgO-Al_2O_3$ system, due to consideration should be given to additions of ultrafine pre-reacted spinel powders with sizes of 0.5 to 4 μm, if the grinding and cost are not barriers.

REFERENCES

1. P. Atkinson et al., "The Introduction of Monolithics in European Steel Ladles: Our Experience", Proceedings of 2nd International Symposium on Advances in Refractories, Montreal, Canada, Aug. 24 – 29, 1996
2. C. Parr et al., "The Design Fundamentals of High Technology Castables – An Understanding for Steelmakers", 82nd Steelmaking Conference Proceedings, Chicago, USA, Vol.82, Mar.21-24, 1999, pp237-249.
3. R. Nakamura et al., "The Current Status of Casting Steel Ladles in Japan", 82nd Steelmaking Conference Proceedings, Chicago, Vol 82, Mar.21-24, Chicago, USA, 1999, pp267-278.
4. S. Asano, "Progress of Steel Making Technology and Refractories Situation in Japan", UNITCER'93, pp69-94.
5. B. Clavaud and J. P. Keihl, "15 Years of Low Cement Castables in Steelmaking", First International Conference on Refractories, Nov. 15-18, Japan, 1983, pp589-606.
6. K. Ide et al., "Development of a Self-flow Castable for Steel Ladles", Takabutsu Overseas, Vol.17, No1, pp53-57.
7. M. Rigaud et al., "Basic Castable for Ladle's Steelmaking Applications: A Review", Journal of Canadian Ceramic Society, Vol. 66, No3, 1997, pp206 209.
8. K. H. Hwang et al., "In-situ Spinel Bond Formation (Expansion/Contraction) during Firing", UNITCER'97, 1997, pp1575-1580.

9. H. Sumimura, T. Yamamura and Y. Kubota et al., "Study on Slag Penetration of Alumina-Spinel Castable", UNITECR'91, pp97-101.

10. Alcan Chemials, "Product Data: Alumina Actibond 101", 1994.

11. L. D. Hart, "Alumina Chemicals Science and Technology Handbook". The American Ceramic Society, Inc. Ohio, pp93-108, 1990.

12. B. Myhre and K. Sunde, "Alumina Castables with very Low Contents of Hydraulic Compound. Part 1: The Effect of Binder and Particle Size Distribution on Flow and Set", UNITECR'95, pp309-316.

13. S. Haling et al, "New Reactive Aluminas for Calcia-Free Low Moisture, Self-Leveling Castables", The 100th American Ceramic Society Meeting and Expo, Cincinnati, May 2-5, 1998.

14. Z. Nakagawa, "Expansion Behavior of Powder Compacts during Spinel Formation", To be published in Mass and Charge Transport in Ceramics.

15. M. Rigaud, S. Palco and N. Wang, "Spinel Formation in the $MgO-Al_2O_3$ System Relevant to Refractory Castables", UNITECR'95, pp387-392.

16. Z. Nakagawa, N. Enomoto, I. Yi, and K. Asano, "Effect of Corundum/Periclase Sizes on Expansion Behavior during Synthesis of Spinel", UNITECR'95, pp379-386.

17. T. Yamamura, Y. Kubota et al., "Effect of Spinel Clinker Composition on Properties of Alumina-Spinel castable", Taikabutsu Overseas, Vol 13, No2. Pp39-44.

18. "Technology of Monolithic Refractories," Plibrico Japan Company, Ltd., Tokyo, Japan, 1984, p598-602.

19. R. E. Fisher "New Developments in Monolithic Refractories," The American Ceramic Society, Inc. Advances in Ceramics, Vol.13, 1985, pp46-66.

20. D. R. Lankard, "Evolution of Monolithic Refractory Technology in the United States", New Developments in Monolithic Refractories, Edited by R. E. Fisher, 1985, pp46-66.

21. P. H. Havranek, "Recent Developments in Abrasion- and Explosive-Resistant Castables", Cement Bulletin (ACerS), Vol. 62, No.2, 1983, pp234-243.

22. K. Adachi and M. Kuwayama et al., "Progress in Ladle Refractories Technology at Kawasaki Steel, Mizushima Works", UNITECR'95, Vol.3, pp242-249.

23. S. D. Majumdar et al., "Development of Cementless and Auto-flow Aluminous Castable for Use in the Production of Cleaner Steel", Stahl und Eisen, Oct. 1994, pp162-167.

24. B. Clavaud, J. P. Kiehl, and J. P. Radal "A New Generation of Low-Cement Castables," The American Ceramic Society, Inc. Advances in Ceramics, Vol.13, 1985, pp274-284.

25. G. MacZura, M. Madono, G. W. Kriechbaum, B. Sewell "Low Moisture Regular Corundum/Spinel Castables with Superior Properties", UNITECR'95, pp179-186.

26. K. Furuta, I. Furusato, I. Takita "Development of Castable for Teeming Ladle in Japan," UNITECR'95, pp334-348.

27. S. Kamei "Progress of Monolithic Refractories for Recent 10 Years in Japan", UNITECR'89, pp46-59.

28. S. Kataoka " Refractoris for Steelmaking in Japan", UNITECR'95, pp1-27.

29. T. Yumoto et al., "Effect of Content of Alumina Cement, Silica Flour and Added Water on Strength of Castable", Taikabutsu Overseas, Vol.13, No.2, pp3-6.

30. J. Mori, N. Watanabe, M. Yoshimura, Y. Oguchi, and T. Kawakami "Material Design of Monolithic Refractories etc. for Steel Ladle ", Ceramic Bulletin (ACerS), Vol. 69, No 7, 1990, pp1172-1176.

31. A. Nagasoe et al., "Refractory Characteristics of Spinels with Various MgO Contents", Taikabutsu Overseas, Vol.11, No.3, pp20-28.

32. H. Kyoden, K. Ichikawa et al., Taikabutsu, Vol.36, 1984, p473.

33. A. Matsuo, S. Miyagawa et al., Taikabutsu, Vol.37, 1985, p279.

34. G. Maczura, V. Gnauck and P. T. Rothenbuehler, "Fine Aluminas for High Performance Refractories", The First International Conference on Refractories, Nov. 15-18, Japan, 1983, pp560-574.

35. K. Oda, H. Itoh, Y. Matsumoto and Y. Ono, "Drying Characteristic of High-Dense Castable", Taikabutsu Overseas, Vol.13, No.2, pp21-28.

36. A. Yamamoto et al., "Development and Application of Unshaped Refractories in Stainless Steel Making", Stahl und Eisen, Oct., 1992, pp88-94.

37. J. Karja and H. Nevala, "Experiences of Monolithic Ladle Linings in RAAHE Steel Works", UNITECR'93, pp1312-1319.

38. K. Kurata, T. Matsui and S. Sakaki, "Castable Lining Technique to Bottom of Teeming Ladle", Taikabutsu Overseas Vol.12, No.1, pp29-39.

39. T. Nishitani et al., "Application of the Alumina-Spinel Castable for BOF Ladle Lining", UNITECR'89, pp529-540.

40. T. Numata et al., "Development of Al_2O_3-MgO Castable Refractories", Tetsu-to-Hagane, 72, S110,1986.

41. T. Yamamura et al., "Alumina-Spinel Castable Refractories for Steel Teeming Ladle", Taikabutsu Overseas, Vol.12, No.1, pp21-27.

42. M. Kobayashi, K. Kataoka, Y. Sakamoto and I. Kifune, "Use of Alumina-Magnesia Castables in Steel Ladle Sidewalls", Taikabutsu Overseas, Vol.17, No.3, pp39-44.

43. A. Ugai, K. Ariyoshi, M. Koyama and M. Hayashi, "Comparison of Corrosion Resistance between Magnesia Carbon and Alumina Magnesia Castables", Taikabutsu Overseas, Vol.17, No.3, p105.

44. B. Clavaud, J. P. Keihl and J. P. Radal, "New Developments in Monolithic Refractories", Advances in Ceramics, Vol. 13, Edided by R. E. Fisher, 1985, pp274-283.

45. H. Teranishi, O. Kawamura, K. Yasui et al., "Application of MgO-C Castable to Ladle Furnace Slag Line", Taikabutsu Overseas, Vol.18, No.1, pp38-42.

46. M. W. Vance et al., "Influence of Spinel Additives on the Performance of High Alumina and Spinel Castables", Technical Bulletin Refractory Products, November, 1994.

47. G. A. Rankin and H. E. Merwin, Journal of the American Ceramic Society, Vol.38, 1916, pp568-588.

48. D. M. Roy, R. Roy and E. F. Osborn, American Journal of Science, Vol. 251, 1953.

49. D. Viechnicki, F. Schmid and J. W. McCauley, "Liquidus-Solidus Determinations in the System $MgAl_2O_4$-Al_2O_3", Journal of American Ceramic Society, Vol.57, No.1, 1974, pp47-48.

50. A. M. Alper, R. N. McNally, P. H. Ribbe, and R. C. Doman, "The System MgO-$MgAl_2O_4$", Journal of American Ceramic Society, Vol.45, No.6, 1962, pp263-268.

51. A. M. Lejus, Rev. Hautes Temp. Refractories, No.1, 1964, pp53-95.

52. A. M. Lejus and R. Collongues, Compt. Rend., 254, 1962, pp2780-2781.

53. G. Eriksson, P. Wu and A. Pelton, "Critical Evaluation and Optimization of the Thermodynamic Properties and Phase Diagrams of the MgO-Al_2O_3, MnO-Al_2O_3, FeO-Al_2O_3, Na_2O-Al_2O_3 and K_2O-Al_2O_3 Systems", CALPHAD Vol.17, No.2, 1993, pp.189-205.

54. S. K. Roy and R. L. Coble, "Solubilities of Magnesia, Titania, and Magnesium Titanate in Aluminum Oxide", Journal of American Ceramic Society, Vol.51, No.1, 1968, pp1-6.

55. R. Morrel, "Handbook of Properties of Technical and Engineering Ceramics", Part 1, HSMO, London, UK, 1985, p82.

56. C. Wagner, "The Mechanism of Formation of Ionic Compounds of Higher Order (Double Salts, Spinel, Silicates)", Z. Physik. Chem., B34, 1936, pp309-316.

57. D. L. Ricoult et al., "Internal Reaction in the (Mg, Me)O System", Journal of Materials Science, Vol.22, 1987, pp2257-2266.

58. J. Beretka and T. Brown, "Effect of Particle Size on the Kinetics of the Reaction between Magnesium and Aluminum Oxides", Journal of American Ceramic Society, Vol.66, No.5, 1983, pp383-388.

59. R. E. Carter, "Mechanism of Solid-State Reaction between Magnesium Oxide and Aluminum Oxide and between Magnesium Oxide and Ferric Oxide", Journal of American Ceramic Society, Vol.44, No.3, 1961, pp116-120.

60. G. H. Stewart, "Science of Ceramics", The British Ceramic Society, Vol.3, 1967, p251-257.

61. W. P. Whitney et al, "Inter-diffusion in the System MgO-$MgAl_2O_4$", Journal of American Ceramic Society, Vol. 54, No.7, 1971, p349-352.

62. R. C. Rossi and R. M. Fulrath, "Epitaxial Growth of Spinel by Reaction in the Solid State", Journal of American Ceramic Society, Vol. 46, No.3, 1963, pp143-149.

63. M. Nakano, G. Yamaguchi, and K. Saito, "On the Thickness Ratio of Two Spinel Layers Formed by Solid State Solution", Yogyo-Kyokai-Shi, Vol.79, No.4, 1971, pp119-123.

64. I. Yasui, G. Yamaguchi, H. Kurosawa, "Interfacial Phenomena and the Orientation of Spinel in $MgO-Al_2O_3$ Solid State Reaction", Yogyo-Kyokai-Shi, Vol.81, No.5, 1973, pp197-202.

65. G. Yamaguchi, K. Shirasuka, and M. Munekata, "Some Aspects of Solid Reaction of Spinel Formation in the System $MgO-Al_2O_3$", Yogyo-Kyokai-Shi, Vol.79, No.2, 1971, pp64-69.

66. Z. Bi et al, "Relationship between Composition and Properties of MgO-Spinel Castables", Vol.1, UNITECR'97, p33-39.

67. Zenbe-e Nakagawa, Takumi Itoh and Naoya Enomoto, "Effect of Compositional Variation ion Expansion Behavior of MgO/Al_2O_3 Compact during Spinel Formation", 35th Annual Conference of Metallurgists, August 24-29, 1996, Montreal, Canada.

68. J. McColm, "Ceramic Science for Materials Technologists", Blackie & Son Ltd, 1983, pp299-306.

69. A. Koller, "Structure and Properties of Ceramics", ASER, Czech Republic, 1994, pp309-311.

70. A. M. Alper, "High Temperature Oxides" Part IV, Academic Press, 1971, pp77-146.

71. T. J .Davies et al, "Alumina-Chromia-Magnesia Refractories", The Third Euro-Ceramics Vol.3, 1993, pp243-248.

72. H. Nagata et al, "Hydration of Magnesia Clinkers", Taikabutsu, Vol.46, No.11, 1994, p599.

73. H. Kyoden, Y. Hamazaki, R. Nakamura, T. Kaneshige, "Basic Castable", Shinagawa Technical Report, No.32, 1989.

74. A. Kitamura, K. Onizuka and K. Tanaka, "Hydration Characteristics of Magnesia", Taikabutsu Overseas, Vol.16, No.3, pp3-11.

75. K. Matsui and K. Saihi, "Effects of Impurities on the Hydration of Magnesia Clinkers ", UNITECR'95, pp513-20.

76. A. M. Alper, "High Temperature Oxides" Part I, Volume 5, Academic Press, 1970.

77. F. Samukawa, M. Yoshimura, T. Yamane, Y. Oguchi and T. Kawakami, "Slaking of Castable Containing Magnesia", Taikabutsu, Vol.40, No.5, pp32-34.

78. A. Watanabe, H. Takahashi et al. "Magnesia Containing Basic Castables", UNITECR'95, pp181-8.

79. Wolfert, "Process for Preparing Magnesia Having Reduced Hydration Tendency, Hydration Resistant Magnesia, Dry Mixture for Preparing Magnesia Based Castables and Magnesia Based Castable", U.S. Patent No. 5 133 648, Feb. 2, 1993.

80. A. Kaneyasu, S. Yamamoto and T. Watanabe, "MgO Raw Material Improved the Hydration Resistance", UNITECR'95, pp533-40.

81. Y. Watanabe, T. Ono etc. "Development and Application of Monolithic Refractory Containing Magnesia Clinker", Proceedings of 2nd International Conference on Refractories, Tokyo, 1987, pp494-506.

82. B. Sandberg and T. Mosberg, "Use of Micro-Silica in Binder System for Ultra-Low Cement Castables and Basic "Cement-Free" Castables", Ceramic Trans. Vol. 4, 1989, pp 245-258.

83. B. Myrhe, "Cement Free Castables; in the System MgO-SiO_2; the Effect of Bond Phase Modifiers on Strength", the 93rd Annual Meeting of American Ceramic Society, Cincinnati, May 1991.

84. K. Nishi, K. Hosokawa et al., "Phosphate Bonded Castable", UNITECR'95, pp237-44.

85. M. W. Vance and K. J. Moody, "Use of Hydratable Alumina Binders in Refractory Compositions and Related Applications", the 97th Annual Meeting of American Ceramic Society, Cincinnati, May 1995.

86. S. C. Maestre Ili et al., "The Effect of Cement Substitution for ρ-alumina Partial Additions on the Thermo-mechanical Properties of a Low Cement Refractory Concrete", UNITECR'95, Vol.1, pp337-342.

87. B. Myhre et al., "Alumina Based Castables with Very Low Contents of Hydraulic Compound. Part II: Strength and High-Temperature Reactions of "No-Cement" Castables with Hydraulic Alumina and Microsilica", UNITECR'95, pp317-24.

88. Ning Wang, Ph.D. dissertation, "Spinel Bonded Magnesia Based Castables with Hydratable Alumina as Binder", Ecole Polytechnique, July 1996.

89. Banerjee and J. To, "Refractories for High Temperature Application", UNITCER'89, pp1140-1156.

90. K. Nishi et al., "Investigation on Basic Castable Refractories for Teeming Ladle", 1st International Conference on Refractories', Tokyo, Nov. 1983, Japan, pp475-493.

91. Kato et al., "Application of Magnesia-Silica Castable Refractories for Slag Line of Steel Teeming Ladle", Trans. I.S.I Japan, Vol. 26, 1986, p92.

92. Y. Oguchi and J. Mori, "Wear Mechanism of Castable for Steel Ladle", Taikabutsu Overseas, Vol. 13, No. 4, pp43-46.

93. Nishii et al., "Investigation on Castable Refractories for Steel Teeming Ladles", first Intnl. Conf. Refract, Tokyo, TARJ, 1983, pp475-494.

94. Francis W. Henry, "Production of basic Castables and Basic Precast Shapes for Steel Applications", UNITECR'95, pp1-8.

95. Udagawa et al., "Slag Penetration into Magnesia and Alumina Monolithic Refractories", UNITCER'93, pp1515-1524.

96. Yaoi et al., "Basic Monolithic Refractories", U.S. Patent No. 5 204 298, April 20, 1993.

97. Nakagawa et al., "Development of Monolithic Refractory Lining for Steel Ladle Slag Line", Stahl und Eisen, No.10, 1992, pp1515-1524.

98. Kawasaki et al., Taikabutsu, Vol.41, No.2, 1989, p12.

99. M. Blanchard, M.Sc.A. dissertation, "Graphite Containing Cement Free Basic Castable", Ecole Polytechnique, June 1998.

100. Yamamura et al., Taikabutsu, Vol.43, No.11, 1991, p. 642.

101. S. Sakamoto et al. "Graphite Containing Unshaped Refractories", UNITECR'95, pp189-96.

102. Mosser, G. Karhut and W. Hammer "New Refractories for Modern Ladel Lining", UNITECR'95, pp195-202.

103. B. Nagai, O. Matsumoto, T. Isobe and Y. Nishiumi, "Wear Mechanism of Castable for Steel Ladle by Slag", Taikabutsu Overseas Vol.12, No.1, pp15-20.

104. Y. Sato, H. Joguchi and N. Hiroki, "Test Results of Alumina-Spinel Castable for Steel Ladle", Taikabutsu Overseas, Vol.12, No.1, pp10-14.

105. T. Kanatani, Y. Imaiida, "Application of an Alumina-Spinel Castable to the Teeming Ladle for Stainless Steelmaking", UNITECR'93, pp1255-66.

106. H. Sumimura, T. Yamamura et al., UNITECR'95, pp97-101.

107. K. Fujii, Isao, F. and I. Takita, "Composition of Spinel Clinker for Teeming Ladle Casting Materials", Taikabutsu Overseas Vol.12, No.1, pp4-9.

108. A. Matsuo, S. Miyagawa et al. Taikabutsu, Vol.40, 1985, p279.

109. Y. Koga, M. Sato, K. Sekiguchi and S. Iwamoto, "Effects of Alumina Cement Grade and Additives on Alumina-Magnesia Castables Containing Aluminum Lactate", Taikabutsu Overseas, Vol.18, No.1, pp43-47.

110. T. Okada, J. Yagi, A. Hayashi, T. Kawamura et al., "Improvement of Castable Refractories for Top Bubbling Lances", Taikabutsu Overseas, Vol.18, No.1, pp22-26.

111. M. Tawara, K. Fujii and T. Taniguchi et al., "Application of Alumina-Magnesia Castable in High Temperature Steel Ladles", Taikabutsu Overseas, Vol.16, No.2, pp17-19.

112. S. Itose, T. Isobe, K. Sugiyama, K. Furukawa, "Optimum Castable Lining for Steel Ladle in Japan", UNITECR'97, pp165-174.

113. T. A. Ring, " Fundamentals of Ceramic Powder Processing and Synthesis", Academic Press, San Diego, 1996.

114. G. Tari et al., "Influence of Magnesia on Colloidal Processing of Alumina", Powder Technology, p1341-1350, 1997.

115. E. Ran and R. W. Wallace, "Thermal Expansion of Refractory Brick", American Ceramic Society Bulletin, Vol.42, No.2, 1963, pp52-56.

116. P. S. Turner, "Thermal-Expansion Stresses in Reinforced Plastics", J. Res. Natl. Bur. Std., Vol.37, No.4, 1946, pp239-50.

117. H. P. Klug et al., "X-Ray Diffraction Procedures", John Willey & Sons, Inc.

118. C. Novak and G. Pokol et al. "Studies on the Reactions of Aluminium Oxides and Hydroxides", Journal of Thermal Analysis, Vol. 36, 1990, pp1895-1909.

119. Z. Jaworska-Galas et al. "Morphological and Phase Changes of Transition Aluminas during their Rehydration", Journal of materials Science, Vol. 28, 1993, pp2075-2078.